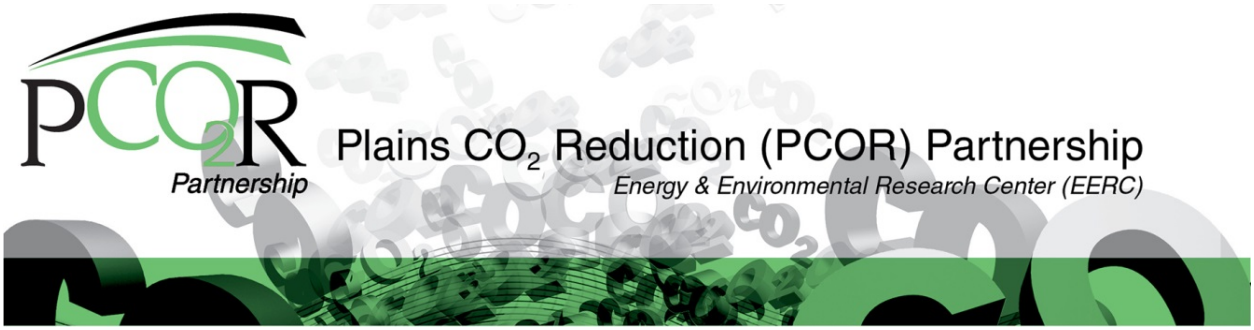

ANALYSIS OF EXPANDED SEISMIC CAMPAIGN

Plains CO_2 Reduction Partnership Phase III
Task 9 – Deliverable D104

Prepared for:

Andrea M. Dunn

National Energy Technology Laboratory
U.S. Department of Energy
626 Cochrans Mill Road
PO Box 10940
Pittsburgh, PA 15236-0940

Cooperative Agreement No. DE-FC26-05NT42592

Prepared by:

Olarinre Salako
Amanda J. Livers
Shaughn A. Burnison
John A. Hamling
Neil Wildgust
Charles D. Gorecki
Kyle A. Glazewski
Loreal V. Heebink

Energy & Environmental Research Center
University of North Dakota
15 North 23rd Street, Stop 9018
Grand Forks, ND 58202-9018

June 2017
2019-EERC-10-19 Approved

EERC DISCLAIMER

LEGAL NOTICE This research report was prepared by the Energy & Environmental Research Center (EERC), an agency of the University of North Dakota, as an account of work sponsored by the U.S. Department of Energy (DOE) National Energy Technology Laboratory (NETL). Because of the research nature of the work performed, neither the EERC nor any of its employees makes any warranty, express or implied, or assumes any legal liability or responsibility for the accuracy, completeness, or usefulness of any information, apparatus, product, or process disclosed or represents that its use would not infringe privately owned rights. Reference herein to any specific commercial product, process, or service by trade name, trademark, manufacturer, or otherwise does not necessarily constitute or imply its endorsement or recommendation by the EERC.

ACKNOWLEDGMENT

This material is based upon work supported by DOE NETL under Award Number DE-FC26-05NT42592.

DOE DISCLAIMER

This report was prepared as an account of work sponsored by an agency of the United States Government. Neither the United States Government, nor any agency thereof, nor any of their employees, makes any warranty, express or implied, or assumes any legal liability or responsibility for the accuracy, completeness, or usefulness of any information, apparatus, product, or process disclosed, or represents that its use would not infringe privately owned rights. Reference herein to any specific commercial product, process, or service by trade name, trademark, manufacturer, or otherwise does not necessarily constitute or imply its endorsement, recommendation, or favoring by the United States Government or any agency thereof. The views and opinions of authors expressed herein do not necessarily state or reflect those of the United States Government or any agency thereof.

TABLE OF CONTENTS

LIST OF FIGURES

Continued . . .

LIST OF FIGURES (continued)

LIST OF TABLES

ANALYSIS OF EXPANDED SEISMIC CAMPAIGN

EXECUTIVE SUMMARY

The Plains CO_2 Reduction Partnership (PCOR) Partnership, led by the Energy & Environmental Research Center (EERC), is working with Denbury Resources Inc. (Denbury) to study incidental carbon dioxide (CO_2) storage associated with a commercial enhanced oil recovery (EOR) project at the Bell Creek oil field located in southeastern Montana, which is operated by Denbury Onshore LLC. As the field operator, Denbury carries out the injection and production operations. The EERC has provided support for site characterization, modeling and simulation, and risk assessment and will aid in the development of the monitoring, verification, and accounting (MVA) plan. As part of this effort, a three-dimensional (3-D) surface seismic survey was acquired in 2012 prior to the start of CO_2 injection. This baseline survey provided detailed information that enhanced the characterization of the reservoir and served as a benchmark comparison for two subsequent surface monitor surveys acquired in 2014 and 2015. The monitor surveys, acquired after CO_2 injection had been implemented in different field development phases, were used to create "difference images" to track where the injected CO_2 had migrated to within the reservoir at the time of the survey. Maps of the seismic amplitude changes associated with injected CO_2 produce powerful images that allow for detailed interpretation of the injection zone, providing significant additional information on permeability barriers and flow channels that were used to refine the characterization, update the geologic models to improve predictive simulations, and help determine the ultimate fate of injected CO_2 (Figure ES-1).

In addition to the 3-D surface seismic surveys, several other geophysical studies have been done or are currently being conducted at Bell Creek as part of the expanded seismic campaign. These include a 2-D test line to assess different sources for use in the baseline 3-D survey that later became instrumental in proving that CO_2 could be observed in the reservoir. 3-D vertical seismic profiles (VSPs) were acquired, processed, and are being interpreted from two observation wells. One observation well, 04-03 OW, contains a 50-level seismic geophone array that was permanently installed. The permanent array was connected to a recording system on the surface, and data were recorded passively and continuously for 3 years in order to detect microseismic events that occurred during the time period when field development Phases 1 and 2 were prepared and brought online with CO_2 flooding. In-house processing and interpretation of the passive data are ongoing. The VSP and passive seismic analyses are not presented in this report.

Key Results and Conclusions from the Bell Creek Expanded Seismic Campaign

- The expanded seismic campaign has been instrumental in gaining a better understanding of incidental CO_2 storage associated with CO_2 EOR. It has provided a means to measure and image physical properties throughout the geologic section on a fine grid over the field that has aided geologic characterization.

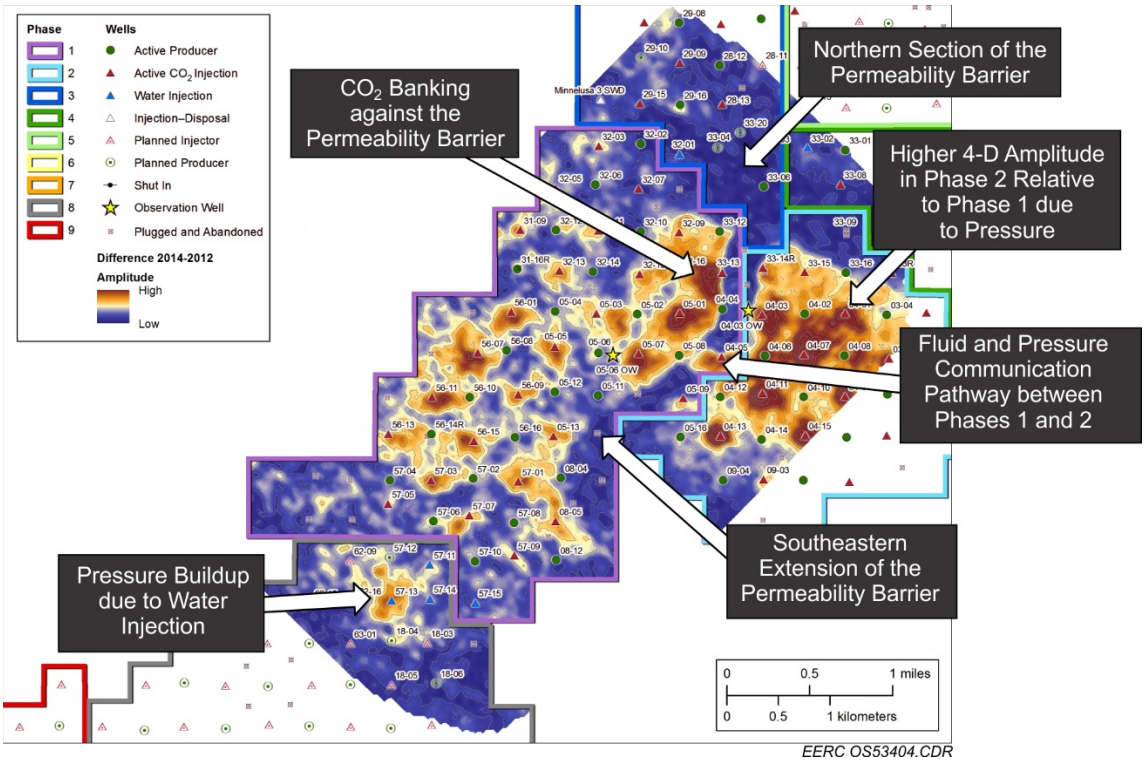

Figure ES-1. Summary of the 2014–2012 4-D amplitude difference map interpretation.

- 4-D analysis improved the understanding of the reservoir heterogeneity and improved the geologic model that was generated using interpretation results from the 2012 baseline data.
- CO_2 acted as a tracer that illuminated geobodies in the 4-D data by delineating permeability barrier boundaries that were not resolved with 3-D baseline data. This illumination gave better insight about the location, extent, and effectiveness of these permeability barriers.
- Understanding and incorporating the newly illuminated features and their geometrical dimensions into the static model significantly improved dynamic simulation of well performance and improved reservoir history matching and forecasting.
- 4-D analysis indicated updip migration of CO_2 in the south–east direction and apparent accumulation of CO_2 against the permeability barrier.
- Inversion of 3-D data was used to calculate volumes of geomechanical properties that were used in the construction of a 3-D mechanical earth model so that geomechanical responses due to injection operations could be modeled in the reservoir and surrounding strata.

The results of the expanded seismic campaign have contributed to the PCOR Partnership's development of practices and technologies that will allow future commercial-scale CO_2 storage projects to make informed decisions regarding site selection, injection operations, and monitoring strategies. Work on the expanded seismic campaign data will continue with in-house processing and interpretation of the passive data to better understand changes in reservoir conditions associated with phase development. New methods of pre- and poststack inversion of 3-D surface data are planned to gain more information about reservoir compartmentalization. Additional efforts may include quantitative 4-D seismic analysis and inversion to independently estimate the amount of CO_2 stored in the reservoir and separate the CO_2 seismic response from the pressure response.

ANALYSIS OF EXPANDED SEISMIC CAMPAIGN

INTRODUCTION

The Plains CO_2 Reduction Partnership (PCOR) Partnership, led by the Energy & Environmental Research Center (EERC), is working with Denbury Resources Inc. (Denbury) to study incidental carbon dioxide (CO_2) storage associated with a commercial enhanced oil recovery (EOR) project at the Bell Creek oil field located in southeastern Montana, which is operated by Denbury Onshore LLC (Figure 1). As the field operator, Denbury carries out the injection and production operations as part of a commercial EOR project. In order to facilitate an improved understanding of incidental CO_2 storage associated with a commercial EOR project and to inform viable characterization, modeling, and monitoring strategies at future CO_2 storage projects, the EERC partnered with Denbury to conduct several types of geophysical studies. This document provides an overview of these different surveys; their acquisition, processing, and interpretation; and their integration with the EERC's characterization program and geologic model.

A significant contribution to this effort has been the acquisition and interpretation of multiple overlapping three-dimensional (3-D) surface seismic surveys acquired over the field. The 2012 baseline survey, acquired prior to the start of CO_2 injection, provided detailed information that enhanced the characterization of the reservoir and served as a benchmark comparison to subsequent surface surveys. When the baseline survey was paired together with overlapping 3-D surface seismic surveys acquired after CO_2 injection had progressed, the changes occurring between the two surveys constituted a direct indication of where the injected CO_2 had migrated within the reservoir at the time of the survey. This provided additional information on permeability barriers and flow channels that were then used to refine the characterization and update the geologic models to improve predictive simulations and help determine the ultimate fate of injected CO_2. At Bell Creek, two 3-D surface seismic surveys were acquired subsequent to the baseline and commencement of injection: the 2014 monitor and the 2015 monitor and baseline extension.

While direct interpretation of the 3-D time-lapse images is powerful, the physical measurements that make up the data sets from the 3-D surveys are a rich source of information that can be mined in other ways. The acquisition geometry provides a wide sampling of shot point and receiver point offsets which, together with subsurface velocity information, allows for the data to be sorted into the various incident angles of the energy raypaths that reflect from any given point in the subsurface. These amplitude-versus-offset relationships can be computationally inverted to geomechanical properties, and this was done to assist in the creation of a 3-D mechanical earth model. The method and purpose for this are described in Appendix C.

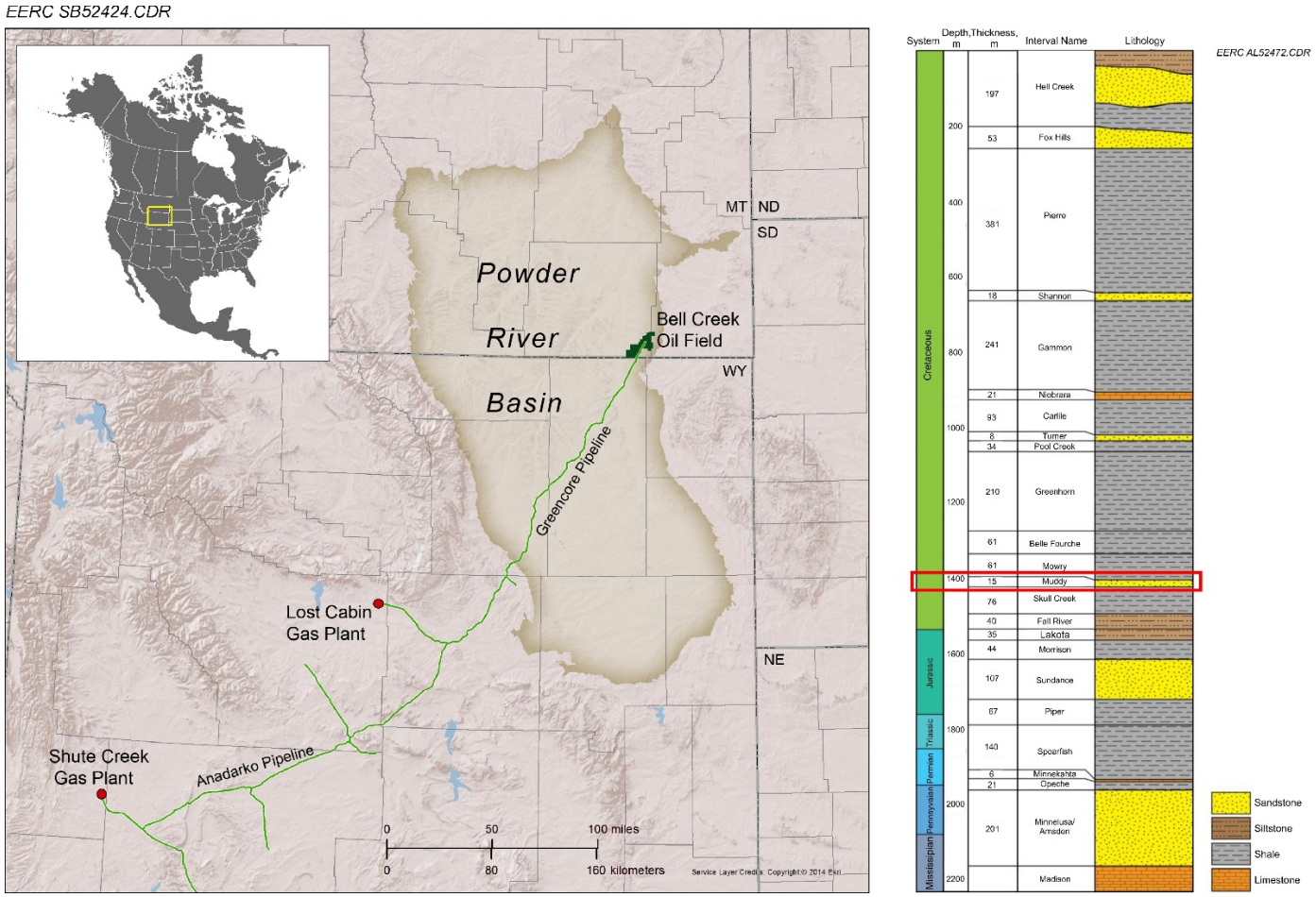

Figure 1. The Bell Creek oil field in southeastern Montana lies on the eastern edge of the Powder River Basin. The CO_2 used for EOR is transported to the field through pipeline from ExxonMobil's Shute Creek gas-processing plant and ConocoPhillips' Lost Cabin natural gas-processing plant (Burnison and others, 2016).

In addition to the 3-D surface seismic surveys, several other geophysical studies have been done at Bell Creek. Figure 2 shows a time line of the geophysical studies that were a part of the PCOR Partnership project's expanded seismic program at Bell Creek. The first study was a 2-D test line to assess different sources for use on the baseline 3-D. It later became instrumental in proving that CO_2 could be observed in the reservoir using time-lapse seismic. Fluid replacement modeling done by Denbury in 2014 indicated that seismic amplitudes for the target interval would be reduced by 17% if CO_2 concentrations were high and dominant frequencies were above 30 Hz. While detectable, this level of change could be ambiguous on real data. To eliminate uncertainty, the 2-D line was reshot approximately 14 months after CO_2 injection had begun in the vicinity of the line. Processed using a time-lapse workflow, the result showed that CO_2 was clearly visible in the reservoir on the difference display.

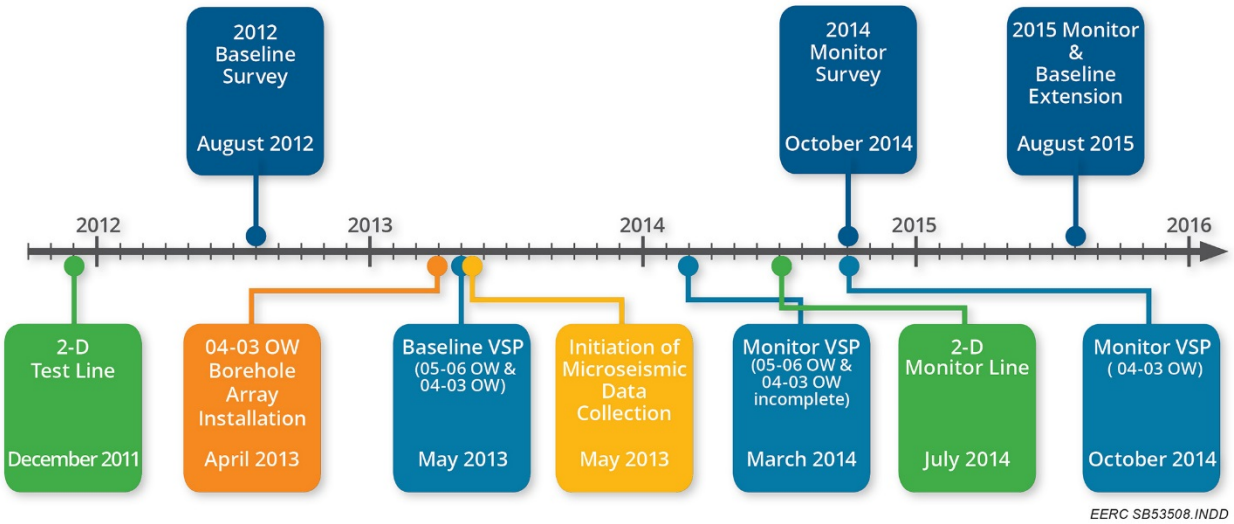

Figure 2. Time line showing the different components of the expanded seismic campaign.

3-D vertical seismic profiles (VSPs) also figured prominently in the expanded campaign. Pre-CO_2 injection baseline 3-D VSPs were acquired in two observation wells (OWs): 05-06 OW and 04-03 OW. The 05-06 OW well employed a removable array, but 04-03 OW is a special case where a 50-level seismic geophone array was permanently installed. After the baseline 3-D VSPs were acquired, the permanent array was connected to a recording system on the surface, and data were recorded passively and continuously for 3 years in order to detect microseismic events that occurred during the time period when field development Phases 1 and 2 were prepared and brought online with CO_2 flooding. Later, while continuously recording, a complete monitor 3-D VSP survey was acquired using the 04-03 OW array concurrently with the first surface seismic monitor survey in October 2014. These geophysical studies are under way, and additional information can be found in Appendixes A and B.

BACKGROUND

The geologic target of interest for CO_2 injection is the oil-bearing Bell Creek Sand reservoir, within the Lower Cretaceous Muddy Formation (also referred to as the Newcastle), at a typical depth of approximately 4500 feet (Figure 3). Burnison and others (2014) reported on the geophysical reservoir characterization efforts at Bell Creek, with analysis and preliminary interpretation of the 3-D baseline survey. The 2012 baseline was the first 3-D data acquired over the field, and the interpretation was able to identify lithofacies and reservoir heterogeneities in greater detail than previously possible. The field had been drilled and developed using 40-acre well spacing which provided 16 data locations per square mile. Normally, this is considered substantial spatial geologic control, but the trace spacing on the 3-D data at Bell Creek is 82.5 feet, or 4096 data points per square mile, which provides the ability to map geologic horizons and facies changes between wells with much more detail. Subsequent interpretation work using the same data led directly to a new and different understanding of the depositional history of the Bell Creek Field (Bosshart and others, 2015; Jin and others, 2016). Insights from the interpretations were incorporated in updated geologic models and used to create more accurate predictive reservoir simulations.

The Muddy Formation is relatively thin, about 60 feet, and there was concern that this could present seismic interpretation challenges due to the depth of the formation (about 4500 ft). Vertical resolution degrades with depth because higher frequencies from the source attenuate more rapidly than do lower frequencies, and both high and low frequencies are needed for resolution. That the Bell Creek sand reservoir within the Muddy is rarely thicker than 30 feet presents even greater challenges. Burnison and others (2014) described in detail the origin of the reservoir reflection, which is due to a large increase in acoustic impedance (AI) at the top of the Springen Ranch Formation and a similar decrease in AI at the top of the Skull Creek (Figure 4). The measured thickness of the Springen Ranch-to-Skull Creek interval in the field varies from about 50 to 75 feet. Spectral bandwidth in the zone of interest on the baseline data was no greater than about 10–50 Hz. Given the average Muddy interval velocity of 10,800 ft/s, this mathematically limits the vertical resolution of the seismic data at reservoir depth to just under 60 feet, roughly equivalent to the thickness of the formation. Therefore, the Muddy Formation acts as a thin-bed reflector, with the appearance of an entering trough followed immediately by an exiting peak. The presence of CO_2 in the Bell Creek sand significantly impacts the amplitude of the entire Muddy reflection, and interpreting the changes in amplitude seen on the monitor surveys and difference displays reveals significant geologic character within the reservoir.

As much of the interpretation effort focuses on the reservoir reflection, images with more context that include annotated well logs and the bounding Springen Ranch and Skull Creek horizons overlaid are useful (Figure 5). Similar images will demonstrate interpretation where CO_2 injection has occurred. Powerful interpretations also result by mapping the amplitude changes over the survey area.

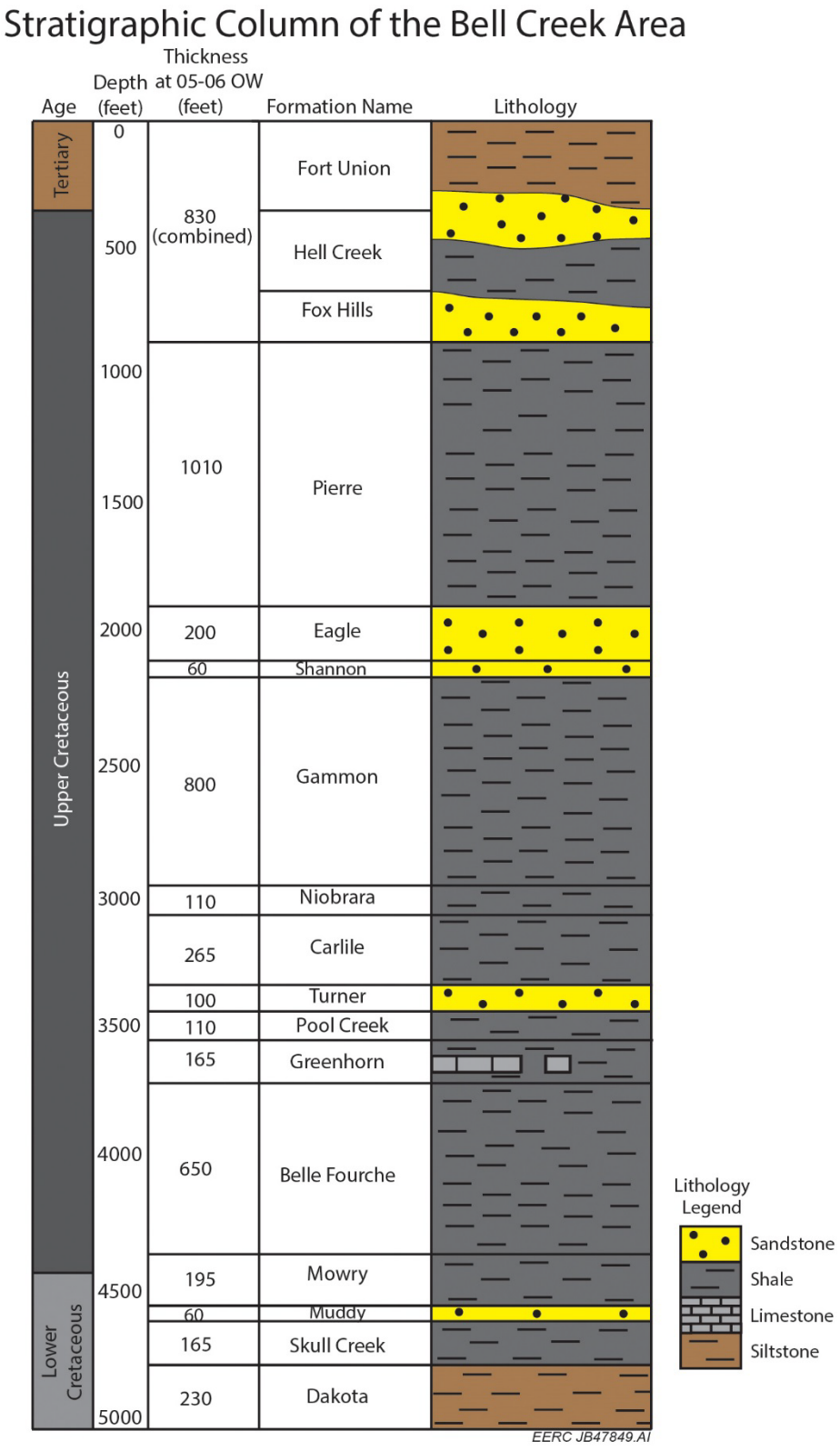

Figure 3. Stratigraphic column for the Bell Creek area. The Muddy Formation at a depth of 4500 feet is the oil-bearing reservoir (modified from Bosshart and others, 2015).

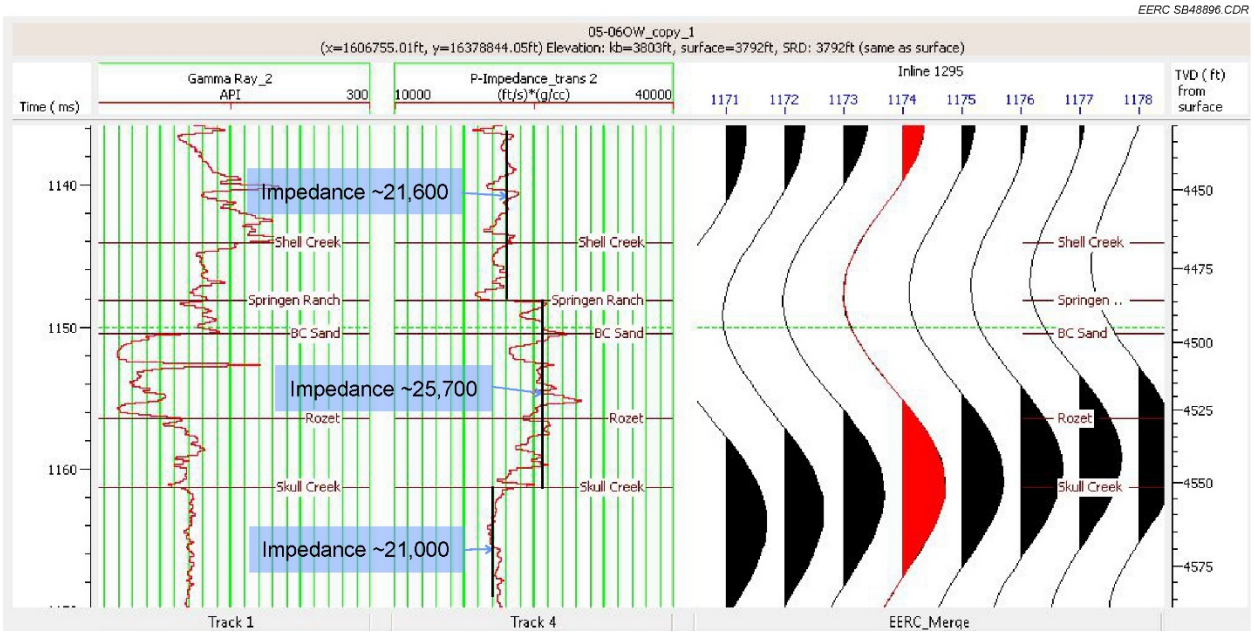

Figure 4. The P-wave acoustic impedance curve (sonic velocity × density) demonstrates that significant impedance changes occur at the Springen Ranch and Skull Creek boundaries and give rise to the Muddy Formation reflection. Bell Creek sand boundaries also exhibit impedance contrasts within this interval but are below the resolution of the wavelet (Burnison and others, 2014).

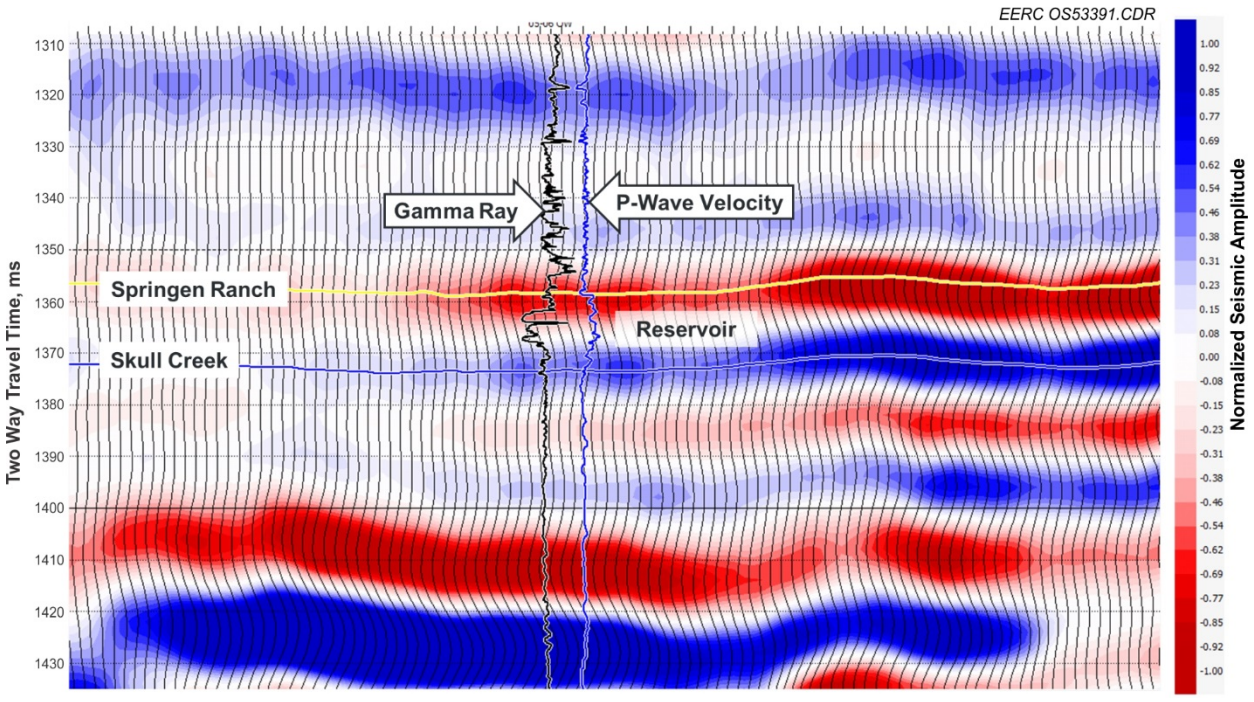

Figure 5. Baseline seismic data with interpreted horizons. GR (gamma ray) and P-wave velocity logs from observation well 05-06 OW are overlaid. The Springen Ranch and Skull Creek represent the top and base of the Muddy Formation.

Jin and others (2016) have described the reservoir depletion and production history of the Bell Creek oil field. In brief, production in the early life of the Bell Creek oil field was driven by primary depletion followed by secondary waterflooding. The mature field, which has been producing since 1967, has experienced pressure depletion and a significant decline in the oil production rate prior to August 2012 when the pre-CO_2 injection baseline 3-D seismic survey was acquired (Figure 6).

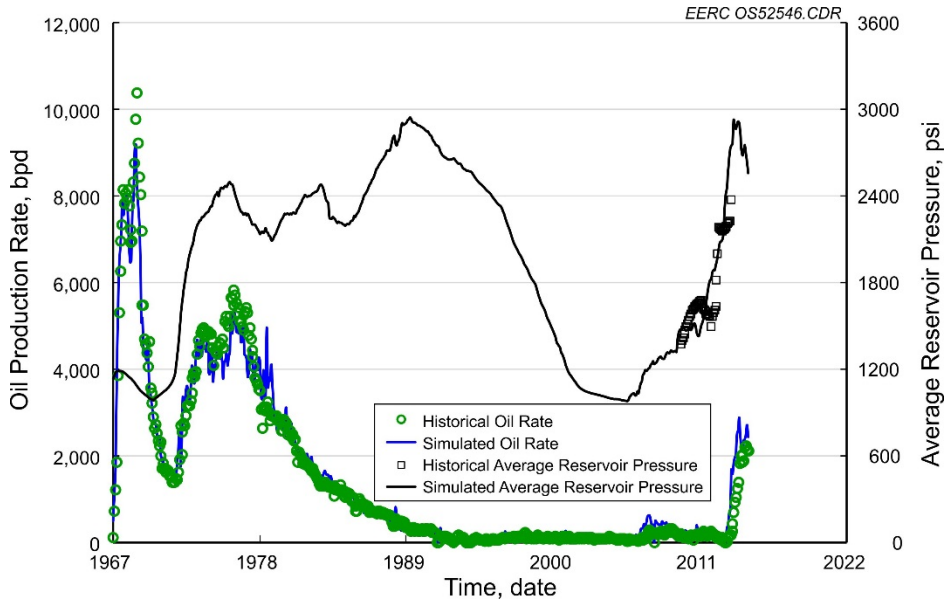

Figure 6. Measured and simulated average reservoir pressure and oil production rate history for development Phases 1 and 2 of the Bell Creek Oil Field. Increases in pressure and oil production in May 2013 are due to CO_2 enhanced oil recovery (Salako and others, 2017).

CO_2 tertiary recovery started in the Phase I development area in May 2013. The CO_2 is sourced from the ExxonMobil Shute Creek gas-processing plant and the ConocoPhillips Lost Cabin natural gas-processing plant, where CO_2 is separated from the process stream during refinement of natural gas. As of August 2016, over 2.9 million barrels of incremental oil has been recovered (Montana Board of Oil and Gas Conservation, 2017). Using these production and accompanying injection data, the EERC calculated that over 3.2 million tonnes of incidental CO_2 storage associated with the CO_2 EOR process has occurred.

At Bell Creek, CO_2 EOR is being implemented in a staged approach with nine planned CO_2 development phases across the field. This is due, in part, to some phases being at least partially geologically isolated by permeability barriers at the reservoir level, allowing them to be pressurized and prepared for CO_2 injection independently of other phases. Hence, mapping the permeability barrier locations is an important part of the characterization of the field. Another reason for phased development is that the infrastructure requirement to implement CO_2 EOR involves substantial capital outlays, and phased development allows for a return on the capital

investment in a staged manner. These factors explain the timing and areal coverage of the 3-D monitor surveys. The 2014 monitor survey was focused on Phase 1 and part of Phase 2, which had been undergoing CO_2 injection for 17 months and 11 months, respectively (Figure 7). The 2015 monitor and baseline extension survey imaged CO_2 injection in Phase 3 and the rest of Phase 2 and provided additional baseline coverage for Phases 4, 5, and 6.

The PCOR Partnership applies a philosophy of integrating site characterization, modeling and simulation, risk assessment, and MVA strategies into an iterative, adaptive management approach (Figure 8) (Ayash and others, 2016). Elements of any of these activities play a role in the understanding and development of the others. The expanded seismic campaign has played a meaningful role in each of the four elements by providing, among other benefits, 1) measurements and images of physical properties throughout the geologic section on a fine grid over the field that has aided geologic characterization, 2) a means of constraining the statistical modeling along geobody boundaries to improve model predictions, 3) a way of identifying potential migration pathways within the reservoir and seal that feeds directly into the risk assessment, and 4) a means of directly indicating the locations of CO_2 accumulation via the time-lapse surveys as part of the MVA plan.

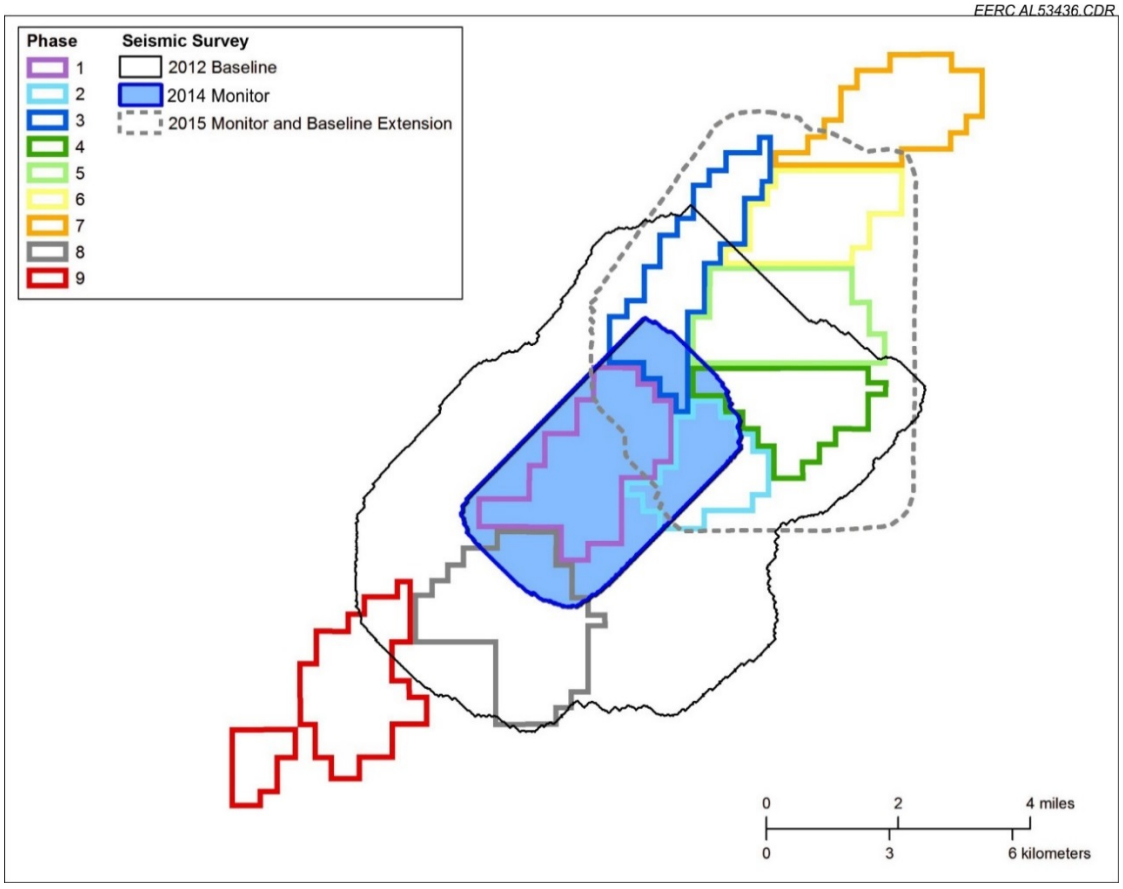

Figure 7. Bell Creek Field with outlines of the three 3-D surface seismic surveys overlaying the nine planned CO_2 EOR development phases in the Bell Creek Field. At the time of the surveys, CO_2 was imaged in Phases 1, 2, and 3 (modified from Jin and others, 2016).

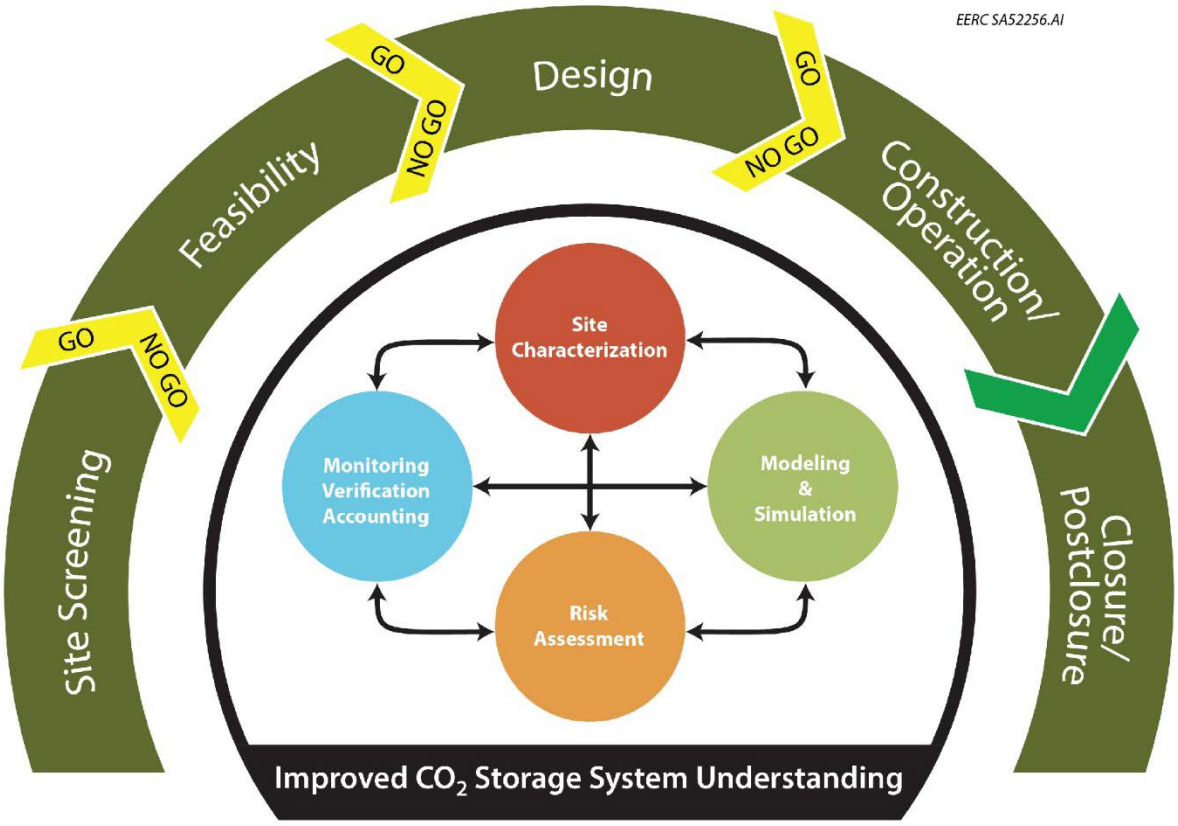

Figure 8. Adaptive management approach for understanding CO_2 storage systems (Ayash and others, 2016).

SEISMIC DATA ACQUISITION AND PROCESSING

3-D Surface Seismic Data Acquisition

Three 3-D seismic surveys have been acquired at the Bell Creek Field to characterize the reservoir and monitor the time-lapse changes within it due to CO_2 injection during EOR. The 2012 baseline survey was collected prior to CO_2 injection. The first monitor survey, the 2014 monitor survey, was collected in 2014 after CO_2 injection had been initiated in development Phases 1 and 2. The second monitor survey, the 2015 monitor and baseline extension, was collected in 2015 after CO_2 injection had been initialized in development Phases 1, 2, and 3.

2012 Baseline Survey

The 2012 baseline survey was acquired in August and September 2012. As the first 3-D seismic survey acquired over the field, its purpose was to enhance reservoir characterization and serve as a baseline data set for future time-lapse analyses. The survey covered an area of 40 square miles (Figure 7). Burnison and others (2014) provide details of the acquisition and processing parameters, with an analysis and initial interpretation of the data that were integrated with the field characterization effort.

2014 Monitor Survey

Approximately 17 months after CO_2 injection was initiated in the field, the 2014 monitor survey was acquired to image the time-lapse changes in the reservoir due to CO_2 injection. The 2014 monitor was an 11.6-square-mile survey acquired over 13 days from October 20, 2014, through November 1, 2014. Survey boundaries include all of Phase 1 and part of Phases 2, 3, 4, 5, and 8 (Figure 9). The survey was designed to overlap the 2012 baseline survey and produce an image of the reservoir in Phase 1 and a portion of Phase 2 that had undergone CO_2 injection since the original baseline survey had been collected.

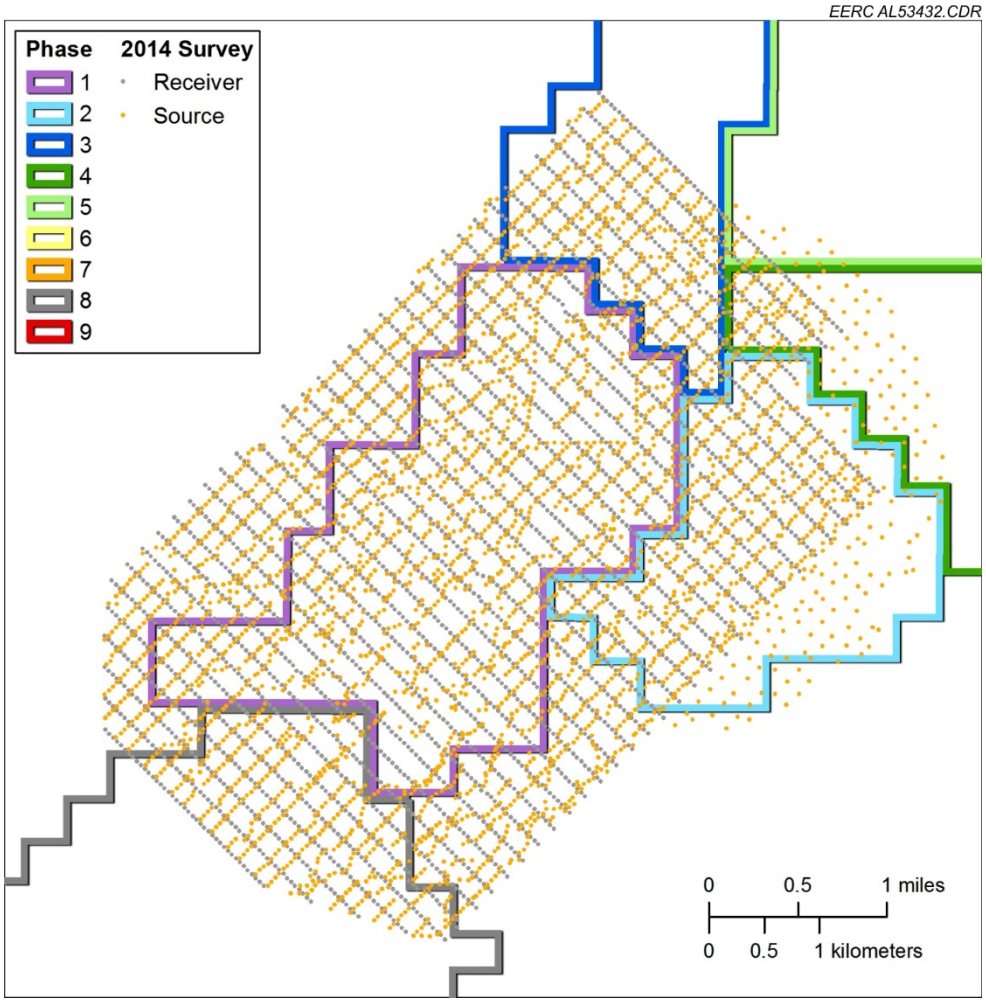

Figure 9. Source and receiver locations for the 2014 monitor survey acquired October 2014. Source locations outside the grid on the east and northeast were part of the concurrently acquired 3-D VSP using the permanent array in 04-03 OW.

The parameters and field layout for the monitor survey were intentionally similar to the 2012 baseline survey with two major differences. The 2012 baseline used a six-geophone array at each receiver location, whereas the 2014 monitor employed a single three-component receiver at each receiver point. Receiver line spacing was also tighter to increase the recorded fold, with an active spread of 26 lines of 126 stations (16 lines for the baseline). Field acquisition parameters for the 2014 monitor survey are listed in Table 1.

Table 1. Acquisition Parameters for the 2014 Monitor Survey and the 2015 Monitor and Baseline Extension Survey

	2014 Monitor	**2015 Monitor and Baseline Extension**
Geophysical Contractor	Dawson	Geokinetics
Energy Source	Two 64,000-lb AHV-IV Vibroseis (Figure 10)	Two 64,000-lb AHV-IV Vibroseis
Source Interval	165 feet	165 feet
Total Source Points	3388	7512
Sensor	GS 1-3C 10-Hz geophone (Figure 11)	DTCC DT- Solo 3C 10-Hz geophone
Group Interval	165 feet	165 feet
Geophone Pattern	One geophone	One geophone
Active Spread	26 lines, 126 stations each	26 lines, 126 stations each
Active Stations	3276	3276
Total Source Stations	3388	7512
Total Receiver Stations	3031	6622
Sweep Parameters	Proprietary	Proprietary
Record Length	4 seconds	4 seconds
Sample Interval	2 millisecond	2 millisecond

Figure 10. Two Vibroseis trucks moving between shot points during the 2014 monitor survey.

Figure 11. 2014 monitor survey receiver station with a single GS-1, 3-component 10-Hz geophone (center), Geospace GSX seismic recorder (bottom), and battery.

The 2014 monitor survey data was processed by Sensor Geophysical Ltd. For time-lapse 4-D analysis, the best practice standard is for both baseline and monitor data to be processed in the same way, so Sensor Geophysical also reprocessed the 2012 baseline survey using the same workflow and velocities to facilitate the time-lapse differencing. The processing workflow is summarized below, with details provided in Appendix C:

- Geometry assignment and trace edits
- Spherical divergence correction with a +4-dB/sec gain
- Surface-consistent scaling
- Singular value decomposition for groundroll removal
- Surface-consistent deconvolution and Vibroseis deconvolution compensation
- Refraction statics and surface-consistent statics
- Velocity analysis, surface-consistent statics, and time alignment statics
- Applying normal moveout correction (NMO)
  - Surface consistent scaling
  - Time and frequency (T-F) adaptive noise suppression
  - Fold-matching the baseline and monitor surveys
  - F-XY filtering
  - Anisotropic diffusion filter
- Removing NMO
- Kirchhoff prestack time migration (PSTM)
- Shift data to final datum

2015 Monitor and Baseline Extension Survey

The 2015 monitor and baseline extension survey was acquired over a 17-day period from August 20, 2015, through September 6, 2015, and has an area of 26 square miles. The survey added area on the north end of the field that had not been covered by the 2012 baseline (Figure 7). Parts of Phases 1, 2, and 3 were repeated for time-lapse analysis (Figure 12).

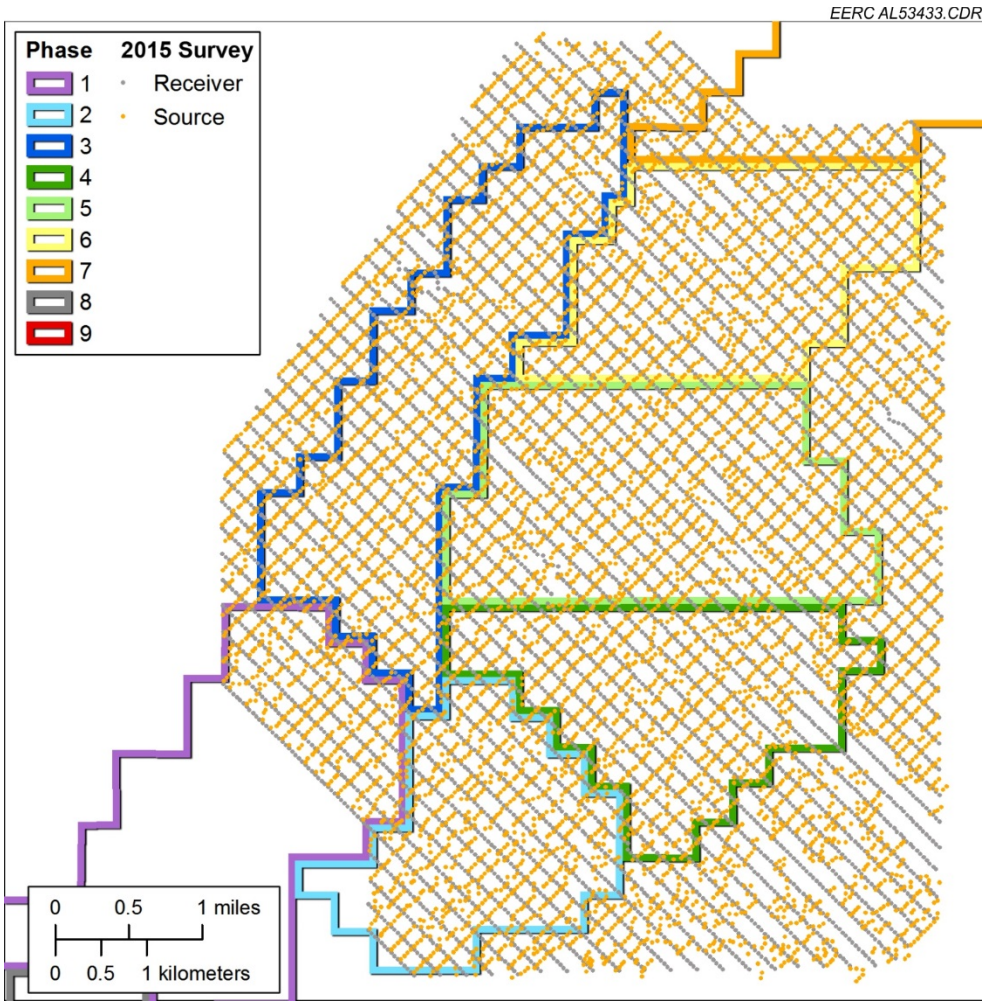

Figure 12. Source and receiver location map for the 26-square-mile 2015 monitor and baseline extension survey acquired September 2015.

Parameters matched the previous survey, with the only difference being the use of Sercel nodal recording instrumentation and a different three-component geophone (Table 1 and Figure 13). Of this data set, 13.2 square miles overlap parts of the 2012 baseline, and 3.8 square miles overlap the 2014 monitor.

Figure 13. 2015 monitor and baseline extension survey receiver stations employed the DTCC (Dynamic Technology Canada Corporation) DT-Solo 3-component 10-Hz geophone, a Sercel UNITE data logger, and battery.

Arcis Seismic Solutions processed the 2015 monitor and baseline extension survey data and reprocessed the 2012 baseline survey data and the 2014 monitor survey data. The processing sequence is summarized below, with details given in Appendix C:

- Minimum phase conversion
- Geometry assignment, trace edits, and 60-Hz noise removal
- Spherical divergence correction
- Surface consistent scaling, groundroll removal, and deconvolution
- Refraction statics, surface consistent statics
- Applying NMO
  - Noise suppression across domains (shot, offset, CMP [common midpoint])
  - Surface consistent deconvolution
  - Noise suppression (offset and CMP)
  - Phase and statics compensation
  - Radon multiple attenuation
  - F-XY noise attenuation
  - 5-D interpolation
- Removing NMO
- Anisotropic velocity analysis

- Anisotropic Kirchhoff PSTM
- Front-end mute
- Stack, filter and AGC (automatic gain control) scaling

4-D SEISMIC DATA INTERPRETATION

Phase Development and Time-Lapse Monitoring

Time-lapse 4-D seismic data analyses and interpretation are possible where the monitor surveys overlap the pre-CO_2 injection 2012 baseline data and where CO_2 injection has occurred. The 2014 monitor survey overlaps Phase 1 and part of Phase 2 where injection had been progressing. The 2015 monitor and baseline extension included parts of Phases 1, 2, and 3, which had been undergoing CO_2 injection at the time (Figure 14). Analysis of incremental injection is possible in areas undergoing injection between monitor surveys.

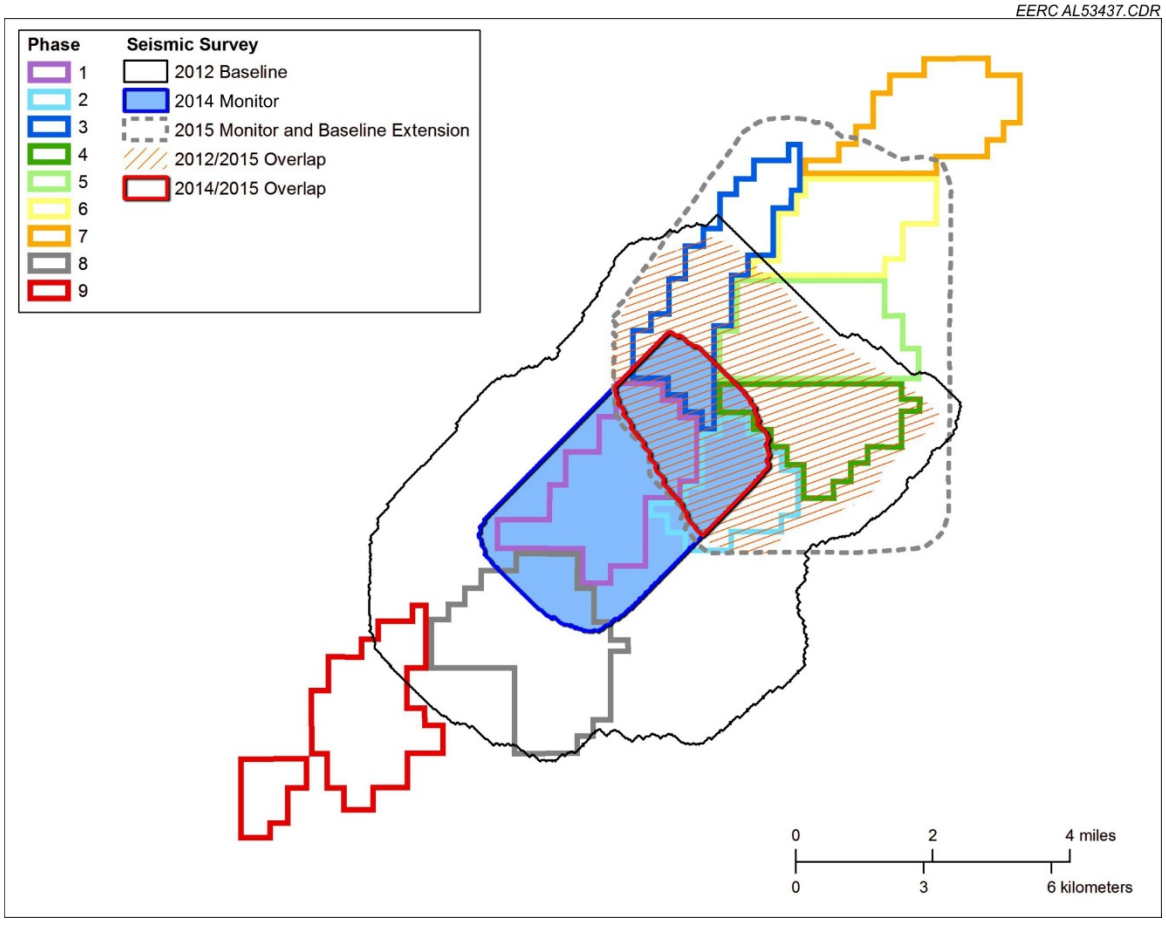

Figure 14. Overlapping areas between the 3-D seismic surveys that were used for time-lapse analysis. The 2014 monitor (blue shading) overlaps the 2012 baseline. The 2015 monitor and baseline extension (black dashed line) overlaps 13.2 square miles of the 2012 baseline. The two monitors also overlap for 3.8 square miles (red outline).

Development Phases 1 and 2 were pressurized sequentially, with CO_2 injection beginning in Phase 1 in May 2013 and in Phase 2 in December 2013. When the 2014 monitor survey was acquired, there had been 17 months of CO_2 injection in Phase 1 and 11 months of CO_2 injection in Phase 2. A total of 1.21 million tonnes of CO_2 had been incidentally stored at that time. The 2015 monitor and baseline extension survey covered parts of Phases 1, 2, 3, 4, and 5 where a total of 1.46 million tonnes of CO_2 had been incidentally stored. Table 2 summarizes CO_2 injection start dates and the calculated amount of CO_2 stored in the different phases of the reservoir at the time of each monitor survey acquisition date (Montana Board of Oil and Gas, 2017).

Table 2. CO_2 Stored in the Muddy Formation within the Extent of the Seismic Surveys (Montana Board of Oil and Gas Conservation, 2017) at the Time of Monitor Seismic Data Acquisition

Seismic Data Acquired	Phase	Start of CO_2 Injection	Calculated Stored CO_2, Mt	Total CO_2 Stored
Oct 2014	1	May 2013	1.04	1.21
	2	Dec 2013	0.17	
Sep 2015	1	May 2013	0.42	1.46
	2	Dec 2013	0.52	
	3	Nov 2014	0.48	
	4	Sep 2014	0.01	
	5	Jan 2015	0.03	

Dynamic Simulation Modeling of Phases 1 and 2

Dynamic simulation modeling prior to CO_2 injection into Phase 1 took into account the north–south trending permeability barrier between Phases 1 and 2 interpreted by Burnison and others, 2014 (Salako and others, 2017). However, several wells along the permeability barrier were unable to be adequately history-matched to production data. These wells were identified as diagnostic wells, indicating that the static and/or dynamic models did not adequately represent the true subsurface geologic conditions. Bottomhole pressure data combined with trial and error dynamic modeling using pseudo production wells provided an indication that fluid and pressure communication across the permeability barrier was occurring in proximity to the diagnostic wells.

Two wells near the fluid and pressure communication pathway were used as water injectors to maintain a fluid and pressure curtain to contain the CO_2 within Phase 1 until Phase 2 was pressurized. Subsequent volumetric analyses, water cut measurements, and the rate of pressure buildup in Phase 2 provided further evidence of fluid and pressure communication across the permeability barrier. Figure 15 shows the zone of suspected fluid and pressure communication across the boundary between Phases 1 and 2. The 4-D seismic interpretation, as described in a later section, helped to define the location and geometry of the permeability barrier and illuminate the communication pathway, which was not discernible on the baseline 3-D data.

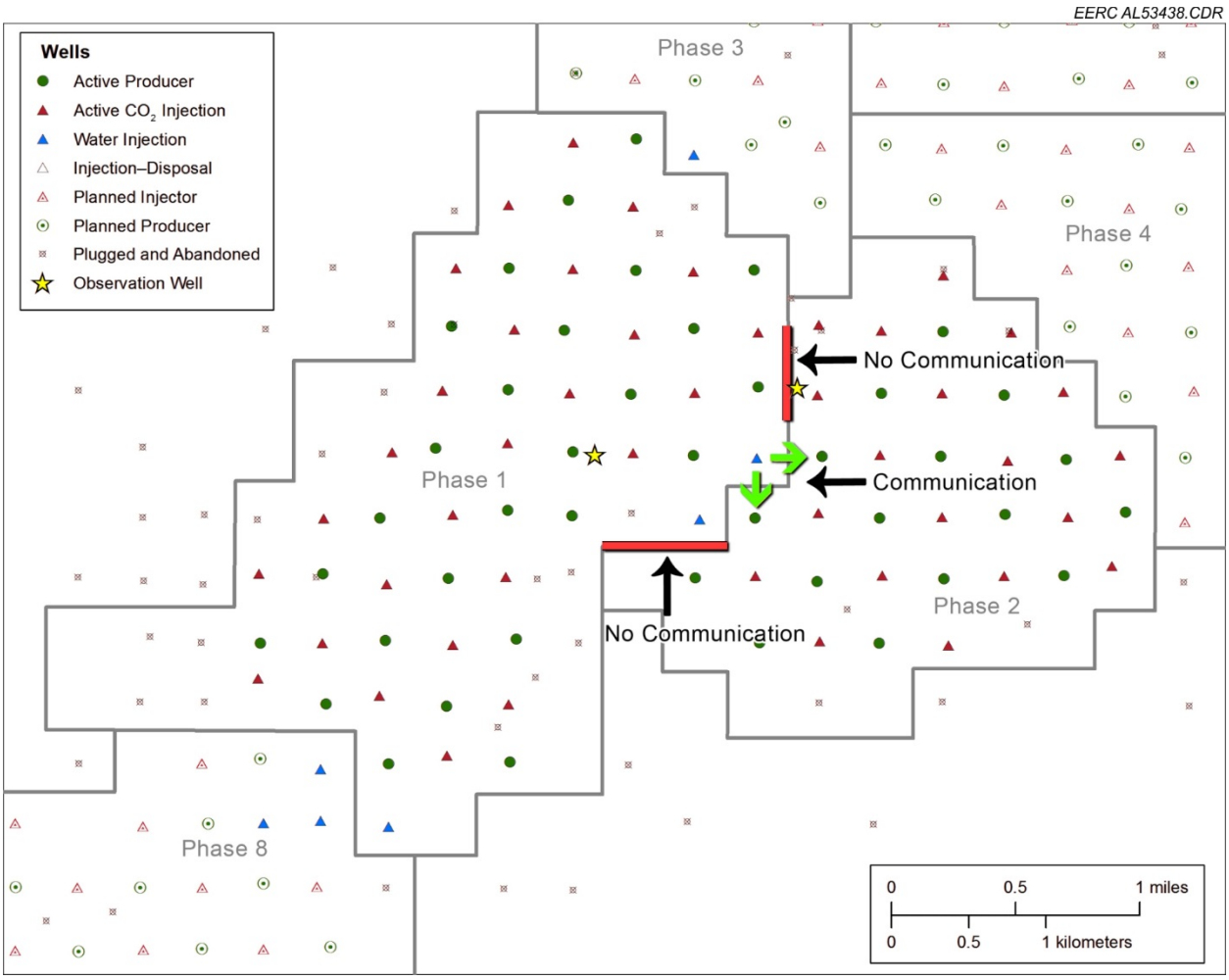

Figure 15. Injector–producer pairs showing zone of anomalous communication in the simulation model (modified from Burnison and others, 2016).

4-D Data Conditioning

Time-lapse analysis involves interpretation of difference displays created by subtracting the monitor data volume from the pre-CO_2 injection baseline data volume. These volumes are created in two steps. In the first step, both volumes are processed using similar workflows to honor the original amplitudes of the seismic data and to minimize the potential differences between the two data sets caused by differences in acquisition parameters, near-surface conditions, and noise. In the second step, the processed volumes are calibrated to enhance the differences only in the injection zone. Conditioning is accomplished with a calibration workflow designed to minimize the differences where they are not expected to occur, such as above or below an injection zone.

After Sensor Geophysical processed the 2012 baseline and 2014 monitor data, initial time-lapse analysis was performed. For these data, the calibration process involved cross-equalization operations that included phase and time-shift estimations between the baseline and monitor, application of the estimated phase and time-shifts, shaping filtering, and shallow static correction.

Shaping filters were computed and applied trace by trace, but other operations were applied to the data set globally. Two repeatability measurements, time-shift maps, and normalized root mean square (NRMS) maps of the baseline and the monitor data sets, before and after cross-equalization, were generated over windows above and below the reservoir. Above the reservoir, a window of 500 ms was used starting 200 ms above the Niobrara horizon. Below the reservoir, a window of 200 ms was examined between 1400 and 1600 ms. These windows included both high and low reflectivity events to avoid NRMS bias toward low or high values. The maps show improvement in the data after the cross-equalization processes. Time-shifts have been significantly reduced to values close to or less than a millisecond (Figure 16), and the value of NRMS amplitude differences have been reduced to a range of 0% to 40%, with a modal value of 25% (Figure 17). Typical values of NRMS reported in the literature indicative of good repeatability are between 10% and 30% (Johnston, 2013).

After data acquisition, the 2015 monitor and baseline extension data were processed by a different contractor, Arcis, who also reprocessed for 4-D analysis the original 2012 baseline and 2014 monitor surveys. Time-lapse processing and cross-equalization workflows were applied by Arcis, including the computation of difference volumes from the several overlapping permutations of the three data sets. The quality of the cross-equalization done by Arcis is demonstrated in Figure 18 by a difference display of the reprocessed 2012 baseline and the reprocessed 2014 monitor. Major amplitude differences between the two data sets are observed at the reservoir, where changes due to CO_2 injection and accumulation are expected. Only minor amplitude differences above the Springen Ranch and below the Skull Creek are observed. This is an indication of good-quality 4-D seismic data that have been processed and cross-equalized.

For some analyses, a phase rotation was applied to the data. Burnison and others (2014) recognized that the reservoir reflection manifests as a thin-bed seismic response, characterized by an entering reflection followed immediately by an exiting reflection of opposite polarity. This results in the situation where the reservoir sand is located at the middle zero-crossing of the reflection. Applying a 90-degree phase shift to the data rotates the reflection so that a positive peak is centered on the reservoir sand, with its amplitude related to the reservoir character or content. The bounding horizons of Springen Ranch and Skull Creek then fall on either side of the reflection peak. Understanding the impact of CO_2 on the reservoir reflection becomes much more intuitive.

CO_2 in the reservoir at a sufficient saturation level significantly reduces the amplitude of the reflection, resulting in an anomaly on the difference section (Figure 19). To illustrate this effect quantitatively, it can be observed at a chosen point within the reservoir (Figure 19, the green dot) that the baseline seismic data (left panel) has a positive 0.667 amplitude value, while the cross-equalized monitor data (middle panel) has a positive 0.335 amplitude value. The difference panel on the right (monitor minus baseline) amplitude value is negative 0.332. The injection of CO_2 has a softening effect by reducing the seismic amplitude. This is an important observation for subsequent interpretation of the time-lapse data sets.

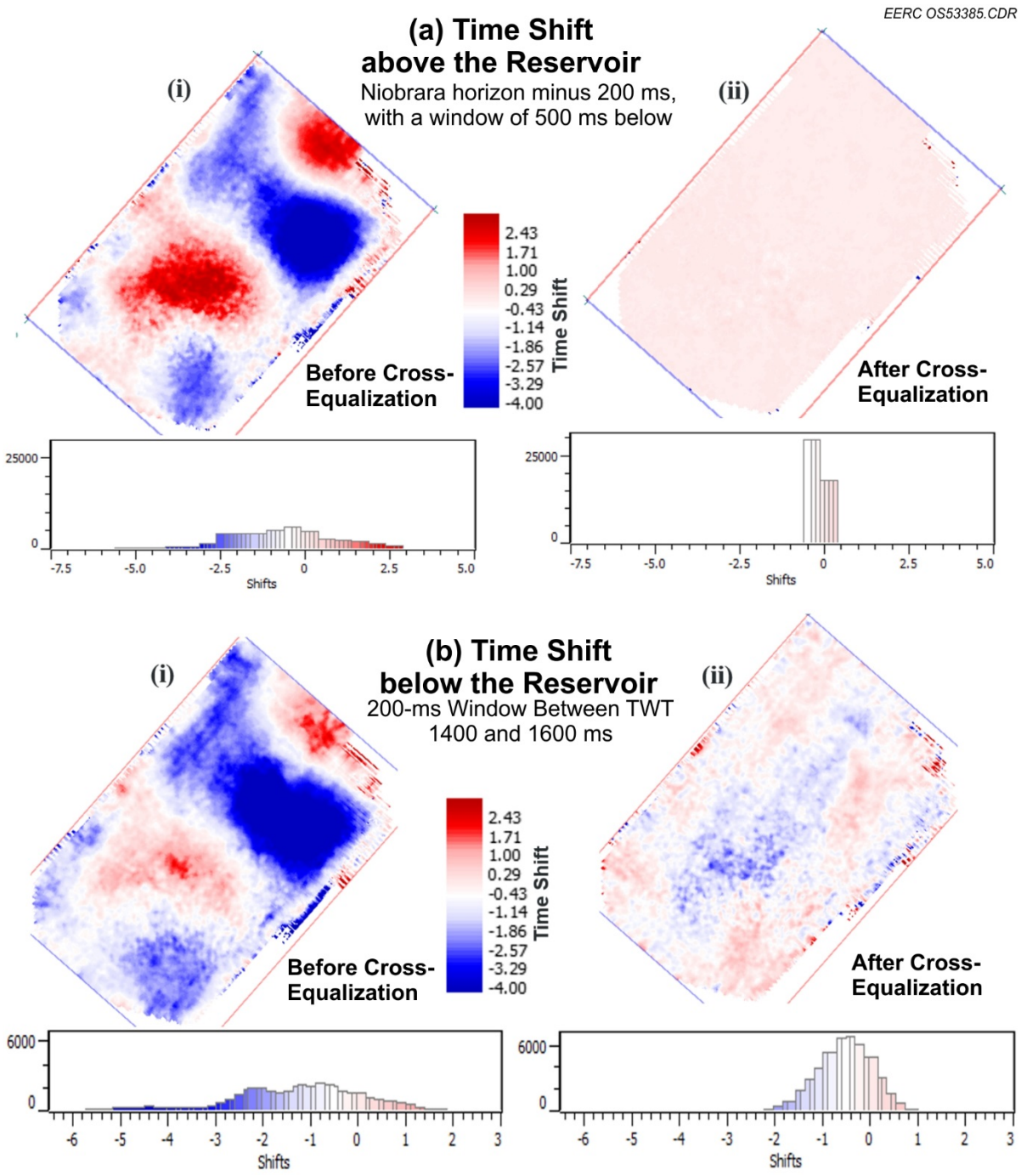

Figure 16. Time shift estimation between the 2012 baseline and the 2014 monitor: a) 500-ms window above the reservoir before (i) and after (ii) cross-equalization; b) 200-ms window below the reservoir. After cross-equalization, time shifts cluster near zero.

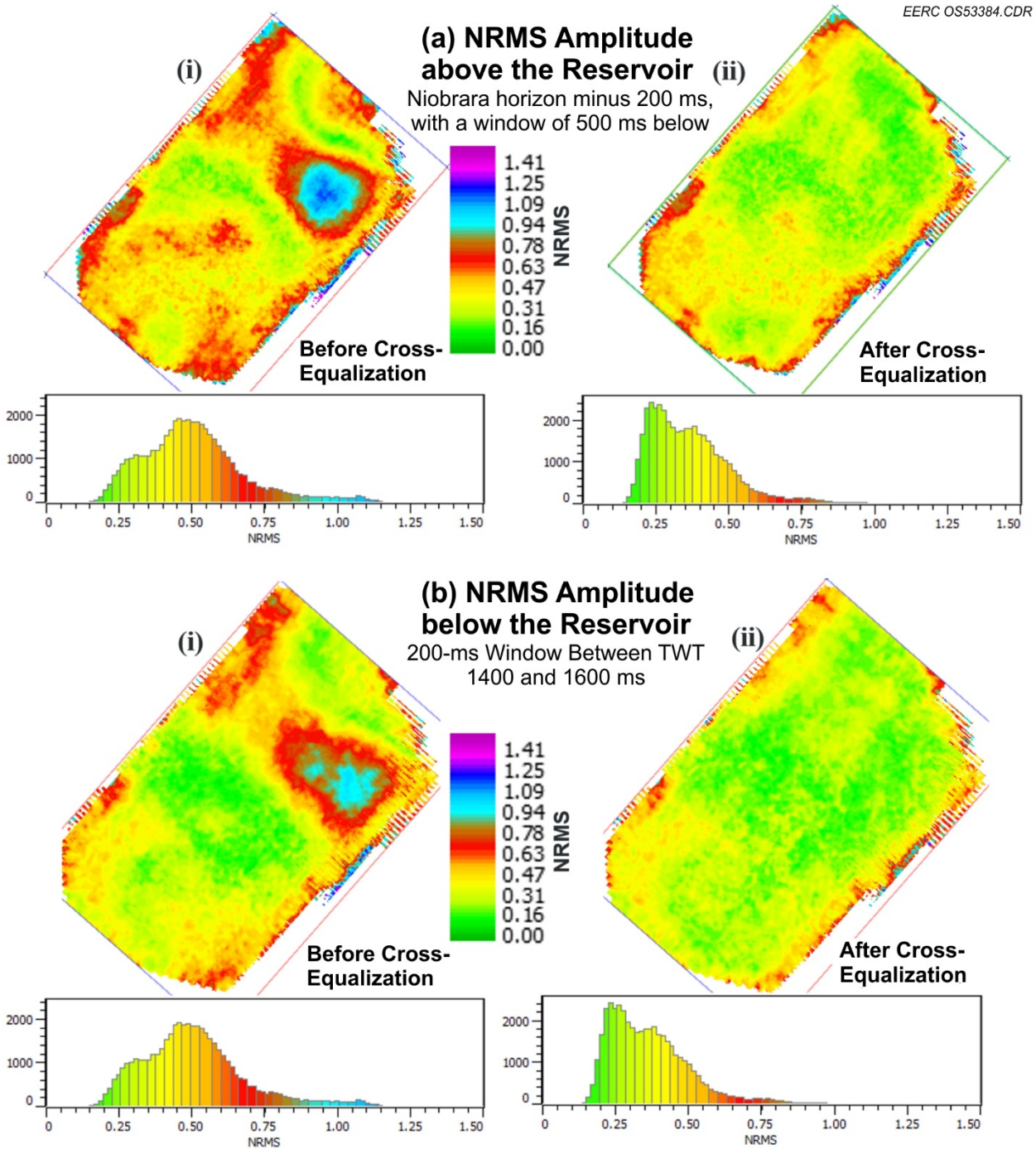

Figure 17. NRMS amplitude computation, 2012 baseline and the 2014 monitor data: a) over a 500-ms window above the reservoir before (i) and after (ii) cross-equalization and b) over a 200-ms window below the reservoir.

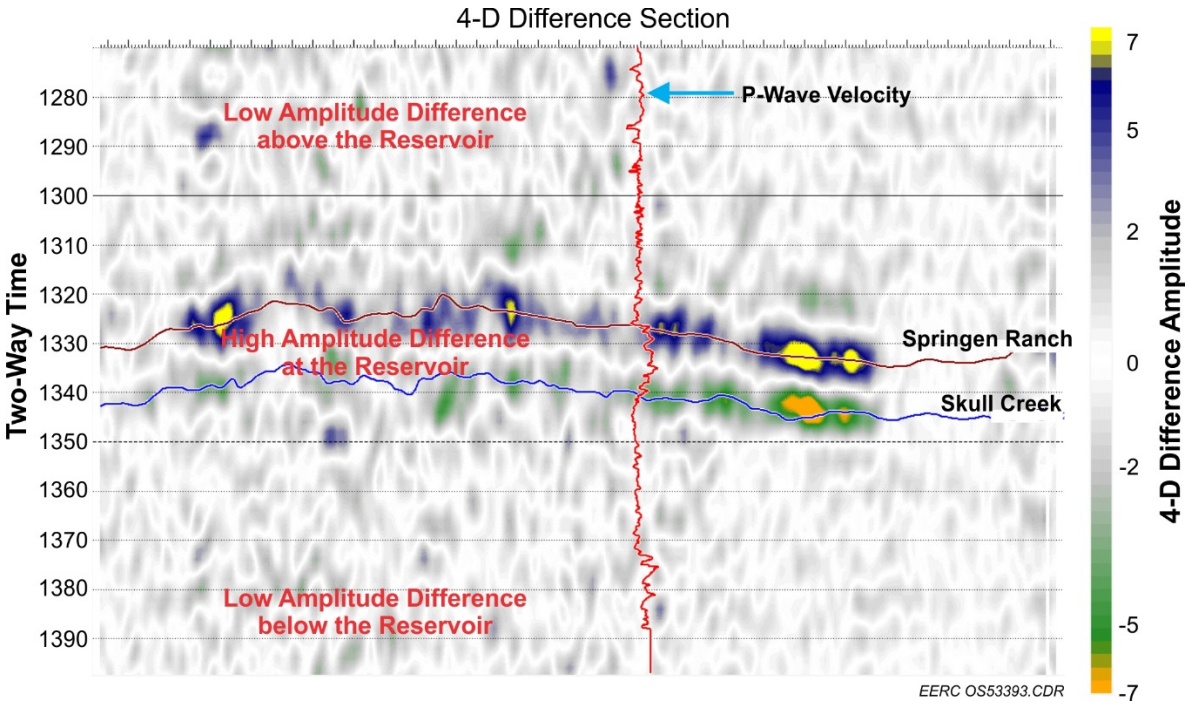

Figure 18. Difference display between the reprocessed 2014 monitor and the 2012 baseline. Highest amplitude differences are in the reservoir as expected (Burnison and others, 2016).

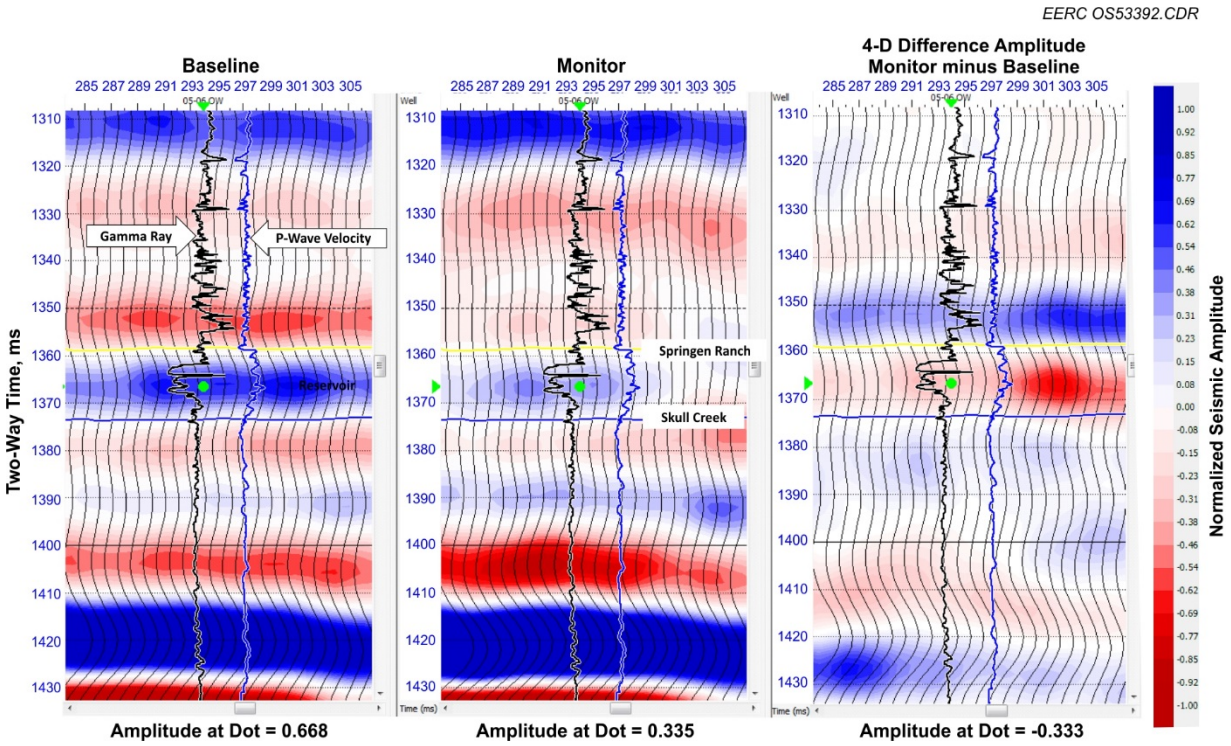

Figure 19. Left panel: 2012 baseline, middle: cross-equalized 2014 monitor data, right: difference display (monitor minus baseline). GR and P-wave velocity logs from 05-06 OW are overlaid. The amplitude color is normalized on a scale of −1 to +1.

4-D Interpretation

4-D interpretation focused on the Arcis processed data sets. Several seismic mapping methods using different amplitude transforms and averaging techniques were examined to generate maps of 2-D slices of the reservoir enclosed within the two-way-travel-time window between horizons Springen Ranch and Skull Creek. Calculating the RMS amplitudes using the raw amplitudes produced the best images. Mapping was done for the 2012 baseline, the 2014 monitor, and 2015 monitor and baseline extension data sets. The baseline maps were subtracted from the respective monitor maps to generate the 4-D amplitude difference maps for the 2014–2012 and 2015–2012 time-lapse periods. These 4-D amplitude difference maps were qualitatively interpreted to assess the changes in the reservoir due to CO_2 saturation changes and pressure changes. The amplitude distributions of these maps illuminate changes in the reservoir and reveal the reservoir architecture and heterogeneities. Interpretations of the time-lapse amplitude maps revealed: a) permeability barriers and baffles (permeability barriers that are less impervious to flow); b) fluid and pressure communication pathways; c) CO_2 migration, banking, and accumulation; and d) pressure buildup, and qualitative discrimination between saturation changes and pressure changes.

2012–2014 4-D Interpretation

The seismic amplitude maps for the 2014 monitor and the resulting 4-D amplitude difference map between the pre- and post-CO_2 injection data sets are shown in Figure 20, Figure 21, and Figure 22, respectively. These maps are jointly interpreted by examining the various features identified on the maps and by correlating these features with the well logs, seismic sections, and the well activities. The negative seismic amplitude changes on the difference map, red to yellow color, observed are diagnostic of the softening effects due to the reduction in the acoustic impedance (i.e., reduction in velocity and density), resulting from the combination of the effect of CO_2 replacing oil and water in the pore spaces and the effect of pressure-up at the injector wells relative to the producer wells (Figure 22). The details of the interpretation are described below.

Permeability Barriers

- In the interpretation of the 3-D baseline survey and well logs, Burnison and others (2014) demonstrated that a high amplitude, meandering fluvial channel feature was shale-filled and acted as a permeability barrier. This feature is visible on the 4-D displays and consists of amplitude values near zero on the difference display. On the 2014 monitor, its character and dimensions along the boundary between Phase 3 (to the west) and Phases 5, 4, and 2 (to the east) are visible on the amplitude map from the monitor data. The feature is clear on the 4-D amplitude difference map between Phases 1 and 2, where CO_2 injection had progressed (Figure 22). Its southern extent had not been discernible on the 2012 baseline data but is visible on the difference display. Knowing the geometry of the permeability barriers proved useful for updating the static and dynamic simulation models.

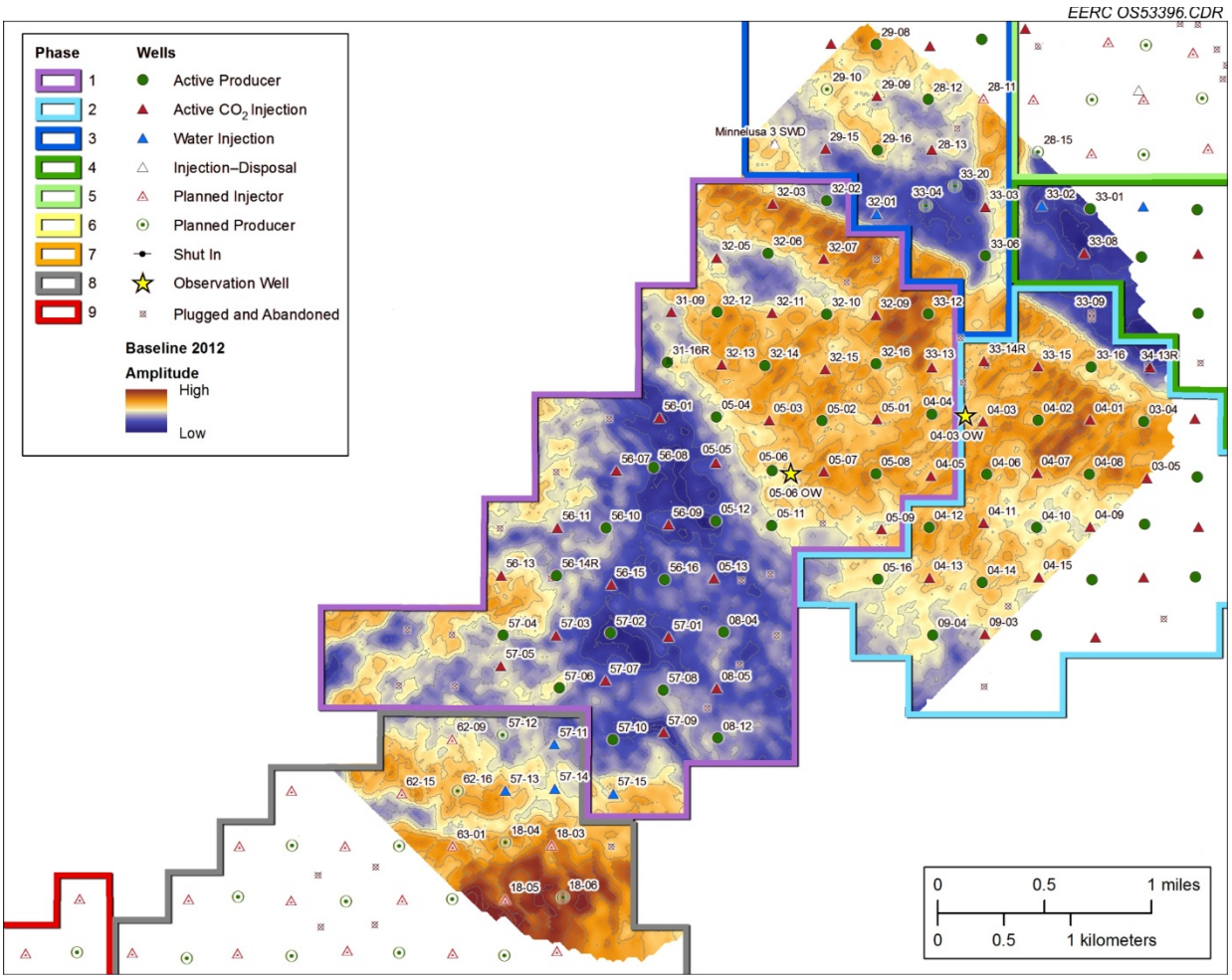

Figure 20. The RMS average amplitude map of the Bell Creek reservoir for the pre-CO_2 injection 2012 baseline (where it overlaps the 2014 monitor) generated between the Springen Ranch and Skull Creek horizons.

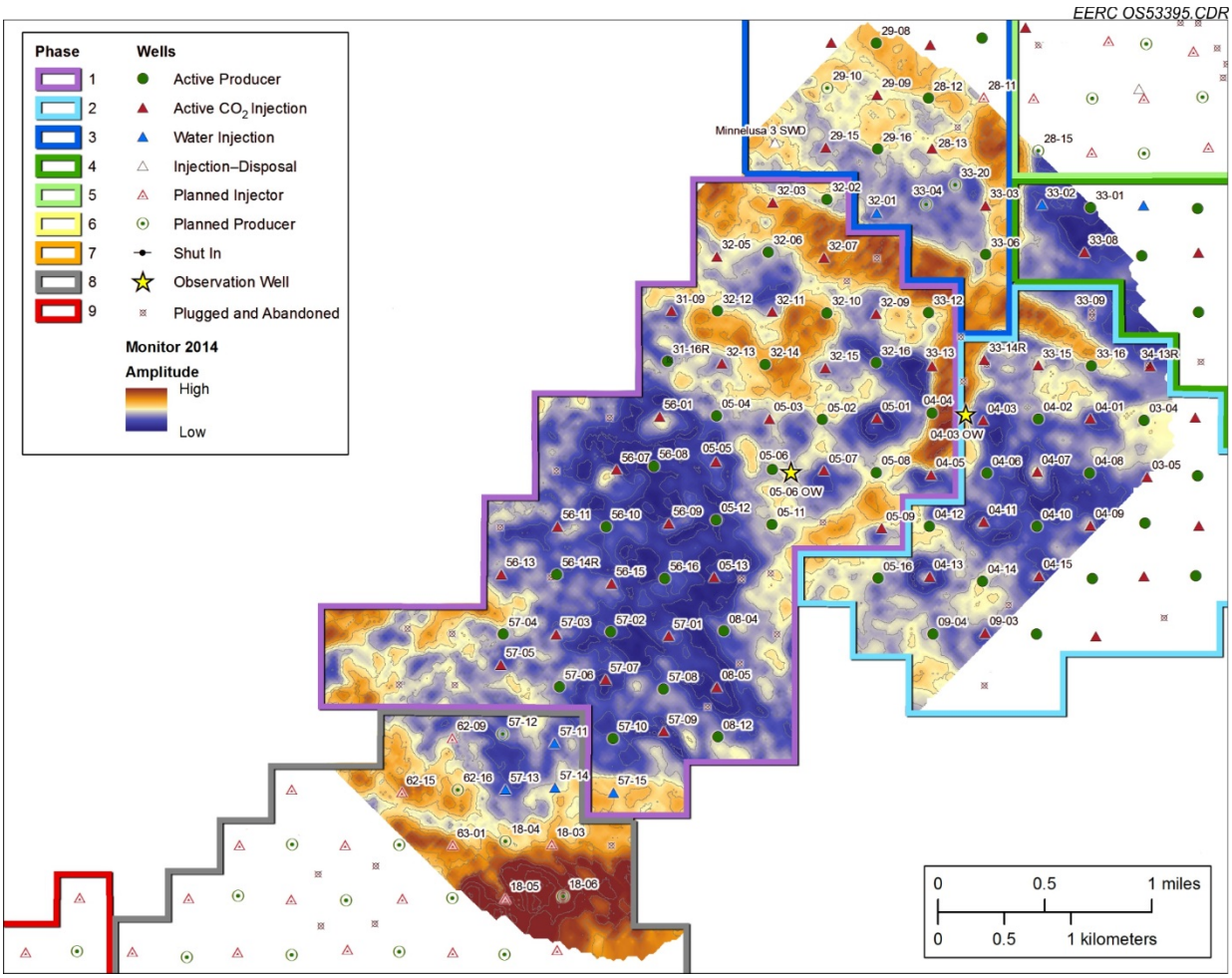

Figure 21. The RMS average amplitude map of the Bell Creek reservoir, for the 2014 monitor, generated between the Springen Ranch and Skull Creek horizons.

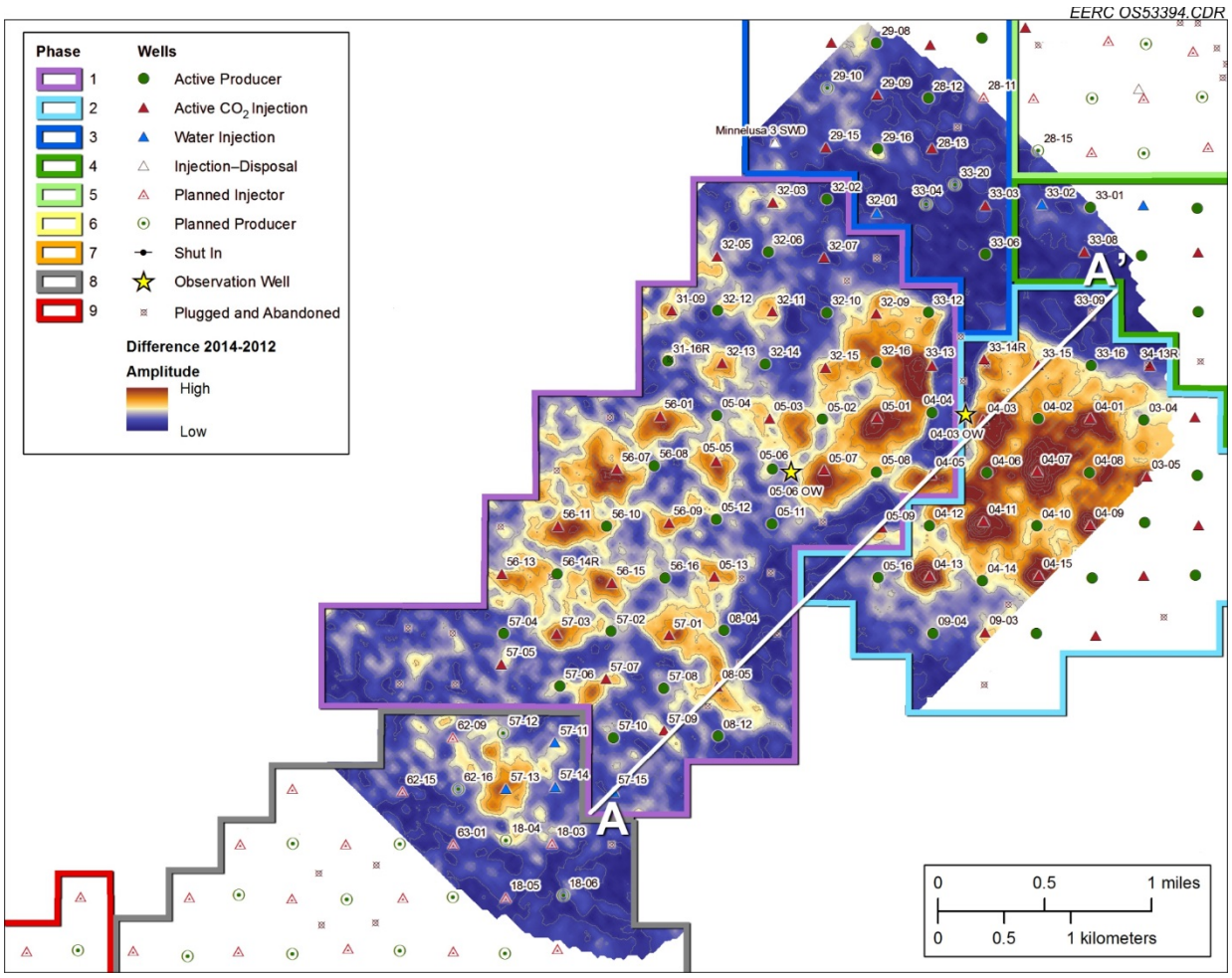

Figure 22. Annotated 4-D amplitude difference map of the Bell Creek reservoir, created by subtracting the 2012 baseline from the 2014 monitor.

- A second permeability barrier that predates the fluvial feature and trends northwest to southeast was also identified during the baseline interpretation. It is seen on the amplitude map of the monitor data, and its character as a barrier to CO_2 is visible on the 4-D display. This barrier prevents fluid communication between Phases 1 and 3 and between Phases 2 and 4.

- A high-amplitude valleylike baffle is also observed within Phase 1, close to Wells 32-10, 32-12, 32-13, 32-14, and 32-15.

- Examination of the 4-D difference map shows that CO_2 movement is restricted at the boundary of the permeability barrier and around the baffle identified in Phase 1. That there is no change in RMS amplitude observed within the permeability barriers and in the area around the baffle is indicative of a lack of CO_2 and confirmation that the barriers and baffle are impermeable to CO_2 flow. The CO_2 acts like a tracer to illuminate these features. Well 32-07, located inside the baffle, and Wells 33-09 and 33-13A, inside the permeability barriers, were found to contain impermeable or tight lithology and were abandoned as dry holes.

A Bridge for Fluid and Pressure Communication

- A permeable pathway traversing the permeability barrier and creating a bridge allowing fluid and pressure communication between Phases 1 and 2 is visible on the 4-D difference map and cross section (Figure 23). This feature was not visible on the baseline seismic data and was not incorporated into the geologic model resulting in history-matching difficulties of the injector–producer pairs nearby. The location of the pathway correlates with interpretations of bottomhole pressure data, from which the existence of a communication channel had been inferred (Bosshart and others, 2015).

- As part of field operations, Wells 04-05 and 05-09 were used to provide a pressure curtain by injecting water to keep CO_2 within the Phase 1 area while Phase 2 was being pressurized. Although these wells fall within the Phase 1 geographic boundary, the 4-D difference display revealed that they were geologically within Phase 2, thereby contributing to an unexpectedly rapid pressurization of Phase 2.

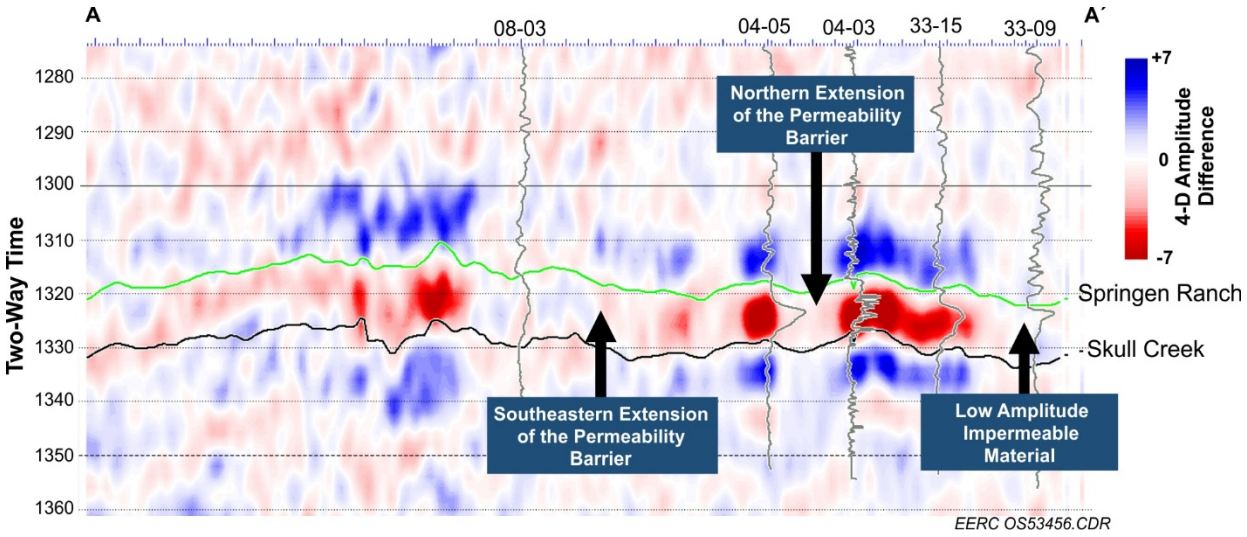

Figure 23. Cross-section line intersecting Wells 08-03 and 33-09 on the 4-D seismic amplitude map. P-wave velocity logs are displayed at well locations.

CO_2 Migration, Banking, and Accumulation

- The 4-D seismic difference map indicates migration of injected CO_2.

- CO_2 exists as a supercritical fluid at reservoir conditions (see Table B-1 and Figure B-3 in Appendix B) and appears to be migrating updip in the south–east direction because of buoyancy.

- The CO_2 appears to be banking and accumulating updip against the permeability barrier, which prevents further CO_2 migration.

- Apart from the areas interpreted as permeability barriers and baffles, with zero 4-D amplitude difference, the connectivity of the CO_2 plumes provides a qualitative indication of efficient sweep. Other areas with zero 4-D amplitude difference are places where CO_2 migration is yet to reach.

Discrimination of Pressure and Saturation Effects

- Phase 2 has a higher or equal amplitude signal compared to Phase 1, despite 0.87 Mt more CO_2 having been injected into Phase 1 (Table 2). This could potentially be due to increased pressure caused by two temporary water curtain injection wells (04-05 and 05-09) actively injecting during the time period between the acquisition of the baseline and monitor surveys. These wells located to the east of the permeability barrier were initially thought to be in Phase 1 but are geologically in Phase 2 (Burnison and others, 2016).

- An example of the effect of pressure buildup only is observed in neighboring Phase 8, at the southern border of Phase 1, where water was injected to create a water and pressure curtain to the south (Figure 23).

2015–2012 4-D Interpretation

- The interpretation of 4-D seismic amplitude difference for the 2015 monitor and extended baseline resulted in similar discoveries. Again, CO_2 acted as a tracer fluid and helped to illuminate features in more detail. The amplitude maps for the 2012 baseline and 2015 monitor and their 4-D amplitude difference map follow (Figures 24, 25, and 26).

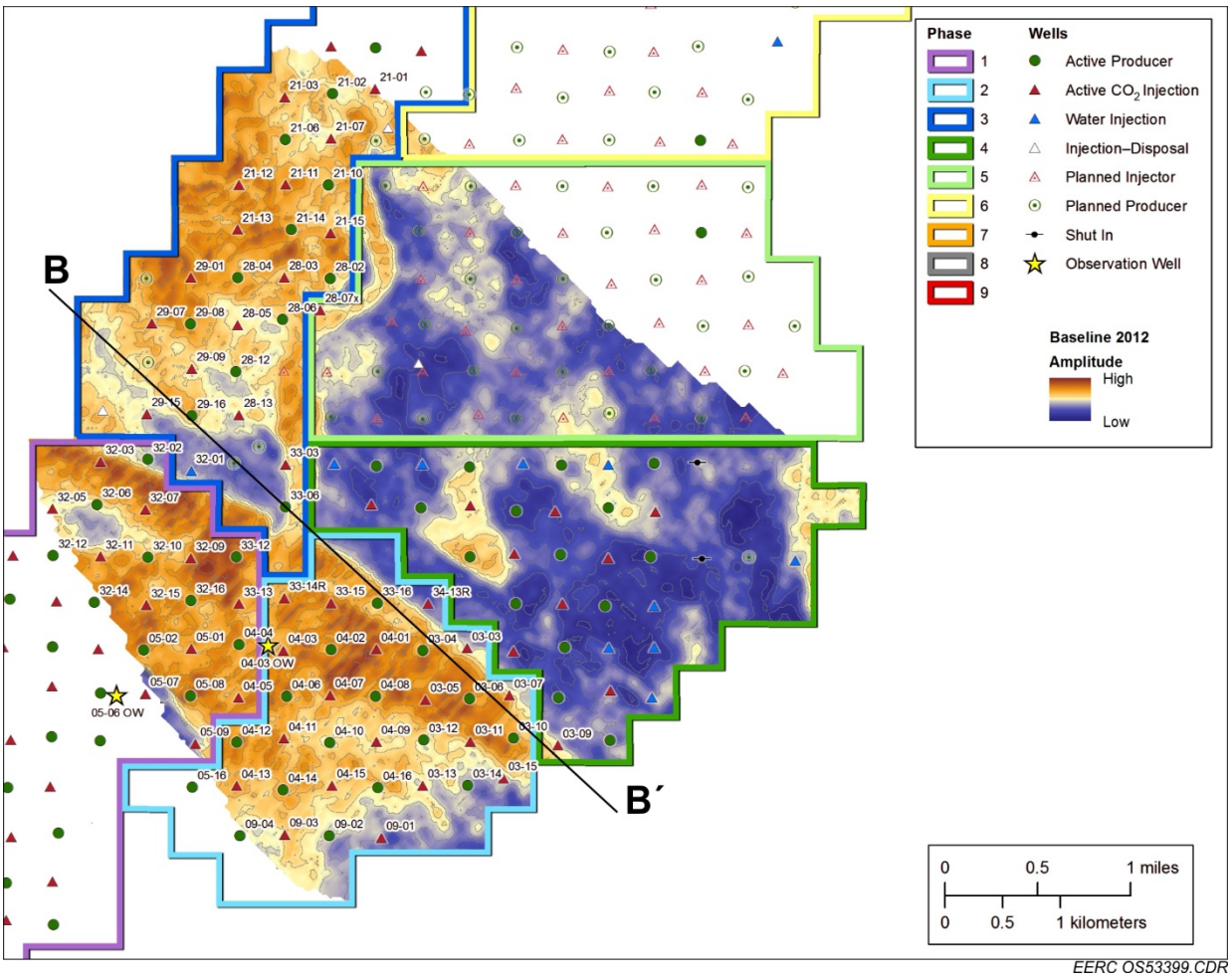

Figure 24. 2012 baseline RMS average amplitude map of the reservoir. A cross-section line is indicated.

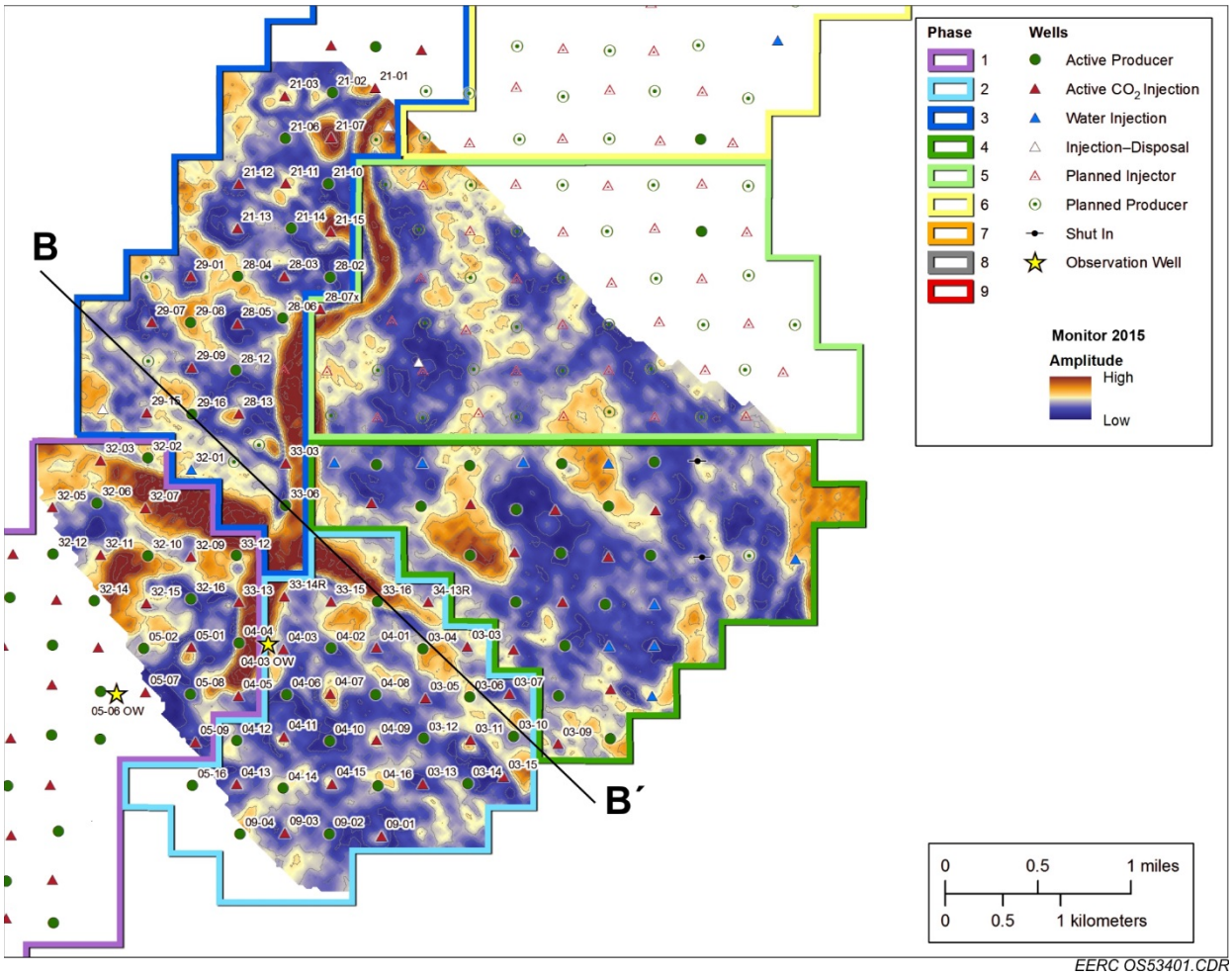

Figure 25. 2015 monitor amplitude map of the reservoir.

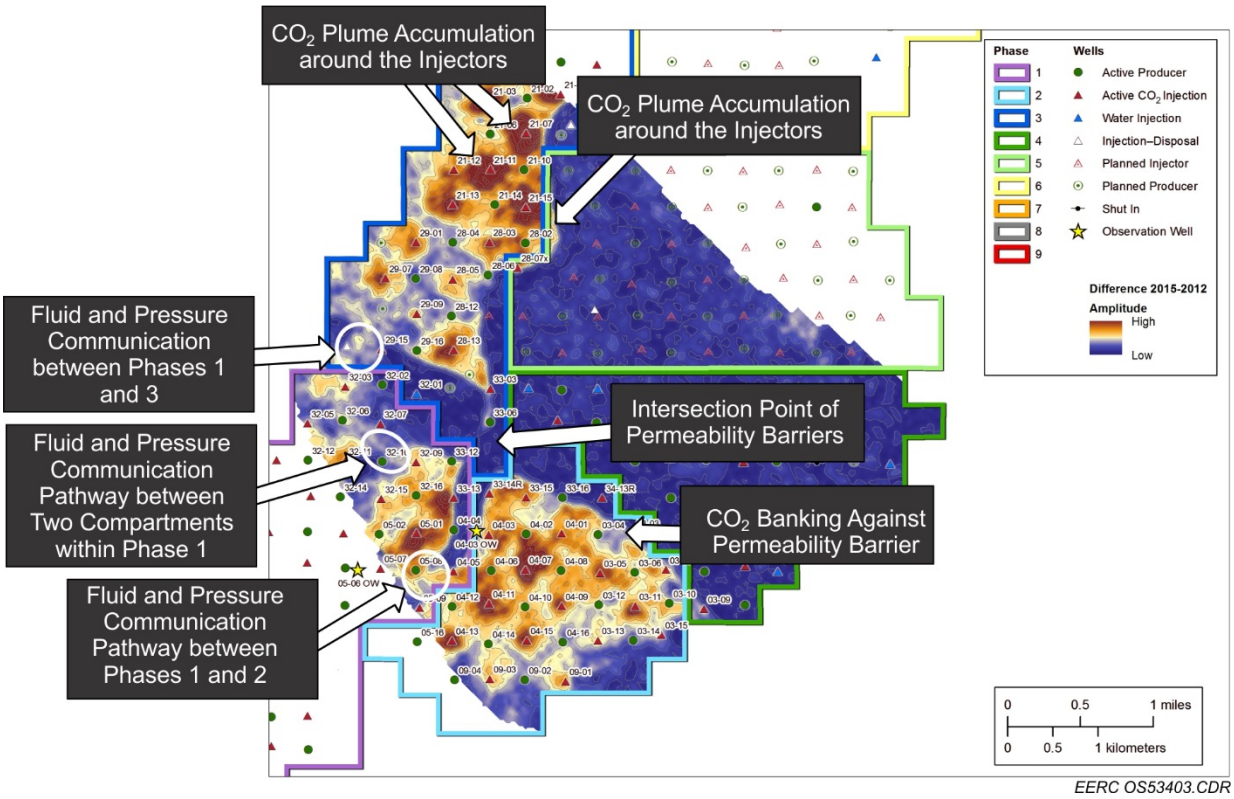

Figure 26. Annotated 4-D difference map from the 2015 monitor.

Permeability Barriers

- There is an improved definition of permeability barriers. The meandering nature of the shale-filled fluvial channel is better revealed in the 2015 monitor time-lapse maps than in the 2014 monitor time-lapse maps because of the larger volume of CO_2 injected. Both the high-amplitude permeability barrier and a lower-amplitude impermeable lithology are shown along the inline cross section (Figure 27).

A Pathway for Fluid and Pressure Communication Between Phases 1 and 3

- Similar to the fluid and pressure communication pathway between Phases 1 and 2 seen on the 2014 monitor amplitude maps, a pathway can be seen between Phases 1 and 3 and between two compartments within Phase 1.

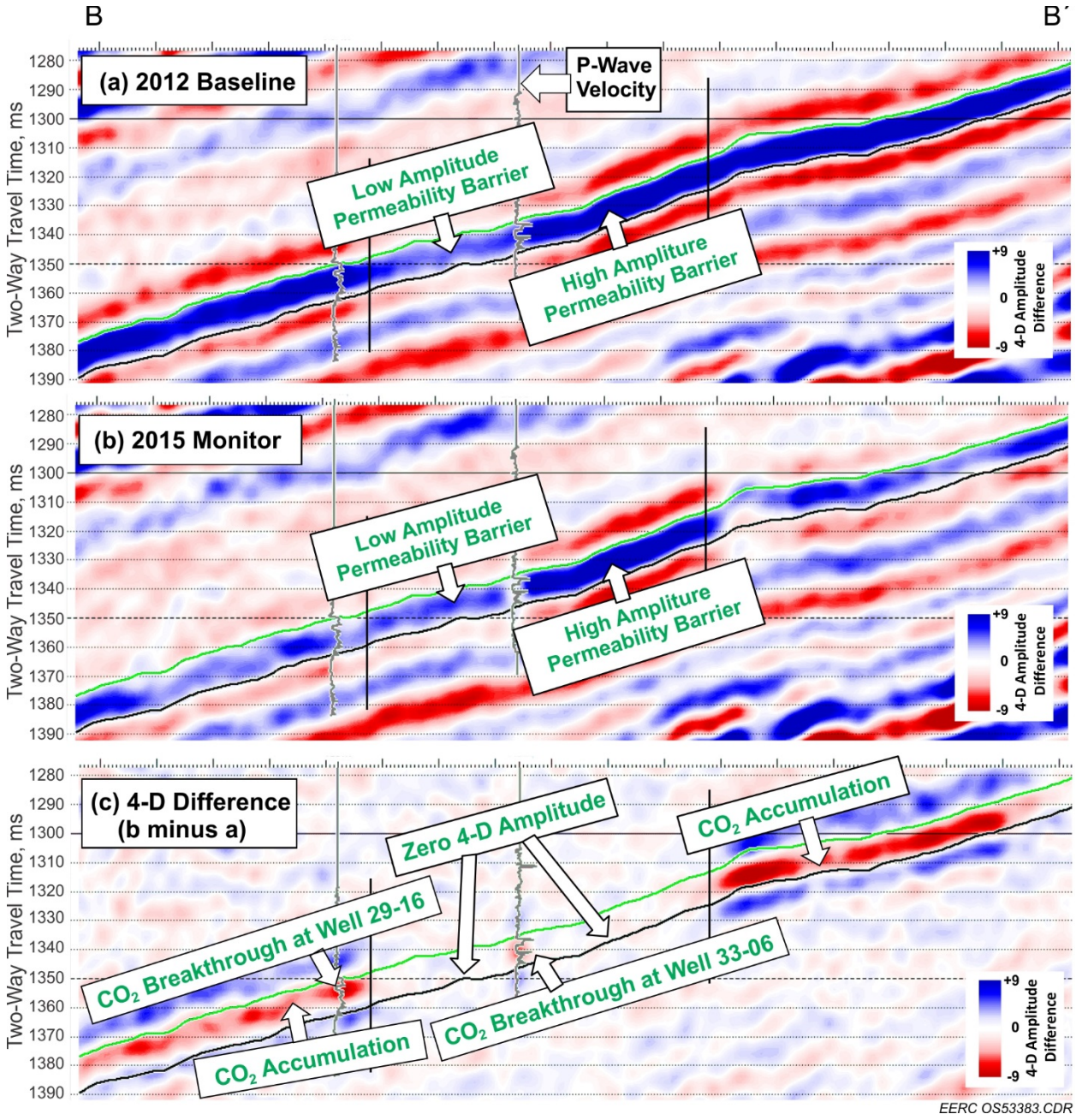

Figure 27. Annotated cross-section line in Figures 23, 24, and 25, respectively: a) baseline, b) 2015 monitor, and c) 4-D difference (b minus a). A 90-degree phase shift has been applied to center the reservoir reflector.

CO_2 Migration, Banking, Accumulation, and Breakthrough

- The 4-D seismic difference map images the injected CO_2 as it migrates away from the injection wells, e.g., Wells 21-01, 21-07, 21-11, 21-13, and Well 21-15 at the northern part of Phase 3.

- Similar to the 2014–2012 4-D interpretation, CO_2 appears to be banking and accumulating against the permeability barrier, which prevents further CO_2 migration.

- There are CO_2 breakthroughs in some of production wells, e.g., Well 33-06 at the intersection of the permeability barrier and Well 29-16 at the upper western end of the fanlike channel at Inline 383.

2015–2014 4-D Interpretation

- The 2014 monitor and 2015 monitor surveys intersect for 3.8 square miles in the center of the field where the permeability barriers cross (Figures 28 and 29). The permeability barriers are visible, as is the impact of additional CO_2 in Phase 3. The communication pathways are visible on the 2015 monitor but are much more ambiguous on the difference display, which is impacted only by the incremental CO_2 injected in the 11 months since acquisition of the 2014 monitor survey. The wells within this overlapping extent had a total of 0.52 million tonnes of incidental CO_2 storage during the time between the two surveys.

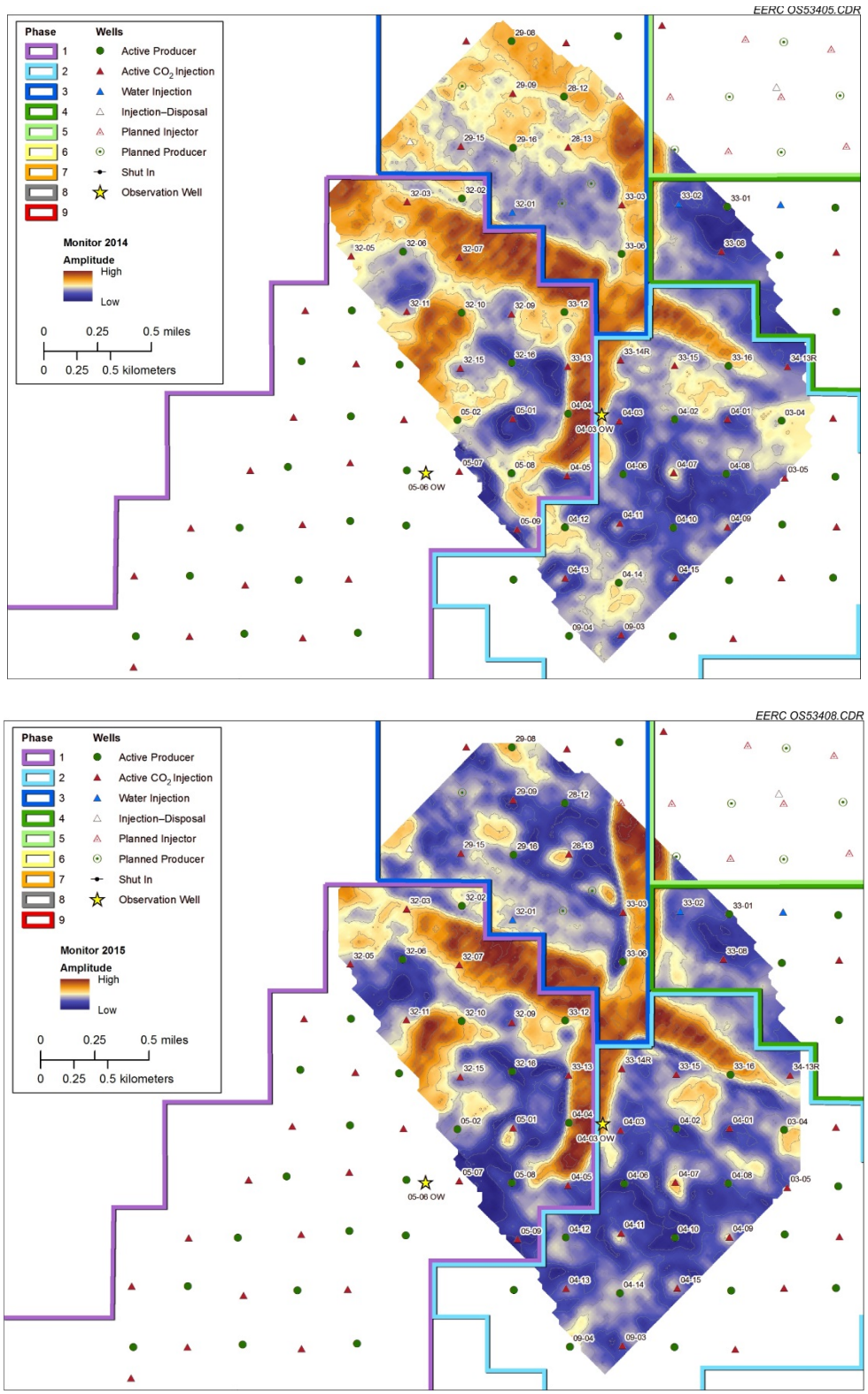

Figure 28. The RMS average seismic amplitude map of the Bell Creek reservoir, for 2014 overlap with 2015 monitor (top panel) and 2015 overlap with 2014 (bottom panel), generated between the Springen Ranch and Skull Creek horizons.

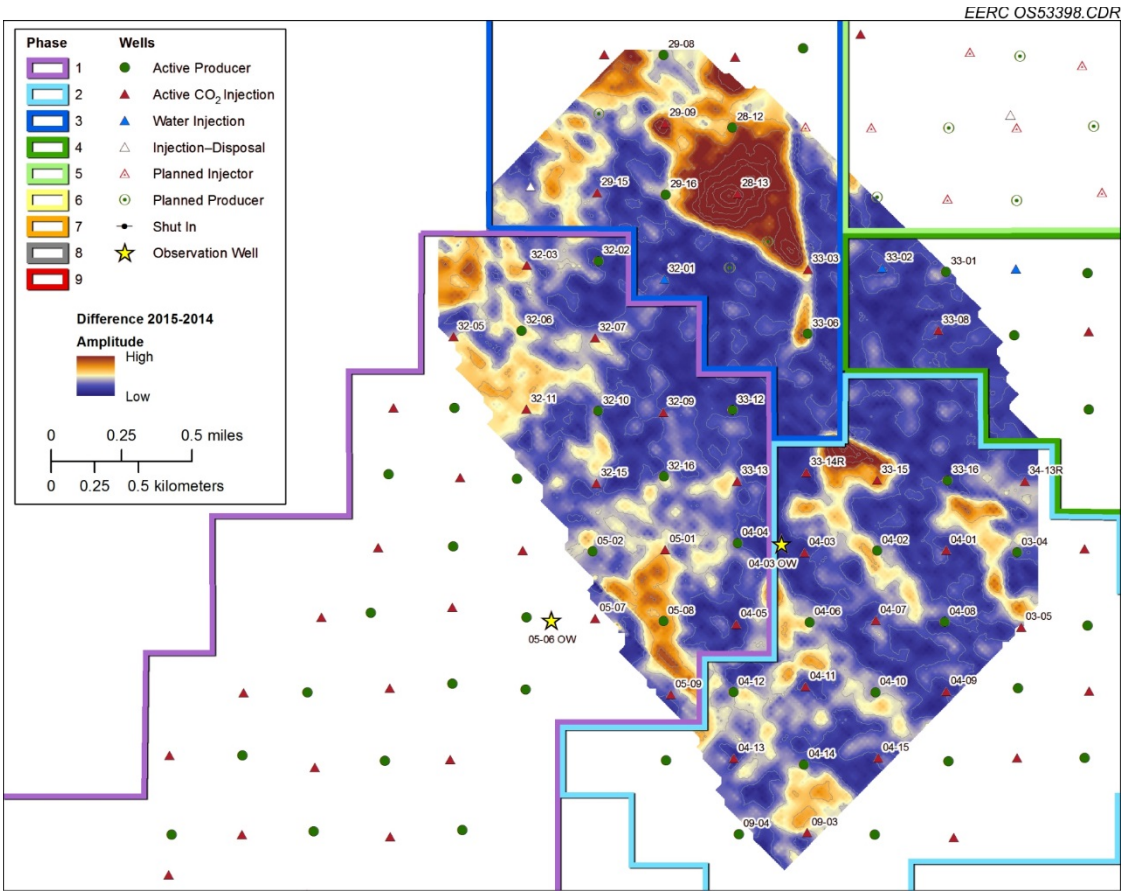

Figure 29. The 4-D difference map for the intersecting region between 2015 monitor and 2014–2015 overlap monitor.

DISCUSSION AND CONCLUSIONS

The expanded seismic campaign at Bell Creek consisting of acquisition, processing, and interpretation of multiple time-lapse seismic data sets (2-D surface seismic data, 3-D surface seismic data, VSP data, and passive seismic data) has been instrumental in gaining a better understanding of incidental CO_2 storage associated with CO_2 EOR. It has provided a means to measure and image physical properties throughout the geologic section on a fine grid over the field that has aided geologic characterization. Inversion of 3-D data was used to calculate volumes of geomechanical properties that were used in the construction of a 3-D mechanical earth model so that geomechanical responses due to injection operations can be modeled in the reservoir and surrounding strata (Ge and others, 2015). 4-D analysis improved the understanding of the reservoir heterogeneity and improved the geologic model that was generated using interpretation results from the 2012 baseline data previously reported on by Burnison and others (2014). CO_2 acted as a tracer and helped illuminate geobodies in the 4-D data by delineating permeability barrier boundaries that were not resolved with 3-D baseline data. This illumination gave better insight about the location, extent, and effectiveness of these permeability barriers.

The expanded seismic campaign also provided a means of directly indicating the locations of CO_2 accumulation via the time-lapse surveys. The tracerlike effect of the CO_2 helped to delineate relatively small permeable pathways transecting the permeability barriers, which allow limited fluid migration and pressure communication between the developmental phases. Understanding and incorporating these features and their geometrical dimensions into the static model significantly improved the dynamic simulation of the well activities and improved reservoir history matching and performance forecasting. 4-D analysis also indicated updip migration of CO_2 in the south–east direction and apparent accumulation of CO_2 against the permeability barrier, which may be preventing further CO_2 movement. This has given insight into the reservoir response to various stages of phase development, including water and CO_2 injection.

The results of the expanded seismic campaign have contributed to the PCOR Partnership's development of practices and technologies that will allow future commercial-scale CO_2 storage projects to make informed decisions regarding site selection, injection programs, operations, and monitoring strategies that improve storage efficiency and effective storage capacity in clastic geologic formations. Related discussion of these practices and technologies has been reported in recent best practices manuals, including in "Best Practices Manual (BPM) for Site Characterization" and "Best Practices for Modeling and Simulation of CO_2 Storage" and will be reported in an upcoming best practices manual "Monitoring for CO_2 Storage and CO_2 EOR." Analysis of the expanded seismic campaign will continue with in-house processing and interpretation of pre- and post-CO_2 injection passive data to better understand changes in reservoir conditions associated with phase development. Future work includes refined interpretation and time-lapse analysis of the VSP data. Additionally, pre- and poststack inversion of 3-D surface seismic data will be performed to gain more information about reservoir compartmentalization to help further refine the geologic model for use in simulations. Future work will also entail quantitative 4-D seismic analysis and inversion to estimate the amount of CO_2 stored in the reservoir and to quantitatively assess the relationship between seismic amplitude change and CO_2 saturation using 4-D difference images and pulse neutron log data.

REFERENCES

Ayash, S.C., Nakles, D.V., Peck, W.D., Sorensen, J.A., Glazewski, K.A., Aulich, T.R., Klapperich, R.J., Azzolina, N.A., and Gorecki, C.D., 2016, Best practice for the commercial deployment of carbon dioxide geologic storage—adaptive management approach: Plains CO_2 Reduction (PCOR) Partnership Phase III draft Task 13 Deliverable D102/Milestone M59 for U.S. Department of Energy National Energy Technology Laboratory Cooperative Agreement No. DE-FC26-05NT42592, Grand Forks, North Dakota, Energy & Environmental Research Center, August.

Bosshart, N.W., Jin, L., Dotzenrod, N.W., Burnison, S.A., Ge, J., He, J., Burton-Kelly, M.E., Ayash, S.C., Gorecki, C.D., Hamling, J.A., Steadman, E.N., and Harju, J.A., 2015, Bell Creek test site – simulation report: Plains CO_2 Reduction (PCOR) Partnership Phase III Task 9 Deliverable D66 (Update 4) for U.S. Department of Energy National Energy Technology Laboratory Cooperative Agreement No. DE-FC26-05NT42592, EERC Publication 2016-EERC-10-09, Grand Forks, North Dakota, Energy & Environmental Research Center, August.

Burnison, S.A., Bosshart, N.W., Salako, O., Reed, S., Hamling, J.A., and Gorecki, C.D., 2016, 4-D seismic monitoring of injected CO_2 enhances geological interpretation, reservoir simulation, and production operations: Presented at the 13th International Conference on Greenhouse Gas Control Technologies (GHGT-13), Lausanne, Switzerland, November 14–18, 2016.

Burnison, S.A., Burton-Kelly, M.E., Zhang, X., Gorecki, C.D., Steadman, E.N., and Harju, J.A., 2014, Bell Creek test site – 3-D seismic and characterization report: Plains CO_2 Reduction (PCOR) Partnership Phase III Task 4 Deliverable D96 for U.S. Department of Energy National Energy Technology Laboratory Cooperative Agreement No. DE-FC26-05NT42592; EERC Publication 2015-EERC-04-04; Energy & Environmental Research Center: Grand Forks, North Dakota, March.

Ge, J., Burnison, S.A., Bosshart, N.W., Dotzenrod, N.W., Liu, G., Braunberger, J.R., Ayash, S.C., Hamling, J.A., Sorensen, J.A., Gorecki, C.D., Steadman, E.N., and Harju, J.A., 2015, Bell Creek Field test site – geomechanical modeling report: Plains CO_2 Reduction (PCOR) Partnership Phase III draft Task 9 Deliverable D32 (update 1) for U.S. Department of Energy National Energy Technology Laboratory Cooperative Agreement No. DE-FC26-05NT42592, Grand Forks, North Dakota, Energy & Environmental Research Center, January.

Jin, L., Bosshart, N.W., Oster, B.S., Hawthorne, S.B., Peterson, K.J., Burton-Kelly, M.E., Feole, I.K., Jiang, T., Pekot, L.J., Peck, W.D., Ayash, S.C., and Gorecki, C.D., 2016, Bell Creek test site – simulation report: Plains CO_2 Reduction (PCOR) Partnership Phase III draft Task 9 Deliverable D66 (update 5) executive summary for U.S. Department of Energy National Energy Technology Laboratory Cooperative Agreement No. DE-FC26-05NT42592, Grand Forks, North Dakota, Energy & Environmental Research Center, August.

Johnston, D.H., 2013, Making a difference with 4D: Practical applications of time-lapse seismic data: SEG distinguished Instructor Short Course.

Montana Board of Oil and Gas Conservation, 2017, MBOGC online oil and gas information system: www.bogc.dnrc.mt.gov/WebApps/DataMiner (accessed June 21, 2017).

Salako, O., Jin, L., Burnison, S.A., Hamling, J.A., Gorecki, C.D., Reed, S., and Richards, T., 2017, The value of 4-D seismic monitoring at Bell Creek—a mature oil field undergoing CO_2 enhanced oil recovery: Paper presented at the 79th EAGE Conference & Exhibition 2017—Energy, Technology, Sustainability – Time to Open a New Chapter, Paris, France, June 12–15, 2017.

APPENDIX A

BRIEF REVIEW OF SEISMIC DATA COLLECTED AT BELL CREEK

BRIEF REVIEW OF SEISMIC DATA COLLECTED AT BELL CREEK

2-D TIME-LAPSE SEISMIC

In December 2011, during seismic source testing in preparation for the 2012 baseline survey to follow, the Energy & Environmental Research Center (EERC) acquired a 2-mile-long 2-D test line on the western edge of Phase 1 (Figure A-1). Originally collected as an exercise to preview the data quality obtainable, the line later provided an important opportunity to test whether CO_2 would be visible on a time-lapse seismic survey in Bell Creek, which was unknown at the time. Fluid substitution modeling had suggested a small but detectable change would occur, but this was not convincing. The uncompleted March 2014 3-D vertical seismic profile (VSP) did not produce unambiguous time-lapse results on 2-D VSP displays.

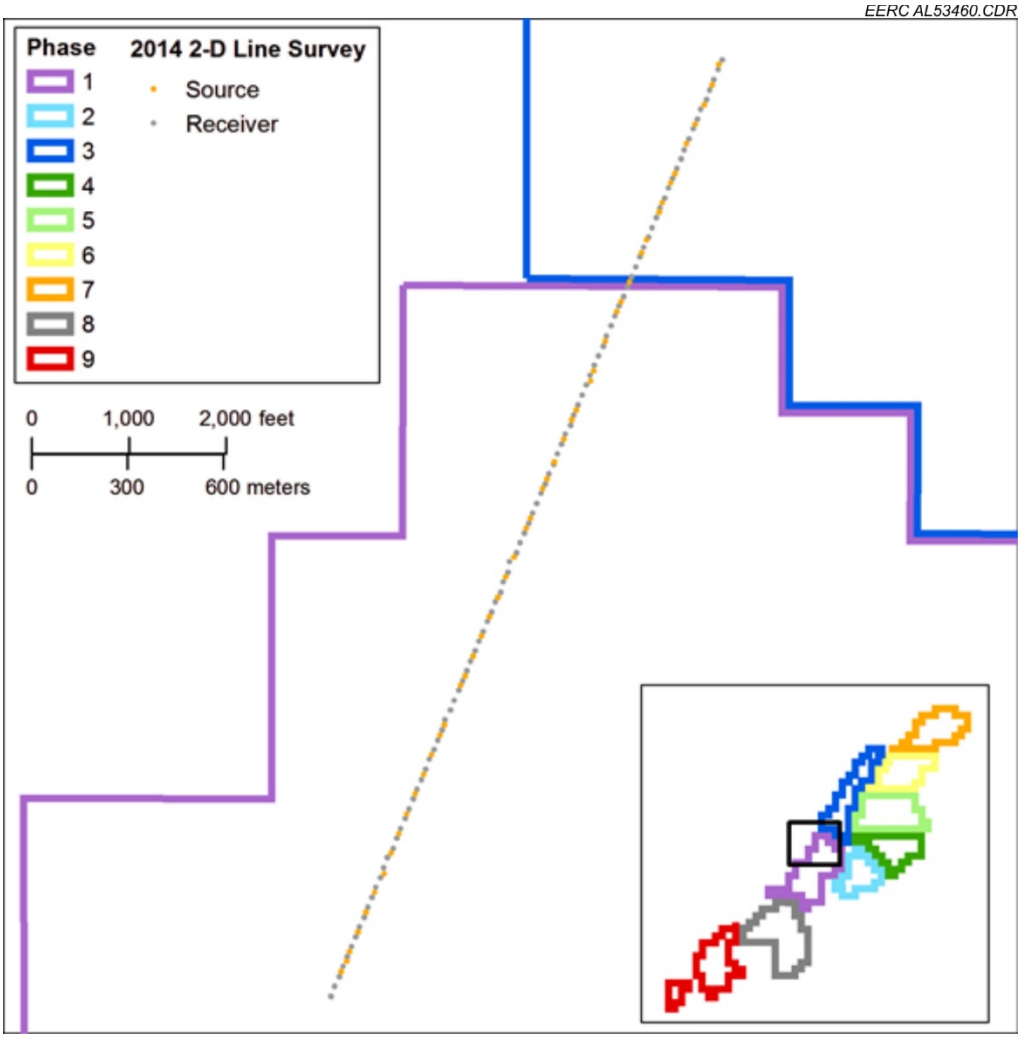

Figure A-1. Source and receiver locations for the 2-D seismic lines collected in 2011 and 2014.

In mid-July 2014, after 14 months of ongoing injection in Phase 1, a repeat of the test line was quickly acquired by a crew that had been mobilized for a larger project in a nearby area (Table A-1). The processed data revealed the presence of CO_2 with a significant detectable amplitude decrease of the reservoir reflection (Figure A-2). The presence of CO_2 was also validated by dynamic simulations of the reservoir along the line traces that were produced by the EERC (Figure A-3).

Table A-1. 2-D Testline and Repeat Acquisition Parameters

	2011 2-D Test Line	2014 2-D Monitor Line
Acquisition Contractor	CGG	Dawson
Energy Source	Two 16,500-lb IVI Mini Vibes	Two 64,000-lb AHV-IV
Source Interval	220 feet	220 feet
Total Source Points	48	48
Geophone	GS 32Ct 10-Hz geophone	SM 24 10-Hz geophone
Group Interval	110 feet	110 feet
Geophone Pattern	3 phones per trace 5-ft inline spacing	6 phones per trace 3-ft inline spacing
Active Spread	NA	NA
Active Stations	96	96
Total Receiver Stations	96	96
Sweep Parameters	Proprietary	Proprietary
Record Length	4 seconds	4 seconds
Sample Interval	2 milliseconds	2 milliseconds

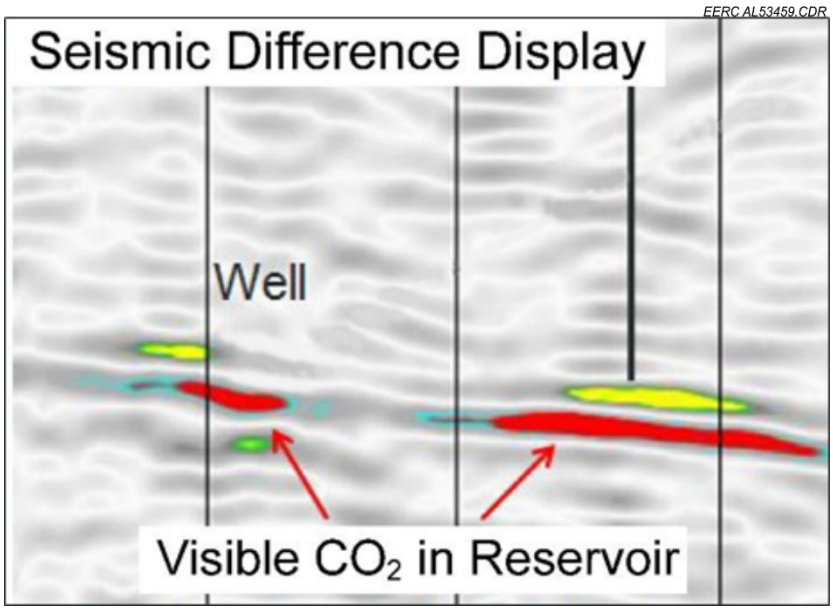

Figure A-2. Seismic difference display from the 2011 and 2014 2-D line data showing amplitude differences in the reservoir due to injected CO_2.

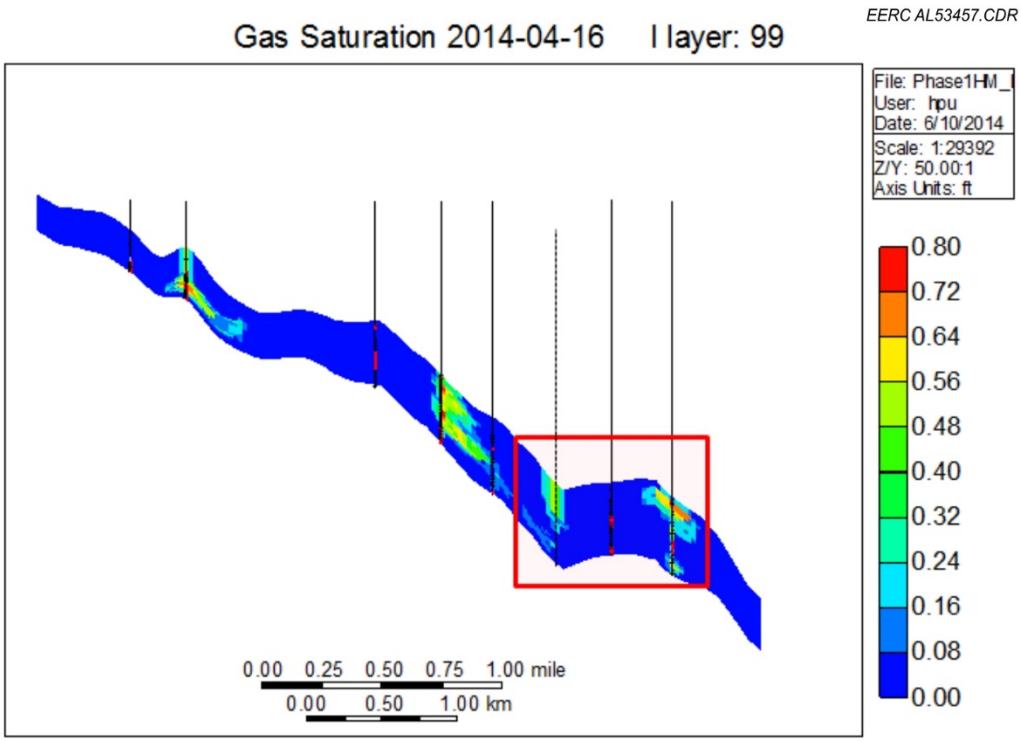

Figure A-3. Cross section of the dynamic reservoir simulations done by the EERC for the 2011–2014 time-lapse period. The red box indicates the simulation extent that corresponds to the seismic difference display shown in Figure A-2.

04-03 OW BOREHOLE ARRAY INSTALLATION

A permanent borehole arrays was installed as part of the monitoring, verification, and accounting (MVA) plan with the intent of using it for microseismic monitoring and use in repeat VSP surveys. The array was installed in 04-03 OW by Apex HiPoint, a seismic services company owned by Sigma Cubed, in April of 2013. The array is a GeoRes DownHole System with 50 levels. Each level consists of a digitized 4C Sensor Module comprising one Deepender™ 5000-X Hydrophone and three orthogonal OMNI-2400 15-Hz geophones (Figure A-4). Additional array parameters can be found in Table A-2.

Figure A-4. Photo of the 4C Sensor Module.

Table A-2. 04-03-0W Borehole Array Parameters

Receiver Type	Digitized 4C Sensor Module (1 Deepender™ 5000-X hydrophone and 3 orthogonal OMNI-2400 15-Hz geophones)
Total Sondes	50
Total Interconnects	50
Total String Length	2460 feet
Sonde Spacing	49.2 feet
First Level	60 feet
Bottom Depth	2461 feet
Coupling Method	Attached to a cemented downhole pipe by bracket

Each 4C Sensor Module was attached to a 2-7/8-inch tubing by a cage and clamp (Figure A-5). This cage and clamp system was specifically designed to protect the sensor module as it descended into the borehole and to allow cable to run under the clamps (Figure A-6). Cable slack was secured to the tubing to prevent damage (Figure A-7). During installation, the array was actively recording data that was analyzed in real time on-site as a quality control method to identify and assess any equipment malfunction caused during installation.

Figure A-5. Photo of the rebar cage and clamp used to secure and protect the sensor modules.

Figure A-6. Photo of a clamp showing the locking mechanism and the spacer, which provides room for cable to safely pass under the clamp without being damaged.

Figure A-7. Photo of secured array cables along the casing.

04-03 OW BOREHOLE ARRAY DATA RECORDING SYSTEM

The 04-03 OW borehole array is connected to a surface data-recording system by a fiber optic cable (Figure A-8). The data-recording system is a GeoRes Imagine HC (high capacity) recording system housed in a recording shack (Figure A-8). This system comprises a GeoRes Topside on-site control, a power controller, a storage controller, and satellite Internet for remote operation (Figure A-9). The GeoRes Topside on-site control is a Windows operating system that contains the GeoRes Imagine operating software, which allows for data recording, display of real-time data, system and sensor testing, power management, multipath data storage, networking, and plotting (Geospace Technologies, 2014). The power controller is used to power the system and can be used to remotely reboot the system using a modem if needed. An uninterruptible power supply (UPS) was also installed with the data-recording system to prevent sudden power outages. The storage controller is a Linux machine that uses multiple drives to store the continuous data. When the borehole array and data-recording system are successfully operating, continuous passive data are recorded by the GeoRes Topside and stored on the storage controller. The surface equipment also includes two power units that supply power to the downhole array.

Figure A-8. Photos of the 04-03 OW wellhead showing the fiber optic cable running from the borehole array to the surface (left) and 04-03 OW recording shack (right). The satellite Internet dish allowing remote operation is mounted on top of the shack.

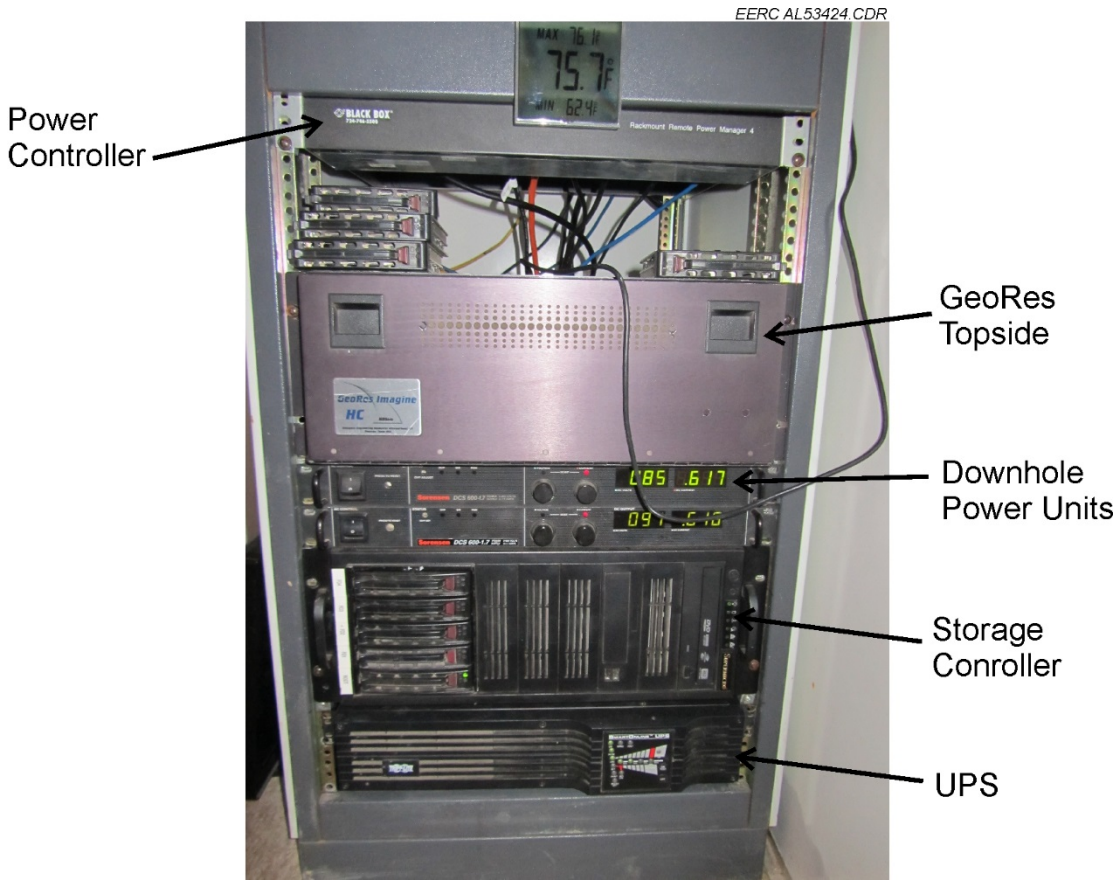

Figure A-9. Photo of the 04-03 OW Borehole Array GeoRes Imagine HC recording system.

PASSIVE DATA ACQUISITION AND PROCESSING

The borehole array was operated and maintained by Sigma Cubed, a geophysical service company, from May 22, 2013, to June 8, 2014. During this time, continuous data was collected using a 0.5 msec sample rate and was saved in 10 second segments as SEG-D files. Sigma Cubed used a software package installed on the storage controller called GeoPro to do near real time event detection. GeoPro scanned the continuous data for coherent events as data were saved to the storage controller. When a coherent event was identified, the field file ID for the file being scanned was logged. File records corresponding to coherent events were validated by hand at the processing center, and if considered legitimate, the events were located and the amplitude of the event at the receiver string noted. Coherent events were mapped (Figure A-10). Sigma Cubed mapped a total of 3648 events. Only 22 of these events occurred between 8:00 p.m. and 7:00 a.m., outside normal field working hours. As there was significant development activity with workover rigs in Phases 2 and 3 during this time period, this suggests that most of the identified events were due to human activity in the field.

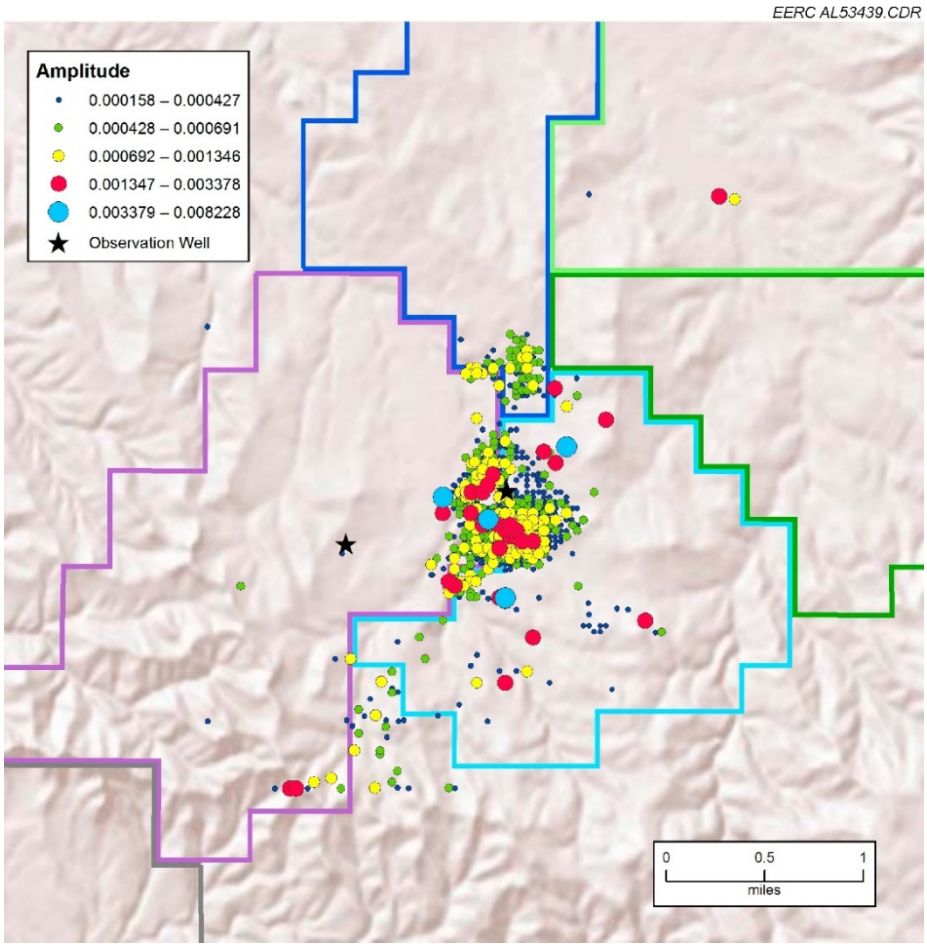

Figure A-10. EERC-generated map showing events mapped by Sigma Cubed. Event amplitude is signified by size of event symbol. (Amplitude does not directly correspond to magnitude. No magnitudes for the mapped events were computed by Sigma Cubed.)

The EERC took over passive data acquisition and continuously recorded data using 1-msec sampling until instability led to the system being shut down for maintenance in May 2016. Maintenance was completed but the recording system remained unstable with frequent crashes making further remote acquisition problematic and intermittent. The EERC is currently processing a subset of this data in-house for location and magnitudes as part of their MVA efforts.

3-D VSP Acquisition

A baseline and two monitor 3-D VSP data sets were collected at Bell Creek as part of the deep monitoring program. The purpose of the surveys was to assess time-lapse changes in the reservoir due to CO_2 around monitor Wells 05-06 OW and 04-03 OW (Figure A-11).

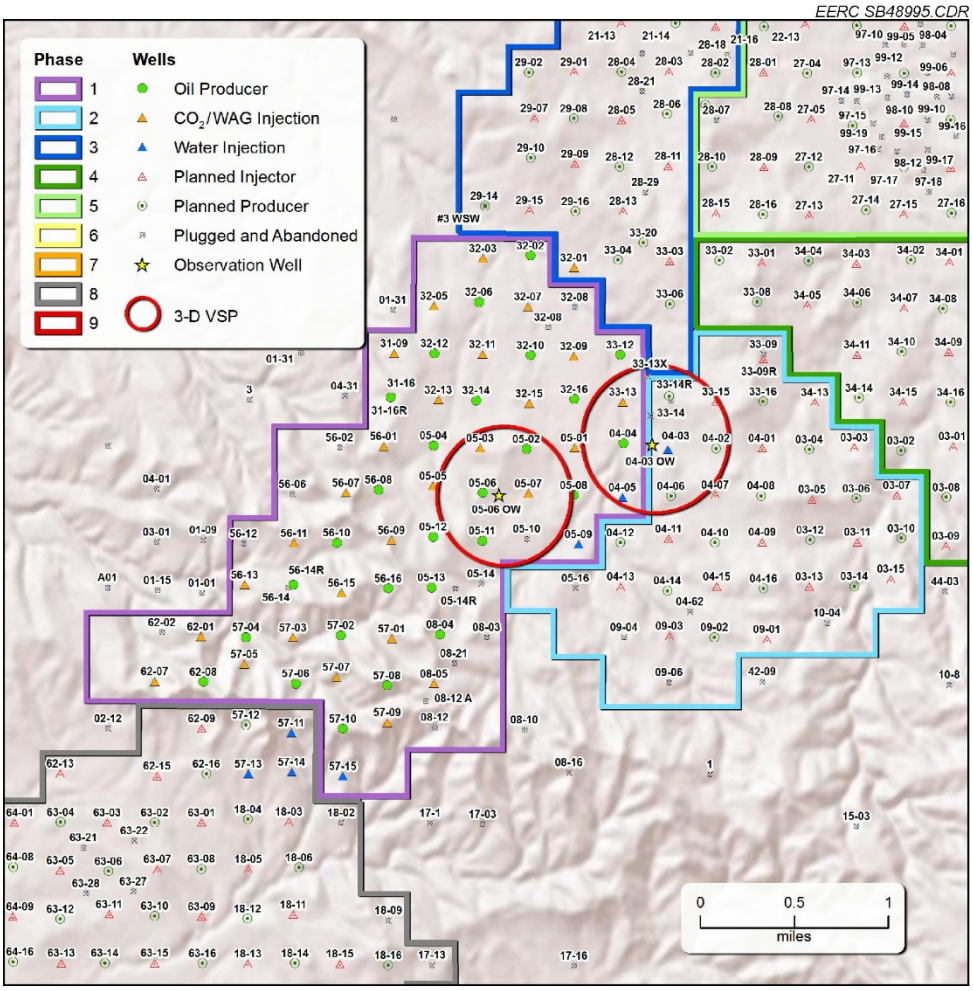

Figure A-11. Location map and notional coverage of the 2013 baseline VSP survey. The area of coverage at the Muddy Formation is within the two outlined circles (Burnison and others, 2014).

2013 Baseline VSP Survey

The baseline VSP survey was collected by Apex HiPoint during a 5-day span from May 15–19, 2013. The receiver arrays were the 50-level permanent borehole array in 04-03 W and a 60-level retrievable array deployed in 05-06-OW. 110 total receivers were used. The borehole array parameters can be found in Table A-2 and Table A-3. The energy source was two 64,000-lb AHV-IV vibrators operating in unison. The total number of shot points was 961(Figure A-12). Data were recorded normally with a time break. The hydrophone data from the 04-03 OW borehole array were not recorded.

Table A-3. 05-06-0W Borehole Array Parameters

Receiver Type	DS 150 3-C 15-Hz Geophone
Total Sondes	60
Total Interconnects	60
Total String Length	2953 feet
Sonde Spacing	49.2 feet
Bottom Depth	3002 feet
First Level	19.2 feet
Coupling Method	Magnets on the receiver casing and pressure buildup using gas

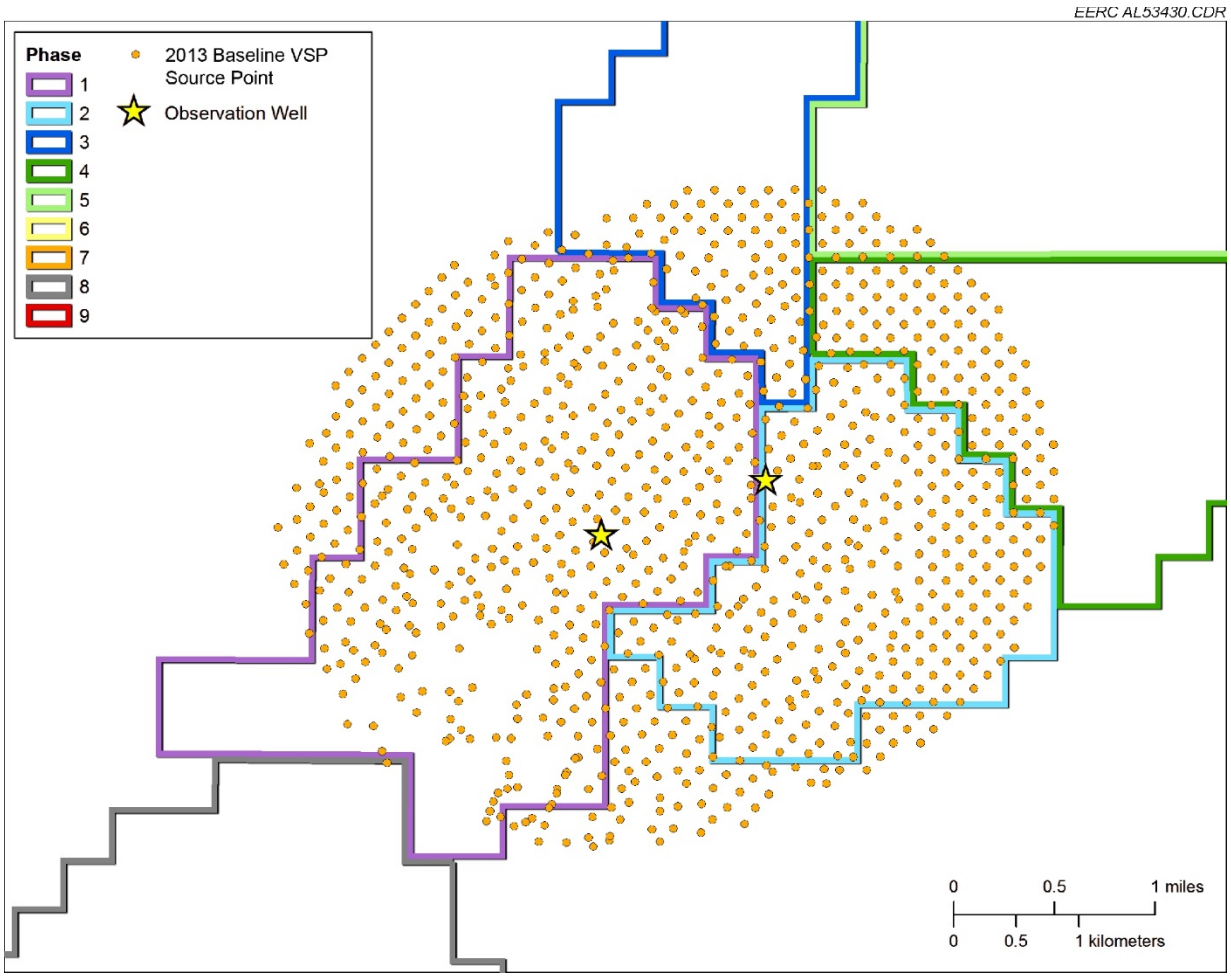

Figure A-12. Map showing source points for a 2013 baseline VSP survey acquired in the Bell Creek Field.

MARCH 2014 MONITOR VSP SURVEY

A monitor survey was started by Apex HiPoint in March 2014. The acquisition equipment and parameters were the same as the 2013 baseline VSP. After 125 shots were collected, the survey team was placed into standby mode because of operator error and equipment malfunctioning that required review. After several days of standby, the survey was aborted for safety and budget considerations. Figure A-13 shows the shot points that were successfully acquired.

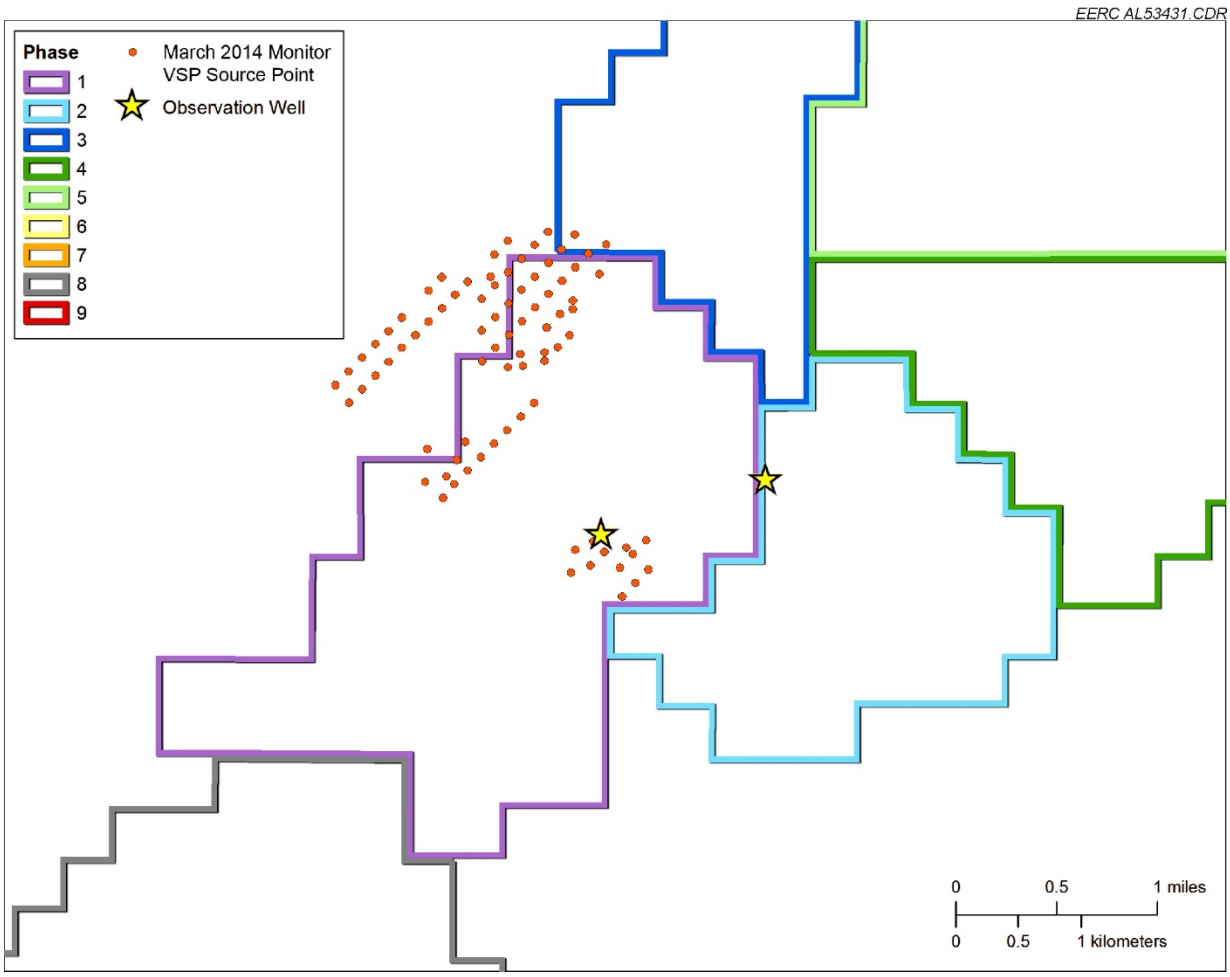

Figure A-13. Map showing source points for a March 2014 monitor VSP survey acquired in the Bell Creek Field.

OCTOBER 2014 MONITOR VSP SURVEY

In October of 2014 during the 2014 3-D surface seismic monitor survey, Dawson Geophysical Company collected a monitor VSP survey. This VSP survey utilized the permanent borehole array in 04-03 OW and shot points collected as part of the 3-D surface survey that overlaid shot point locations from the baseline VSP. 442 shots were selected from the 3-D surface seismic survey shot lines, and an additional 238 shots were specifically collected for the VSP survey for a total of 680 shots (Figure A-14). The energy source was two 64,000-lb AHV-IV vibrators operating in unison. No repeat VSP data were collected for 05-06 OW. No time break was used for data collection. Active shot records were extracted from the continuous data recorded by the 04-03 OW array using GPS (global positioning system) time stamps. Hydrophone data were recorded.

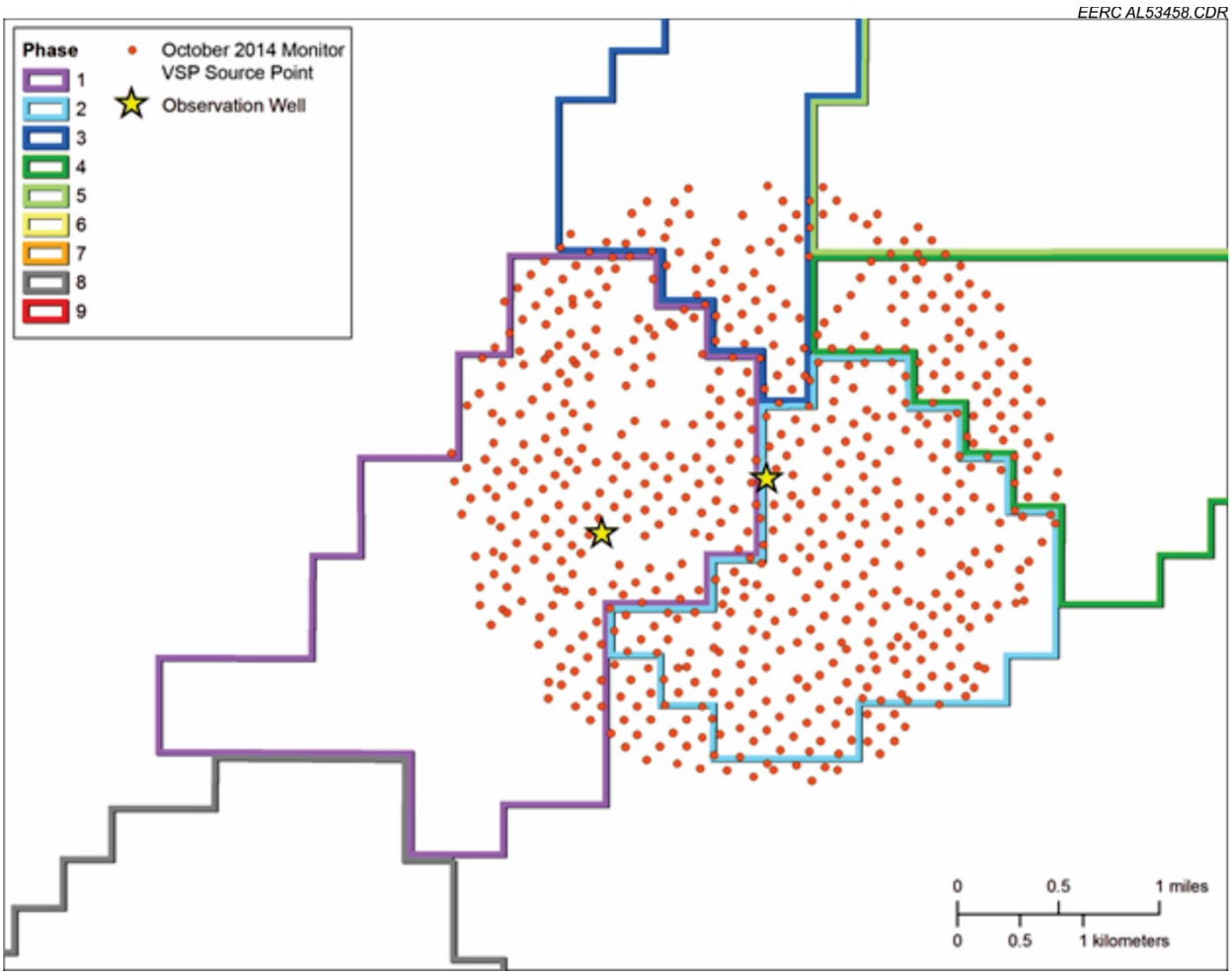

Figure A-14. Map showing source points for October 2014 monitor VSP survey acquired in the Bell Creek Field.

3-D VSP DATA PROCESSING

Apex HiPoint processed the 2013 baseline VSP survey data with the following summarized sequence (greater detail is provided in Appendix C):

- Reformatting and geometry assignment
- Geophone orientation analysis and rotation
- First arrival picking
- Time-variant rotation
- Spherical divergence correction
- Removal of downgoing energy
- Upward continuation to pseudo-receivers at surface
- Surface consistent scaling and deconvolution
- 3-D gridding, CMP (common midpoint) sort, and stack
- Surface consistent scaling and deconvolution, trace balancing

- Velocity analysis and residual statics
- Kirchoff PSTM (prestack time migration)
- NMO (normal moveout correction), mute, stack, and filter
- Datum statics

In 2014, Apex HiPoint processed the shot points from the 2013 baseline and March 2014 monitor VSP survey data that were repeated with the following summarized sequence (greater detail is provided in Appendix C):

- Reformatting and geometry assignment
- Geophone orientation analysis and rotation
- First arrival picking
- Time-variant rotation
- Spherical divergence correction
- Match filter
- Source wavelet estimation and wavelet deconvolution
- Removal of downgoing energy
- Linear moveout correction (LMO)
- Filter and shift to final datum

In 2015, Paulsson, Inc., processed the geophone data from the 04-03 OW permanent borehole array collected during the 2013 baseline survey and October 2014 monitor VSP survey with the following summarized sequence. Paulsson also included the hydrophone data from the October 2014 monitor VSP survey (greater detail is provided in Appendix C):

- Geometry assignment, geometry QC, data subset selection, and trace editing
- Geophone orientation analysis and rotation
- First arrival picking
- Datum statics
- Source wavelet estimation and wavelet deconvolution
- Velocity analysis
- Update receiver locations using well deviation and first arrivals
- Spherical divergence correction and surface consistent scaling
- Removal of downgoing energy
- Surface consistent scaling, and statics
- Kirchhoff prestack depth migration (Kirchhoff PSDM)
- Residual statics and refined velocity analysis
- Spectral balancing
- Anisotropic velocity analysis and anisotropic Kirchhoff PSDM

References

Burnison, S.A., Burton-Kelly, M.E., Zhang, X., Gorecki, C.D., Steadman, E.N., and Harju, J.A., 2014, Bell Creek test site—3-D seismic and characterization report: Plains CO_2 Reduction (PCOR) Partnership Phase III Task 4 Deliverable D96 for U.S. Department of Energy National Energy Technology Laboratory Cooperative Agreement No. DE-FC26-05NT42592; EERC

Publication 2015-EERC-04-04; Energy & Environmental Research Center: Grand Forks, North Dakota, March.

Geospace Technologies, 2014, GeoRes Subsea System: www.geospace.com/wp-content/uploads/2012/10/592-03140-01-GeoResSubseaSystem-Rev-A.pdf (accessed August 19, 2014).

APPENDIX B

SEISMIC INVERSION OF GEOMECHANICAL PROPERTIES AND PHYSICS OF THE BELL CREEK FLUIDS – FEASIBILITY STUDY

SEISMIC INVERSION OF GEOMECHANICAL PROPERTIES AND PHYSICS OF THE BELL CREEK FLUIDS – FEASIBILITY STUDY

SEISMIC INVERSION OF GEOMECHANICAL PROPERTIES

Computation of Geomechanical Properties

As part of characterization for CO_2 storage, geomechanical properties were computed by simultaneous prestack inversion of 3-D gathers. The data set used was the 2012 baseline that was reprocessed after the 2014 monitor survey. Three volumes were computed; bulk density, Poisson's ratio (PR), and Young's modulus from the surface to a depth of 8000 feet. The volumes of geomechanical properties were used in the construction of a 3-D mechanical earth model so that geomechanical responses due to injection operations could be modeled in the reservoir and surrounding strata (Ge and others, 2015).

Importance of Geomechanical Properties

3-D geomechanical modeling can help in understanding the stress and strain states of the reservoir and the surrounding rocks (above and below the reservoir) prior to CO_2 injection. When incorporated with fluid flow simulation modeling, 3-D geomechanical modeling can help to assess possible impacts of the changes in the stress and strain conditions during and after CO_2 injection. Among the inputs required to build a 3-D geomechanical model are 1) density, 2) Poisson's ratio, and 3) Young's modulus. These three inputs were obtained from inversion of the 3-D prestack seismic data. Density is a direct inversion output, and Poisson's ratio and Young's modulus are calculated from the inversion outputs (density, P-wave velocities, and S-wave velocities).

Poisson's Ratio

PR (σ), unitless, is connected with the P-wave and S-wave velocities by the equation:

$$\sigma = \frac{\gamma^2 - 2}{2\gamma^2 - 2} \qquad \text{[Eq. C-1]}$$

Where

$$\gamma = \frac{V_p}{V_s} \qquad \text{[Eq. C-2]}$$

and V_p and V_s are P-wave and S-wave velocities (km/s), respectively.

An image of PR obtained is shown (Figure B-1). Typical values inside the reservoir, between the Springen Ranch and Skull Creek horizons, are approximately 0.38.

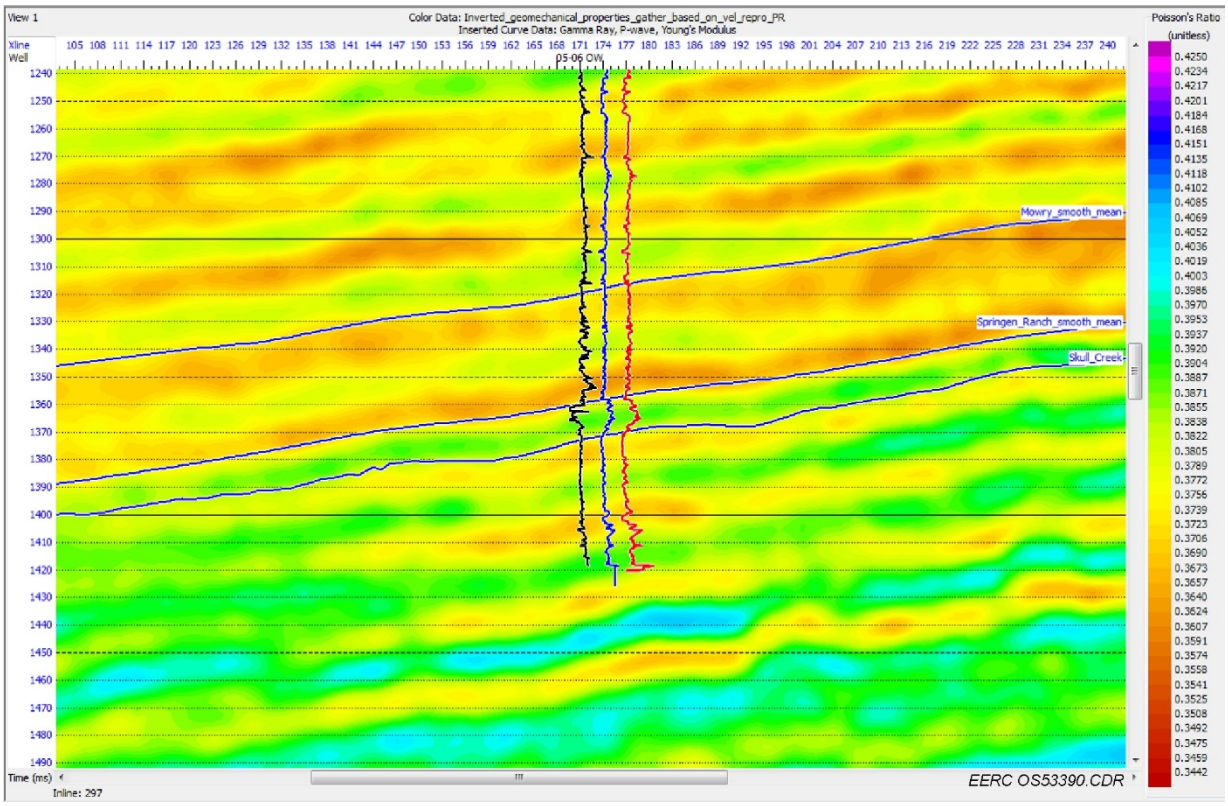

Figure B-1. Color image of PR in the vicinity of the reservoir. Logs from 05-06 OW are overlaid: GR (gamma ray, black), Sonic P-wave velocity (blue), and PR (red) as computed from the array sonic log.

Young's Modulus

To obtain Young's modulus, shear and bulk moduli were calculated.

The shear modulus (μ) is the resistance to change in shape. It has units of gigapascals (GPa) and is given by:

$$\mu = V_s \times \rho \qquad \text{[Eq. C-3]}$$

where ρ is the density (g/cm^3) and V_s (km/s) is a direct output of prestack inversion.

The bulk modulus (K), in GPa, is the resistance to a change in volume and is given by:

$$K = \left(V_p^2 \times \rho\right) - \frac{4\mu}{3} \qquad \text{[Eq. C-4]}$$

From these, the Young's modulus (E), in GPa, is computed:

$$E = 3K(1 - 2\mu) \qquad \text{[Eq. C-5]}$$

Typical values of Young's modulus within the reservoir are between 9 and 10 GPa (Figure B-2).

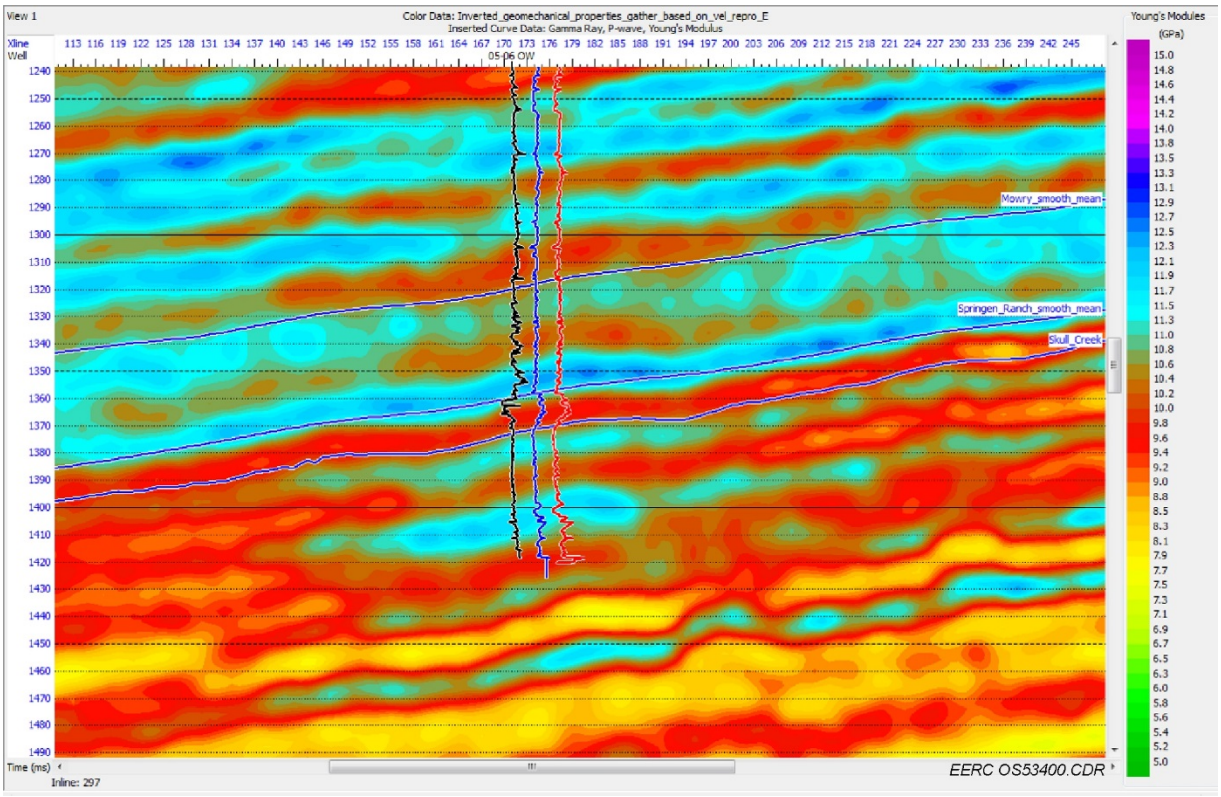

Figure B-2. Color image of Young's modulus in the vicinity of the reservoir. Logs from 05-06 OW are overlaid: GR (black), sonic P-wave velocity (blue), and Young's modulus (red) as computed from the array sonic log.

PHYSICS OF THE BELL CREEK FLUIDS – FEASIBILITY STUDY

Earlier feasibility studies performed by the field operator – Denbury, using amplitude versus offset (AVO) fluid substitution, have shown that CO_2 injection can produce detectable changes in time-lapse seismic amplitude. The Energy & Environmental Research Center (EERC) carried out the fluid physics analysis to examine how seismic might respond to the water alternating gas (WAG) enhanced oil recovery mechanism at Bell Creek Field. Using empirical equations (Batzle and Wang, 1992; Han and Batzle, 2000), engineering data from the reservoir, and thermodynamic properties of CO_2 (NIST, 2017) the seismic acoustic parameters (density, bulk modulus, P-wave [primary or compressional wave] velocity, and P-impedance) of the Bell Creek, reservoir fluids

(oil, water, and CO_2) are calculated. This aided the interpretation of the 4-D seismic data for fluid discrimination as a result of CO_2 injection. Table B-1 shows the summary of the reservoir fluid properties and conditions used in calculating acoustic parameters.

Table B-1. Summary of Bell Creek Engineering Data Showing Reservoir Fluid Properties and Conditions Used in Calculating Acoustic Parameters (Jin and others, 2016)

Properties		Value
Depth		4300–4500 ft
Thickness		30–45 ft
Average Porosity		25%–35%
Reservoir Temperature		108.0°F
Oil API Gravity at 108.0°F		35.6
Solution Gas–Oil Ratio at 108.0°F		173.38 scf/stb
Connate Water Saturation		0.25
Salinty		5000 ppm (TDS*)
Pressure, psia	Average Initial	1200
	Average in 2012	1600
	Average in 2014	2500
	Injection Range	2700–2900
	Average Production	2300

* Total dissolved solids.

The pressure and temperature conditions of the reservoir show that the CO_2 exists at supercritical condition, which means CO_2 can behave either as a gas or as a liquid (Figure B-3).

Density and bulk modulus are two fundamental seismic acoustic parameters. The calculated density (Figure B-4) indicates that the density of CO_2 is slightly larger than the density of oil, for the injection pressure ranging between 2700 to 2900 psia and at average reservoir temperature of 108°F. This indicates the point at which CO_2 behaves as a supercritical liquid. Whereas at, and below, the average production pressure of 2300 psia, the density of CO_2 is much less than the density of oil. This indicates the point at which CO_2 behaves as a supercritical gas. In comparison with the density of brine, the density of CO_2 is significantly less than the density of brine at reservoir conditions. It is about 0.25 g/cm^3 less at production pressure and about 0.2 g/cm^3 less at injection pressure.

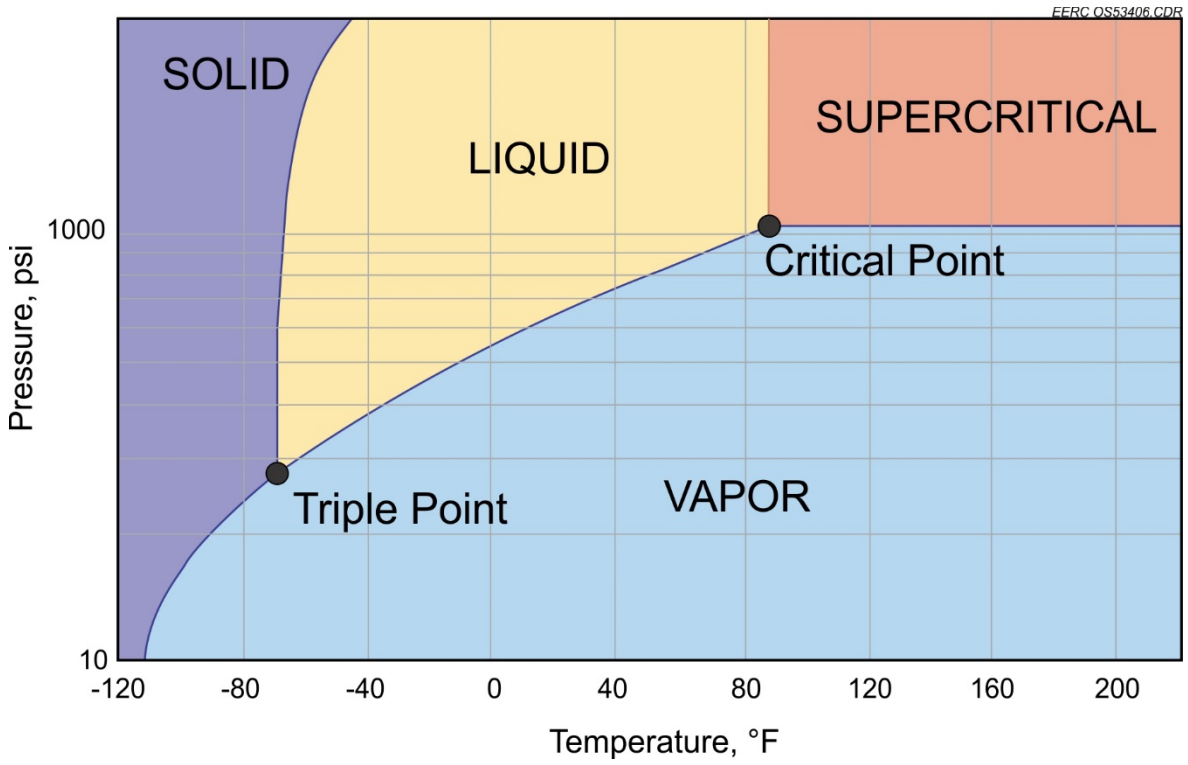

Figure B-3. CO_2 phase diagram showing that, at the reservoir pressure and temperature conditions shown in Table B-1 above, CO_2 exists in a supercritical condition (BPS International, 2017).

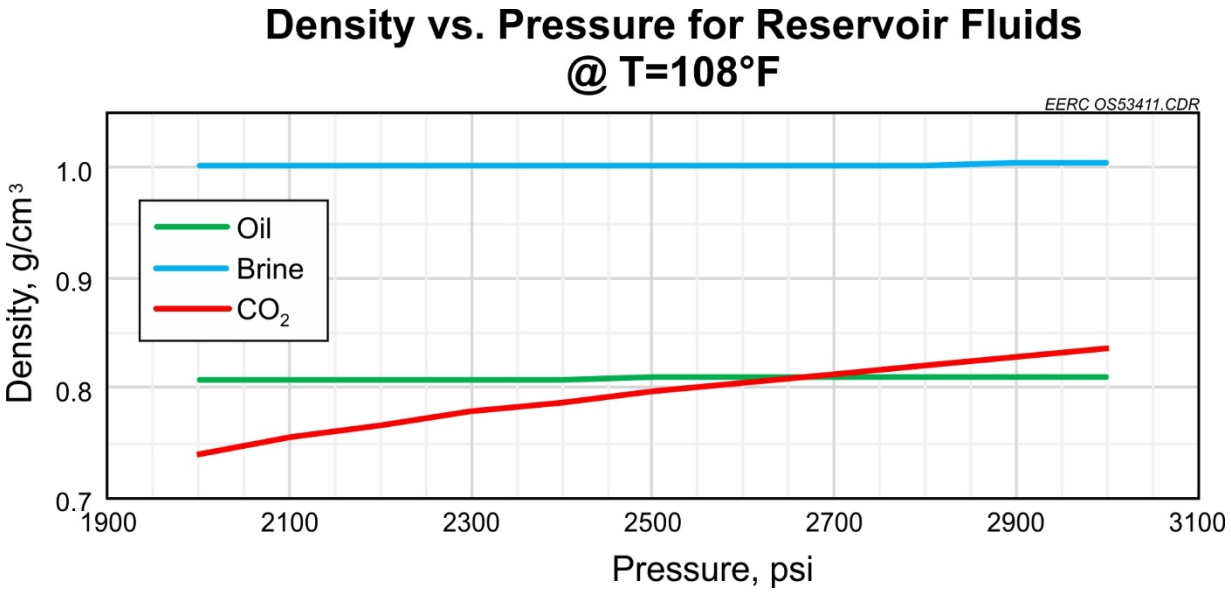

Figure B-4. Comparison of Bell Creek fluid densities. Calculations were made using empirical equations from Batzle and Wang (1992) and Han and Batzle (2000), CO_2 properties from the National Institute of Standards and Technology (2017), and engineering data from Table B-1.

In terms of the bulk modulus, Figure B-5 shows that the CO_2 bulk modulus is about 70 to 200 times less than the bulk modulus of oil and much less than the bulk modulus of brine at reservoir conditions. This shows that whether the CO_2 exists as a liquid or as a gas at supercritical conditions, its compressibility is still much higher than those of oil and brine, thus having a much lower bulk modulus than those of oil and brine. In terms of homogeneous fluids mixing in the pore space and using Wood's equation (Wood, 1955), CO_2 which has the lowest bulk modulus (i.e., highest compressibility) will dominate the effective bulk modulus of the mixed fluid.

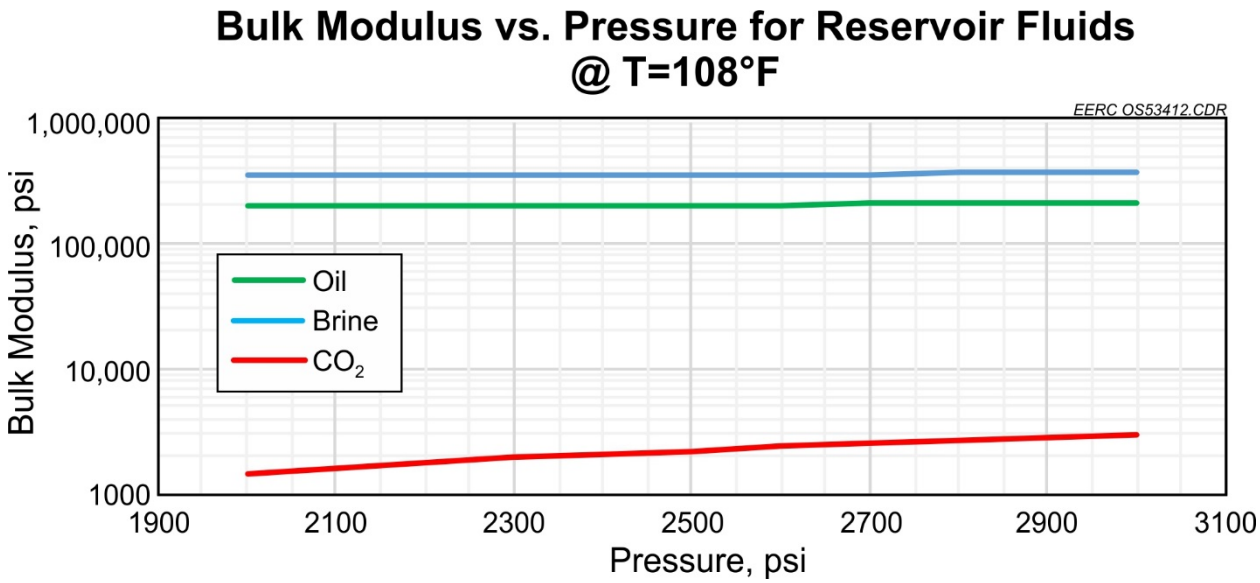

Figure B-5. Comparison of Bell Creek fluid bulk moduli. Calculations were made using empirical equations from Batzle and Wang (1992) and Han and Batzle (2000), CO_2 properties from the National Institute of Standards and Technology (2017), and engineering data from Table B-1.

$$\frac{1}{K_f} = \frac{S_{CO_2}}{K_{CO_2}} + \frac{S_o}{K_o} + \frac{S_b}{K_b} \qquad \text{[Eq. C-6] (Wood, 1955)}$$

Where S_{CO2}, S_o, S_b are CO_2, oil, and brine saturations, respectively, and K_{CO2}, K_o, K_b, and K_f are CO_2, oil, brine, and combined mixed fluid bulk moduli, respectively.

While fluid density variation, especially between oil and CO_2, may not be significant in this case, the fluid bulk modulus variation is significant. It has a large impact on the two derived acoustic parameters, P-wave velocity and P-impedance, which in conjunction with the rock acoustic parameters, give rise to the two-way travel times measured in seismic data. Figure B-6 shows that there is a significant difference between the velocity of CO_2 and the velocities of oil and brine. The velocity of CO_2 is on the order of 8 to 10 times less than the velocity of oil and much less than the velocity of brine.

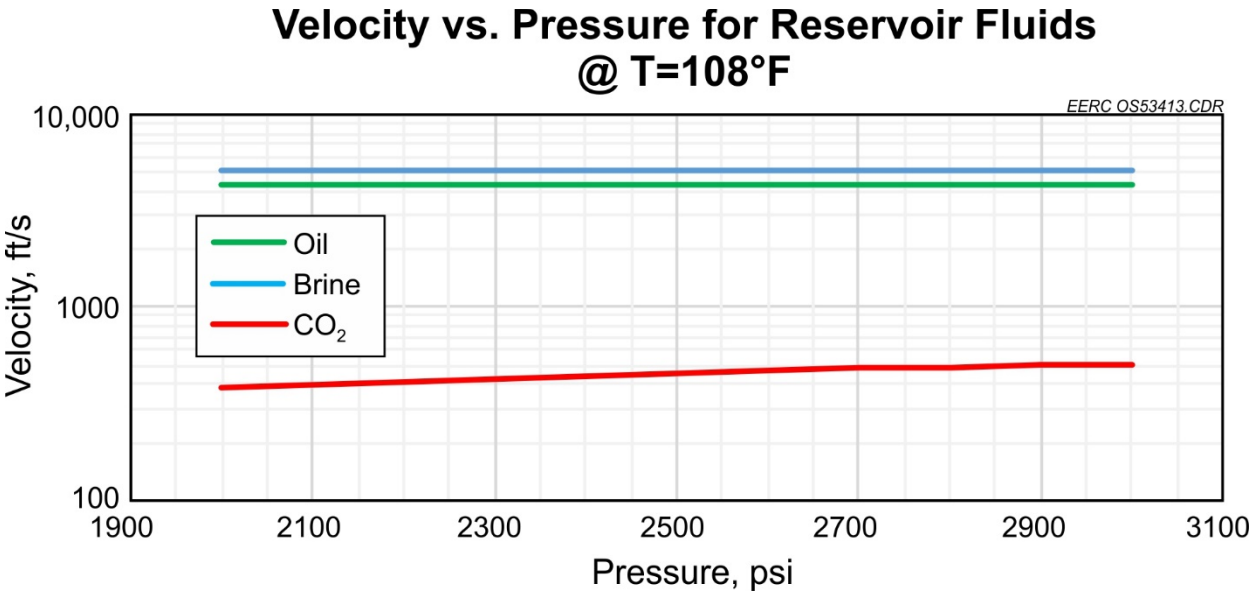

Figure B-6. Comparison of Bell Creek fluid P-wave velocities. Calculations were made using empirical equations from Batzle and Wang (1992) and Han and Batzle (2000), CO_2 properties from the National Institute of Standards and Technology (2017), and engineering data from Table B-1.

Similarly, P-impedance of CO_2 is approximately 8 to 10 times less than the impedance of oil and much less than the impedance of brine (Figure B-7). This study, focused mainly on the fluid effect on seismic response, shows that CO_2 injection can produce significant change in P-wave velocity and impedance. The addition of reservoir rock properties has a scaling effect and requires more detailed modeling to generate the seismic response. Nevertheless, with an average porosity of 25% to 35%, the rock matrix of the Bell Creek reservoir is expected to be compressible enough such that the P-wave velocity would be sensitive to the change in pore-fluid compressibility.

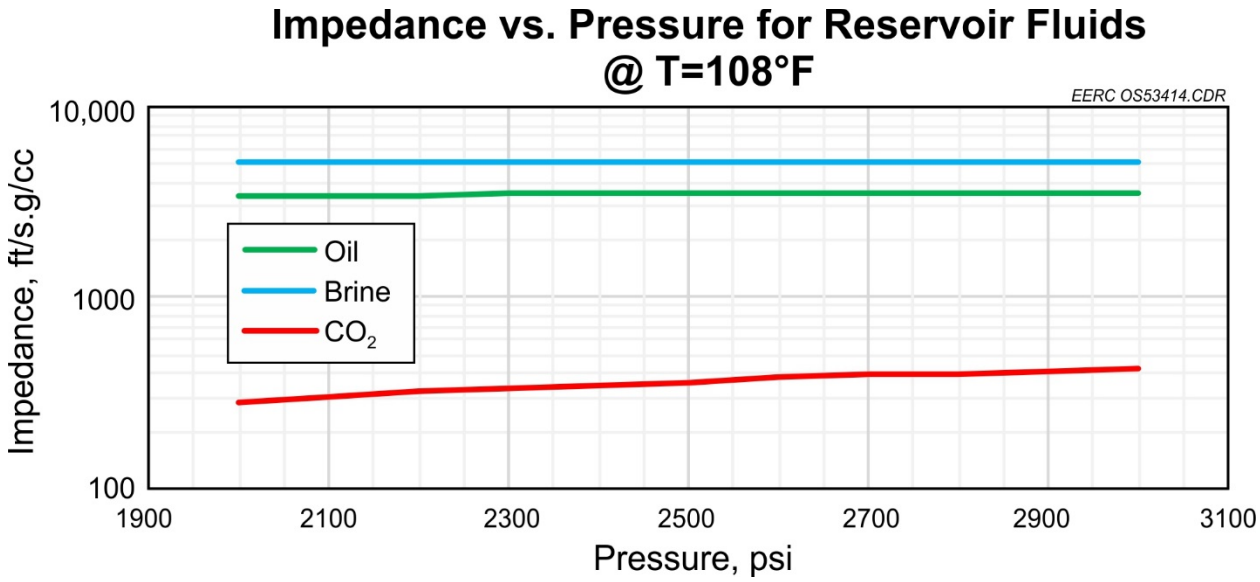

Figure B-7. Comparison of Bell Creek fluid P-impedance. Calculations were made using empirical equations from Batzle and Wang (1992) and Han and Batzle (2000), CO_2 properties from National Institute of Standards and Technology (2017), and engineering data from Table B-1.

The change in pressure, as a result of injection, also impacts the rock framework and can result in change in moduli and in the P-wave and S-wave velocities. Since S-wave (shear waves) do not travel through fluid, they might be used in combination with P-wave to separate the effect of fluid saturation from the effect of pressure which has more impact on the rock framework than the fluid. To do this, inversion of P-wave and S-wave velocities and impedances from the prestack 4-D seismic data was done.

REFERENCES

Batzle, M.L., and Wang, Z.-J., 1992, Seismic properties of pore fluids: Geophysics, v. 57, p. 1396–1408, http://dx.doi.org/10.1190/1.1443207.

BPS International, 2017, http://botanicalprocesssolutions.com/ (accessed June 2017).

Ge, J., Burnison, S.A., Bosshart, N.W., Dotzenrod, N.W., Liu, G., Braunberger, J.R., Ayash, S.C., Hamling, J.A., Sorensen, J.A., Gorecki, C.D., Steadman, E.N., and Harju, J.A., 2015, Bell Creek Field test site – geomechanical modeling report: Plains CO_2 Reduction (PCOR) Partnership Phase III draft Task 9 Deliverable D32 (Update 1) for U.S. Department of Energy National Energy Technology Laboratory Cooperative Agreement No. DE-FC26-05NT42592, Grand Forks, North Dakota, Energy & Environmental Research Center, January.

Han, D., and Batzle, M., 2000, Velocity, density and modulus of hydrocarbon: SEG Technical Program Expanded (p. 1892–1866), Tulsa: Society of Exploration Geophysicists.

Jin, L., Bosshart, N.W., Oster, B.S., Hawthorne, S.B., Peterson, K.J., Burton-Kelly, M.E., Feole, I.K., Jiang, T., Pekot, L.J., Peck, W.D., Ayash, S.C., and Gorecki, C.D., 2016, Bell Creek test site – simulation report: Plains CO_2 Reduction (PCOR) Partnership Phase III draft Task 9 Deliverable D66 (Update 5) executive summary for U.S. Department of Energy National Energy Technology Laboratory Cooperative Agreement No. DE-FC26-05NT42592, Grand Forks, North Dakota, Energy & Environmental Research Center, August.

National Institute of Standards and Technology (NIST Chemistry WebBook, SRD 69), 2017, http://webbook.nist.gov/chemistry/fluid/ (accessed June 2017).

Wood, A.W., 1955, A textbook of sound: MacMillan, *in* Johnston, D.H., 2013, Making a difference with 4D—practical applications of time-lapse seismic data: SEG distinguished Instructor Short Course.

APPENDIX C

SURFACE SEISMIC DATA PROCESSING

SURFACE SEISMIC DATA PROCESSING

2014 SURFACE SEISMIC DATA PROCESSING

The 3-D surface seismic data from the 2012 baseline survey and 2014 monitor survey were processed by Sensor Geophysical Ltd. in 2014. A summary of the processing can be found in the SEG-Y format data file headers. Processing statistics can be found in Table C-1. The processing sequence was as follows, with a brief explanation of each step:

- Geometry assignment and trace editing
  - Assign x, y, and z values to each record trace associated with each shot to allow sorting by shot, receiver, offset, and common midpoint (CMP). Identify and edit defective traces.

- Apply spherical divergence spreading correction
  - A time-variant, approximate correction for the geometrical decay of energy as the wavefront propagates away from the source.

- +4 dB/sec gain
  - A time-variant, approximate correction for the geometrical decay of energy as the wavefront propagates away from the source.

- Surface consistent scaling
  - A time-invariant trace amplitude correction incorporating source, receiver, offset, and CMP factors.

- Singular value decomposition for groundroll removal
  - A filtering method that treats shot gathers as matrices and utilizes eigenvectors and eigenvalues to remove uncorrelated traces.

Table C-1. Processing Statistics

	2012 Baseline	2014 Monitor
Prestack Traces	1,634,584	1,634,566
Stacked Traces	48,313	48,343
Record Length	3.0 sec	3.0 sec
Sample Interval	2 msec	2 msec
Inline Fold	24	24
Bin Size	82.5 ft × 82.5 ft	82.5 ft × 82.5 ft
No. of Inlines	288	288
No. of Crossline	193	193
Seismic Datum	4500 ft ASL*	4500 ft ASL
Datum Velocity	7000 ft/s	7000 ft/s

* Amplitude source location.

- Surface consistent deconvolution: 100-ms spiking operator with 1% white noise
  - A deconvolution operator to flatten the spectrum of the data. White noise prevents zero division. Incorporates source, receiver, offset, and CMP factors.

- Vibroseis deconvolution compensation
  - Phase correction to transform the correlated and decomposed wavelet to minimum phase (Poletto and Miranda, 2004)

- Delay time refraction statics: one layer, datum elevation 4500 ft; correction velocity 7000 ft/s
  - A model of the near-surface layer is computed using first break times from the traces, allowing the data to be corrected for elevation differences and time-shifted to the seismic reference datum.

- Surface consistent statics
  - After correcting trace gathers for normal moveout using the new velocities, small static shifts that increase event coherence among trace gathers are computed incorporating source and receiver components.

- Time alignment statics
  - Another form of residual static correction. Algorithm used is not disclosed in the header.

- Normal moveout correction
  - A time correction applied to flatten reflections in CMP gathers. The time correction is calculated using the velocity functions determined during velocity analysis.

- Surface consistent scaling
  - A time-invariant trace amplitude correction incorporating source, receiver, offset, and CMP factors.

- T-F adaptive noise suppression
  - A filtering method that models noise in the time and frequency (T-F) domain over sliding windows and uses the noise model to predict and subtract noise.

- Fold match
  - A process performed to select a subset of data from the monitor and baseline surveys that have similar fold in each bin in order to accurately compare the two data sets for time-lapse changes due to changes in the reservoir and not acquisition.

- F-XY filtering
  - A filter used to remove random noise using frequency-shot-receiver (f-x-y) domain. Specific details about the algorithms were not provided in the header. There are several algorithms that can be described as F-XY noise attenuation filters.

- Anisotropic diffusion filtering
  - A filtering method used to remove random noise and enhance coherent horizontal events without removing coherent energy from dipping structure that is not corrected to horizontal events using NMO (normal moveout correction).

- Remove NMO
  - The time corrections applied during NMO are subtracted.

- Kirchhoff prestack time migration
  - The processed gathers, with the migration velocities applied, are migrated using a Kirchhoff algorithm. This imaging process repositions amplitudes from their apparent reflected location to their actual geometric location in space.

- Shifted to final datum
  - CDP (common depth point) gathers are shifted to the final datum. Processed data were output to data files in SEG-Y format for transfer to the client.

The 2014 monitor survey data were acquired with reference to the NAD (North American Datum) 1927 State Plane Montana South FIPS 2503. Both data sets were processed with reference to the NAD 1927 State Plane Montana South FIPS 2503, units in U.S. feet. Corner points of the 3-D surface are denoted as follows:

Inline	Crossline	X-Coordinate	Y-Coordinate
1001	1001	3101457.0	417537.8
1001	1410	3126826.0	395289.9
1558	1001	3131755.5	452086.8

2015 SURFACE SEISMIC DATA PROCESSING

The 3-D surface seismic data from the 2012 baseline survey, 2014 monitor survey, and 2015 monitor and extended baseline surveys were processed by Arcis Seismic Solutions in 2015. A summary of the processing can be found in the SEG-Y format data file headers. Processing statistics can be found in Table C-2. The processing sequence was as follows, with a brief explanation of each step:

- Minimum phase conversion
  - A filter is used to transform the phase of the data to minimum phase.

- Geometry assignment and trace editing
  - Assign x, y, and z values to each record trace associated with each shot to allow sorting by shot, receiver, offset, and CMP. Identify and edit defective traces.

Table C-2. Processing Statistics

	2012 Baseline	2014 Monitor	2015 Monitor and Baseline Extension
Stacked Traces	163,639	49,614	105,459
Record Length	3.5 sec	3.5 sec	3.5 sec
Sample Interval	2 msec	2 msec	2 msec
Inline Fold	24	24	24
Bin Size	82.5 ft × 82.5 ft	82.5 ft × 82.5 ft	82.5 ft × 82.5 ft
No. of Inlines	550	289	415
No. of Crossline	380	189	378
Seismic Datum	4500 ft ASL	4500 ft ASL	4500 ft ASL
Datum Velocity	7000 ft/s	7000 ft/s	7000 ft/s

- 60-Hz noise removal
  - Data are transformed into the frequency domain, and a filter is applied to remove 60-Hz signal. 60-Hz noise is typically associated with power line noise.

- Apply spherical divergence spreading correction
  - A time-variant, approximate correction for the geometrical decay of energy as the wavefront propagates away from the source.

- Surface consistent scaling
  - A time-invariant trace amplitude correction incorporating source, receiver, offset, and CMP factors.

- Groundroll attenuation
  - Algorithm used is not disclosed in the header.

- Surface consistent scaling
  - A time-invariant trace amplitude correction incorporating source, receiver, offset, and CMP factors.

- Surface consistent deconvolution: 100-ms spiking operator with 1% white noise
  - A deconvolution operator to flatten the spectrum of the data. White noise prevents zero division. Incorporates source, receiver, offset, and CMP factors.

- Delay time refraction statics: one layer, datum elevation 4500 ft; correction velocity 7000 ft/s
  - A model of the near-surface layer is computed using first break times from the traces, allowing the data to be corrected for elevation differences and time-shifted to the seismic reference datum.

- Surface consistent statics
  - After correcting trace gathers for NMO using the new velocities, small static shifts that increase event coherence among trace gathers are computed incorporating source

and receiver components. Although not noted in the header, this process was likely preceded by velocity analysis.

- Velocity analysis (second pass)
  - Gathers that have the surface consistent static correction applied are corrected for NMO with a range of constant velocities. The velocity at a given time resulting in the greatest coherence is saved.

- Surface consistent residual statics (second pass)
  - As before, after application of refined velocities.

- NMO
  - A time correction is applied to flatten reflections in CMP gathers. The time correction is calculated using the velocity functions determined during velocity analysis.

- SCORE
  - A surface consistent amplitude correction used to account for amplitude effects caused by the near surface.
- Noise suppression (shot and offset domain)
  - Algorithm used is not disclosed in the header.

- Noise suppression (CMP domain)
  - Algorithm used is not disclosed in the header.

- Surface consistent deconvolution: 100-ms spiking operator with 1% white noise
  - A deconvolution operator to flatten the spectrum of the data. White noise prevents zero division. Incorporates source, receiver, offset, and CMP factors.

- Noise suppression (CMP and offset domain)
  - Algorithm used is not disclosed in the header.

- Phase and statics compensation
  - Phase and static differences between the different vintages of data are corrected for using standard 4-D calibration routines

- Radon multiple attenuation
  - NMO-corrected data are transformed into the ray parameter two-way intercept time domain. In this domain, the flattened primary reflections are mapped to different locations from the undercorrected multiples, and a filtering or muting operation is applied to remove the signal associated with the multiples. Then the inverse parabolic radon transform is performed. Another common approach is to remove the primary reflections in the ray parameter two-way intercept time domain, apply the inverse radon transform, and then subtract these data containing primarily the multiples from the input data.

- F-XY noise attenuation
  - A filter used to remove random noise using frequency-shot-receiver (f-x-y) domain. Traces within a window are transformed into the frequency domain, and a filter is designed to enhance signal that is spatially predictive for every frequency in a user-specified range.

- 5-D interpolation
  - Trace interpolation is done in the inline, crossline, offset, azimuth, and frequency domain to regularize the data. Some of its uses include correcting for missing shot or receiver points because of acquisition constraints.

- Remove NMO
  - The time corrections applied during NMO are subtracted.

- Anisotropic velocity analysis
  - A process that uses the NMO velocity functions determined in velocity analysis which are determined assuming reflected energy has a hyperbolic trajectory to solve for the more realistic nonhyperbolic trajectory defined by the anisotropic moveout equation.

- Anisotropic Kirchhoff prestack time migration
  - The processed gathers, with the anisotropic migration velocities applied, are migrated using a Kirchhoff algorithm. This imaging process repositions amplitudes from their apparent reflected location to their actual geometric location in space.

- Culling by SFIDST
  - Algorithm is not disclosed in the header.

- Front-end mute
  - A mute applied to far offset traces to zero the parts of the trace where refracted energy overlaps reflected energy.

- Stack
  - The traces in each migrated CMP gather are summed together to create a single CMP trace centered in each 82.5-ft × 82.5-ft surface bin.

- Filter
  - Filter parameters are not disclosed in the header.

- AGC (automatic gain control)
  - A trace-by-trace amplitude scaling process using a moving window. Parameters not disclosed. Processed data were output to data files in SEG-Y format for transfer to the client.

The 2015 monitor and baseline extension data were acquired in NAD 1927 State Plane Montana South FIPS 2503, units in U.S. feet. The 2012 baseline survey, 2014 monitor survey, and

2015 monitor and baseline extension data were delivered with coordinates into the NAD 83 UTM 13N projections. Corner points of the 3-D surface are denoted:

Inline	Crossline	X-Coordinate	Y-Coordinate
1001	1001	1579652.70	16371915.72
1001	1410	1603733.59	16348279.58
1697	1001	1619874.59	16412894.44
1697	1410	1643955.48	16389258.30

2013 VSP DATA PROCESSING

In October 2013, Apex HiPoint processed the 2013 baseline VSP data with the following summarized sequence. A summary of the processing can be found in the SEG-Y format data file headers. Additional processing information was delivered in PowerPoint format. The processing sequence was as follows, with a brief explanation of each step:

- Reformat
  - Convert field data to internal format for processing.

- Geometry assignment
  - Assign x, y, and z values to each record trace associated with each shot to allow sorting by shot, receiver, offset, and CMP.

- Geophone orientation analysis
  - Analysis of hodograms (time versus distance of motion plots) for signal from the horizontal component geophones to determine the arrival direction of waves and determine each component's orientation.

- Rotation
  - Correction of phase changes resulting from rotation of tool during installation to signal consistent with radial and transverse geophone orientation. Another rotation of geophones was applied to maximize direct arrival energy on one component for first arrival picking (Apex HiPoint, 2013; Hinds and others, 1996)

- First arrival picking
  - Times corresponding to the first arrival of energy on each channel are selected or picked.

- Time-variant rotation
  - Rotation to maximize P-wave reflection energy on one single component (Apex HiPoint, 2013)

- Apply spherical divergence spreading correction
  - A time-variant, approximate correction for the geometrical decay of energy as the wavefront propagates away from the source.

- Removal of downgoing energy
  - Attenuation of downgoing direct arrivals leaving upgoing reflections (Apex HiPoint, 2013)

- Upward continuation to pseudo-receivers at surface
  - Upward continuation of seismic data using a proprietary method to pseudo-receivers at surface allowing for standard surface seismic processing flows.

- Surface consistent scaling
  - A time-invariant trace amplitude correction incorporating source, receiver, offset, and CMP factors.

- Surface consistent deconvolution: 240-ms spiking operator with 1% white noise
  - A deconvolution operator to flatten the spectrum of the data. White noise prevents zero division. Incorporates source, receiver, offset, and CMPt factors.

- 3-D gridding CMP sort and stack
  - A 3-D grid was applied to the data to make 82.5-ft by 82.5-ft bins and assign CMPs.

- Surface consistent scaling
  - A time-invariant trace amplitude correction incorporating source, receiver, offset, and CMP factors.

- Surface consistent deconvolution: 240-ms spiking operator with 1% white noise
  - A deconvolution operator to flatten the spectrum of the data. White noise prevents zero division. Incorporates source, receiver, offset, and CMP factors.

- Trace balancing
  - A time-invariant trace amplitude correction.

- Velocity analysis
  - Gathers are corrected for NMO with a range of constant velocities. The velocity at a given time resulting in the greatest coherence is saved.

- Residual statics
  - After correcting trace gathers for normal moveout using the new velocities, small static shifts that increase event coherence among trace gathers are computed.

- Kirchhoff prestack time migration
  - The processed gathers, with the migration velocities applied, are migrated using a Kirchhoff algorithm. This imaging process repositions amplitudes from their apparent reflected location to their actual geometric location in space.

- NMO correction
  - A time correction applied to flatten reflections in CMP gathers. The time correction is calculated using the velocity functions determined during velocity analysis.

- Mute
  - Top and bottom mute was applied to the stack to remove areas with poor resolution due to survey geometry.

- Stack
  - The traces in each migrated CMP gather are summed together to create a single CMP trace centered in each 82.5-ft × 82.5-ft surface bin.

- Filter
  - An F-XY deconvolution was applied which is a filter used to remove random noise using frequency-shot-receiver (f-x-y) domain. Specific details about the algorithms were not provided in the header. Several algorithms can be described as F-XY noise attenuation filters. A 4-140-Hz bandpass filter was applied.

- Shifted to final datum: one layer, datum elevation 3700 ft; correction velocity 6500 ft/s
  - Data are shifted to the final datum. Processed data were output to data files in SEG-Y format for transfer to the client.

2014 VSP Data Processing

In April 2014, ApexHi Point processed the shot points from the 2013 baseline and March 2014 monitor VSP data that were repeated with the following summarized sequence. A summary of the processing can be found in the SEG-Y format data file headers. The processing sequence was as follows, with a brief explanation of each step:

- Reformat
  - Convert field data to internal format for processing.

- Geometry assignment
  - Assign x, y, and z values to each record trace associated with each shot to allow sorting by shot, receiver, offset, and CMP.

- Geophone orientation analysis
  - Analysis of hodograms (time versus distance of motion plots) for signal from the horizontal component geophones to determine the arrival direction of waves and determine each component's orientation.

- Rotation
  - Correction of phase changes resulting from rotation of tool during installation to signal consistent with radial and transverse geophone orientation. Another rotation of geophones was applied to maximize direct arrival energy on one component for first arrival picking (Apex HiPoint, 2013; Hinds and others, 1996).

- First arrival picking
  - Times corresponding to the first arrival of energy on each channel are selected or picked.

- Time-variant rotation
  - Rotation to maximize P-wave reflection energy on one single component (Apex HiPoint, 2013).

- Apply spherical divergence spreading correction
  - A time-variant, approximate correction for the geometrical decay of energy as the wavefront propagates away from the source.

- Match filter
  - Filter designed and applied to match source signature of one vintage of data to another in order to equalize amplitudes and minimize phase differences (Hoeber and others, 2005).

- Source wavelet estimation and wavelet deconvolution
  - Source wavelet is estimated for each shot and used to design a deconvolution operator to flatten the spectrum of the data.

- Removal of downgoing energy
  - Attenuation of downgoing direct arrivals leaving upgoing reflections (Apex HiPoint, 2013).

- Linear moveout correction (LMO)
  - Reflections were flattened using the first arrival time picks.

- Filter
  - A 4-140-Hz bandpass filter was applied.

- Shifted to final datum: one layer, datum elevation 3700 ft; correction velocity 6500 ft/s
  - Data are shifted to the final datum. Processed data were output to data files in SEG-Y format for transfer to the client.

2015 VSP Data Processing

In May 2015, Paulsson, Inc., processed the geophone data from the 04-03 OW permanent borehole array collected during the 2013 baseline and October 2014 monitor VSP surveys with the following summarized sequence. A summary of the processing cannot be found in the SEG-Y format data file headers. The following information is a processing flow proposed prior to actual data processing and may not reflect the processing flow used.

- Geometry assignment and trace editing
  - Assign x, y, and z values to each record trace associated with each shot to allow sorting by shot, receiver, offset, and CMP. Identify and edit defective traces.

- Data subset selection
  - Shot records from shot points that were repeated from the 2013 baseline VSP to the October 2014 monitor VSP survey were compiled into a subset of data used for processing.

- Geophone orientation analysis
  - Analysis of hodograms (time versus distance of motion plots) for signal from the horizontal component geophones to determine the arrival direction of waves and determine each component's orientation.

- First arrival picking
  - Times corresponding to the first arrival of energy on each channel are selected or picked.

- Datum statics: datum elevation 3730 ft; correction velocity not disclosed
  - Data are shifted to an elevation datum.

- Source wavelet estimation and wavelet deconvolution
  - Source wavelet is estimated for each shot and used to design a deconvolution operator to flatten the spectrum of the data.

- Velocity analysis
  - Evaluate velocity model generated from zero offset VSP velocities by performing moveout analysis on prestack gathers.

- Update receiver locations using well deviation and first arrivals
  - X, Y, and Z coordinates were updated to account for well deviation.

- Apply spherical divergence spreading correction
  - A time-variant, approximate correction for the geometrical decay of energy as the wavefront propagates away from the source.

- Surface consistent scaling
  - A time-invariant trace amplitude correction incorporating source, receiver, offset, and CMP factors.

- Removal of downgoing energy
  - Attenuation of downgoing direct arrivals leaving upgoing reflections (Apex HiPoint, 2013).

- Surface consistent scaling
  - A time-invariant trace amplitude correction incorporating source, receiver, offset, and CMP factors.

- Surface consistent statics
  - After correcting trace gathers for NMO using the new velocities, small static shifts that increase event coherence among trace gathers are computed incorporating source and receiver components.

- Kirchhoff prestack depth migration (Kirchhoff PSDM)
  - The processed gathers, with the migration velocities applied, are migrated using a Kirchhoff algorithm. This imaging process repositions amplitudes from their apparent reflected location to their actual geometric location in space.

- Residual statics
  - After correcting trace gathers for NMO using the new velocities, small static shifts that increase event coherence among trace gathers are computed.

- Refined velocity analysis
  - Evaluate velocity model generated from zero offset VSP velocities by performing moveout analysis on prestack gathers.

- Spectral balancing
  - The frequency spectra are shaped in order to balance the amplitudes of the frequencies in the desired bandwidth and improve data resolution.

- Anisotropic velocity analysis
  - Algorithm not disclosed.

- Anisotropic Kirchhoff PSDM
  - The processed gathers, with the anisotropic migration velocities applied, are migrated using a Kirchhoff algorithm. This imaging process repositions amplitudes from their apparent reflected location to their actual geometric location in space.

REFERENCES

Apex HiPoint, 2013, Denbury/EERC Belle Creek 3-D VSPs—final imaging update: Presented to Energy & Environmental Research Center.

Hinds, R.C., Anderson, N.L., and Kuzmiski, R.D., 1996, VSP interpretive processing—theory and practice: Society of Exploration Geophysicists.

Hoeber, H., Lecerf, D., Zaghouani, H., and Whitcombe, D., 2005, Matching of multiple time-lapse data using multi-coherence analysis: Presented at 67th EAGE Conference & Exhibition.

Poletto, F., and Miranda, F., 2004, Seismic while drilling, fundamentals of drill-bit seismic for exploration: SEG, Handbook of Geophysical Exploration, Seismic Exploration, Elsevier 35.